CENTRAL EQUATORIAL PACIFIC SEA SURFACE TEMPERATURES OVER THE LAST GLACIAL CYCLE

A Dissertation
Presented to
The Academic Faculty

by

Minda Moriah Monteagudo

In Partial Fulfillment
of the Requirements for the Degree
Doctor of Philosophy in the
School of Earth and Atmospheric Sciences

Georgia Institute of Technology
December 2021

CENTRAL EQUATORIAL PACIFIC SEA SURFACE TEMPERATURES OVER THE LAST GLACIAL CYCLE

Approved by:

Dr. Jean Lynch-Stieglitz, Advisor
School of Earth and Atmospheric Sciences
Georgia Institute of Technology

Dr. Jenny McGuire
School of Biological Sciences
Georgia Institute of Technology

Dr. Kim Cobb
School of Earth and Atmospheric Sciences
Georgia Institute of Technology

Dr. Kevin Haas
School of Civil and Environmental Engineering
Georgia Institute of Technology

Dr. Emanuele Di Lorenzo
School of Earth and Atmospheric Sciences
Georgia Institute of Technology

Date Approved: December 7, 2021

ACKNOWLEDGEMENTS

I would first like to first thank my advisor, Jean Lynch-Stieglitz, for her guidance and unwavering support throughout my Ph.D. I feel lucky to have spent such a formative time in my life, as both a researcher and person, learning from someone who motivates her students to meet her high expectations through confidence in their abilities, even when they most doubt themselves. I would also like to thank my committee members – Kim Cobb, Manu Di Lorenzo, Jenny McGuire and Kevin Haas – for their input and guidance throughout the years. Thank you to Tom Marchitto and Matthew Schmidt, who have both hosted me in their labs and patiently answered all my trace element-related questions. I am also grateful to Tammy Chang for her help in the lab, which supported all the work presented in this thesis.

I would not be here without the support of family and friends throughout my entire life, but especially in the last five years. First and foremost, to my parents whose unending love and support has formed the foundation from which everything I do builds. Your work ethic is the example I have always followed and I hope I made you proud. It's been a long road but I promise I'm done with school now. To my siblings who, among other things, have been incredibly understanding when I retreat into research for weeks at a time, but are also ready to welcome me back with open arms and a supportive shoulder to cry on. You are my first and best friends. To Miles Sakwa-Novak, for being the most supportive partner I could have ever asked for. Thank you for reminding me not to sweat the small stuff. It's not a lesson I have learned yet but your efforts are appreciated. I am also indebted to Team Paleo past and present for their friendship: Shannon Valley, Tyler Vollmer, Karim Lakhani, Shelby Ellis, Annika Jersild, and Hussein Sayani.

Finishing a Ph.D. is never easy, and a global pandemic certainly does not help. To everyone mentioned above, I would like to also acknowledge the additional support and kindness they have shown me during the last year and a half as we all navigated difficult and uncertain circumstances.

TABLE OF CONTENTS

LIST OF TABLES

LIST OF FIGURES

LIST OF SYMBOLS AND ABBREVIATIONS

Al	Aluminum
BP	Before present
Ca	Calcium
CLIMAP	Climate: Long Range Investigation, Mapping and Prediction
CMIP	Coupled Model Intercomparison Project
CO_2	Carbon dioxide
$[CO_3^{2-}]$	Carbonate ion concentration
$\Delta[CO_3^{2-}]$	Delta carbonate ion concentration
$\delta^{18}O$	Ratio of oxygen-18 to oxygen-16
$\delta^{18}O_c$	Ratio of oxygen-18 to oxygen-16 in calcite
ECS	Equilibrium climate sensitivity
Fe	Iron
ka	Thousands of years before present
kyr	Thousand years
LGM	Last Glacial Maximum
LIG	Last Interglacial
MARGO	Multiproxy Approach to Reconstructing the Glacial Surface Ocean
Mg	Magnesium
Mn	Manganese
MIS	Marine Isotope Stage
NADW	North Atlantic Deep Water
NECC	North Equatorial Counter Current
PDB	Pee Dee Belemnite

PMIP	Paleoclimate Modelling Intercomparison Project
psu	Practical salinity unit
SEC	South Equatorial Current
SMOW	Standard Mean Ocean Water
SST	Sea surface temperature
$U_{37}^{k\prime}$	Alkenone unsaturation index
Ω	Saturation state of calcite in seawater

SUMMARY

The tropical Pacific is a dominant influence on global climate, from interannual to glacial-interglacial timescales. How this system will respond to anthropogenic greenhouse gas forcing, however, remains an area of large uncertainty. In order to better our understanding of how the tropical Pacific ocean-atmosphere system has responded to greenhouse gas forcing in the past, I have generated new reconstructions of sea surface temperature (SST) in the central equatorial Pacific over the last ~150,000 years.

In Chapter 1, I investigate Pacific SSTs during the Last Glacial Maximum (LGM, 19,000-23,000 years before present), the most recent interval in earth history when atmospheric CO_2 was significantly lower than the Pre Industrial. Our new Mg/Ca records show that the central equatorial Pacific cooled by an average of ~2 °C during the LGM, providing the first geochemical records of LGM SST in this region. Our data resolve a decades-old disagreement between older microfossil proxies that suggested warming of the glacial tropical central Pacific and climate models which, like our data, show a ~1.5-2.0 °C cooling.

To further improve our understanding of the glacial surface ocean, I present a Mg/Ca record from VM19-74 in the southeastern tropical Pacific in Chapter 2. Mg/Ca data from this site suggests no glacial SST change, a puzzling finding given our understanding of glacial climate. Interestingly, VM19-74 oxygen isotopes show a ~1.4 ‰ glacial enrichment, which, when corrected for ice volume, suggests the southeastern tropical Pacific could have been ~1.5 °C cooler, ~0.3 psu saltier, or some combination of the two. I explore possible geochemical explanations for these high glacial Mg/Ca data, and show that an attempt to corroborate this record using nearby core RC11-34TRI is not possible

given evidence of sediment disturbance. This study highlights the need for continued work to improve our spatial understanding of past SST patterns.

In Chapter 3 I extend our SST reconstructions to the Last Interglacial (LIG), a period between 115,000-130,000 years before present which has been studied as a possible analogue for future climate change. Here I show that the central equatorial Pacific was ~1.1 °C warmer during the LIG. I compile additional tropical Pacific Mg/Ca and alkenone records which also support a warmer LIG, unlike climate models that struggle to simulate this magnitude of tropical SST change. There is also significant evidence that seasonal insolation, not atmospheric CO_2 forcing, is the dominant driver of LIG climate. We explore some of the prevailing mechanisms proposed linking seasonal insolation forcing to mean annual temperature response, though it remains unclear which mechanism explains tropical proxy records. This study underscores the importance of disentangling the components of LIG warming driven by greenhouse gas and orbital forcings.

Finally, in Chapter 4 I incorporate new Equilibrium Climate Sensitivity estimates from CMIP6 models contributing to the recent IPCC Sixth Assessment Report into the discussion of the results from Chapters 1 and 3. I conclude by outlining some of the questions that remain which may be resolved by future paleocenographic work.

CHAPTER 1. CENTRAL EQUATORIAL PACIFIC COOLING DURING THE LAST GLACIAL MAXIMUM

(Previously published as: Monteagudo, M.M., Lynch-Stieglitz, J., Marchitto, T. and M.W. Schmidt (2021) Central Equatorial Pacific Cooling during the Last Glacial Maximum. Geophysical Research Letters, 48, DOI: 10.1029/2020GL088592)

1.1 Introduction

The tropical Pacific has been shown to be a dominant influence on global climate, from interannual to glacial timescales; however, much uncertainty surrounds the evolution of the tropical Pacific ocean-atmosphere system in response to varying atmospheric CO_2 levels. The Last Glacial Maximum (LGM, 19-23 ka) serves as an important interval for studying equilibrium climate sensitivity since the forcing is both large and fairly well-constrained, and multiple proxies exist to estimate the temperature response. LGM tropical SSTs, in particular, may be more significantly correlated with climate sensitivity than mean global temperature, given the lessened impact of high latitude forcings on tropical records (Hargreaves, Annan, Yoshimori, & Abe-Ouchi, 2012; Hopcroft & Valdes, 2015; Schmidt et al., 2014). Thus, the magnitude of tropical cooling during the LGM from proxy-based reconstructions is an important constraint on equilibrium climate sensitivity estimates (Hargreaves et al., 2012; Lea, 2004).

At present, both the magnitude and spatial pattern of tropical Pacific SST changes during the LGM remain uncertain. The Climate Long-Range Investigation Mapping and Prediction (CLIMAP) project's synthesis of glacial SST showed little to no SST change in the glacial central equatorial Pacific, based largely on foraminiferal assemblages (CLIMAP Project Members, 1976). More recently, the Multiproxy Approach for the Reconstruction of the Glacial Ocean Surface (MARGO) project incorporated

geochemical SST proxies, yet reiterated CLIMAP's finding of little to no SST change in the central equatorial Pacific (Waelbroeck et al., 2009). However, it should be noted that there were very few geochemical measurements in the MARGO compilation from the central tropical Pacific and the MARGO project had to rely on foraminiferal assemblage data, much of it generated for the early CLIMAP study. In contrast, geochemical records from the eastern and western equatorial Pacific from Mg/Ca (Benway et al., 2006; de Garidel-Thoron et al., 2005; de Garidel-Thoron et al., 2007; Koutavas & Lynch-Stieglitz, 2002; Koutavas & Joanides, 2012; Lea et al., 2000; Lea et al., 2006; Rosenthal et al., 2003; Stott et al., 2002; Stott et al., 2007), alkenones (Kienast et al., 2001; Koutavas & Sachs, 2008; Leduc et al., 2007), TEX_{86} (Hertzberg et al., 2016) and clumped isotopes (Tripati et al., 2014) indicate 1-4 °C cooling. Several proxy-based analyses indicate that the magnitude of overall tropical ocean cooling was likely 2.0-3.0 °C (Ballantyne et al., 2005; Crowley, 2000), much larger than the moderate cooling suggested by CLIMAP and MARGO. Most recently, a multi-proxy data assimilation study showed 3.5 °C of global tropical ocean cooling (Tierney et al., 2020). Terrestrial proxy records are also incompatible with CLIMAP/MARGO SSTs, as depressed tropical snowlines indicate ~4-6 °C cooling (Rind & Peteet, 1985; Webster & Streten, 1978). Given that lower atmospheric CO_2 should cause cooling, it remains difficult to explain why central equatorial Pacific SSTs would be similar to modern during the LGM. Global climate model simulations driven with LGM boundary conditions suggests 2.0-2.5 °C cooling in the central tropical Pacific and suggest a similar degree of cooling in the central equatorial Pacific as in the eastern and western parts of the basin (Brady, Otto-Bliesner, Kay, & Rosenbloom, 2013; DiNezio et al., 2011; Otto-Bliesner et al., 2009).

Here we present the first estimates of central equatorial Pacific SSTs during the LGM using the Mg/Ca ratio of the surface-dwelling foraminifera *Globigerinoides ruber* from a meridional transect of sediment cores from the Line Islands. We also combine our data with existing equatorial *G. ruber* Mg/Ca data to present a more complete view of tropical SST changes during the LGM.

1.2 Materials and Methods

1.2.1 Line Islands Sediment Cores and Age Models

The cores used in this study (Figure 1) were collected along the Line Islands Ridge, a NW-SE trending bathymetric rise in the central equatorial Pacific (Table 1), west of the Eastern Pacific Cold Tongue. Seasonal temperature and salinity variability at the Line Islands is low: 0.7-1.0 °C and 0.2-0.5 PSU, respectively, increasing from the equator to 7 °N (Schmidtko et al., 2013). Locations south of 2 °N (~27 °C) are supplied with cooler water from the subsurface by equatorial upwelling, as well as from the Eastern Pacific via the South Equatorial Current. Warmer surface waters (~28 °C) north of 2° latitude are supplied from the Western Pacific via the North Equatorial Countercurrent.

The cores presented in this study span from 0.22°S - 7.04 °N, 155.96 - 161.63 °W and 2371-3597 m water depth. Sedimentation rates range from ~1.7 - 3.5 cm/kyr, decreasing with distance from the equator (Lynch-Stieglitz et al., 2015). Radiocarbon measurements were made on samples of the planktonic foraminifera *Globigerinoides ruber* or *Globigerinoides sacculifer* (350-500 µm size fraction) at the National Ocean Sciences Accelerator Mass Spectrometry facility at Woods Hole. Radiocarbon ages (Table 2) were converted to calendar ages using CALIB 7.1 and the Marine13 calibration curve, with the

standard marine reservoir correction (R=400 years) (Reimer et al., 2013). Age models for each core were constructed by linearly interpolating between radiocarbon measurements. Due to low sedimentation rates above 2 °N and recent carbonate dissolution, Late Holocene (0-4 ka) core-tops were available only for the southern portion of our transect. The age models were used to establish the depth ranges for Late Holocene (0-4 ka), Mid-Holocene (4-8 ka) and LGM (19-23 ka) time slices. Samples from depths within the above time slices were analyzed for Mg/Ca. Cores 27BB, 34BB and 36BB feature age reversals in the upper 8 cm; data above the age reversal are not used.

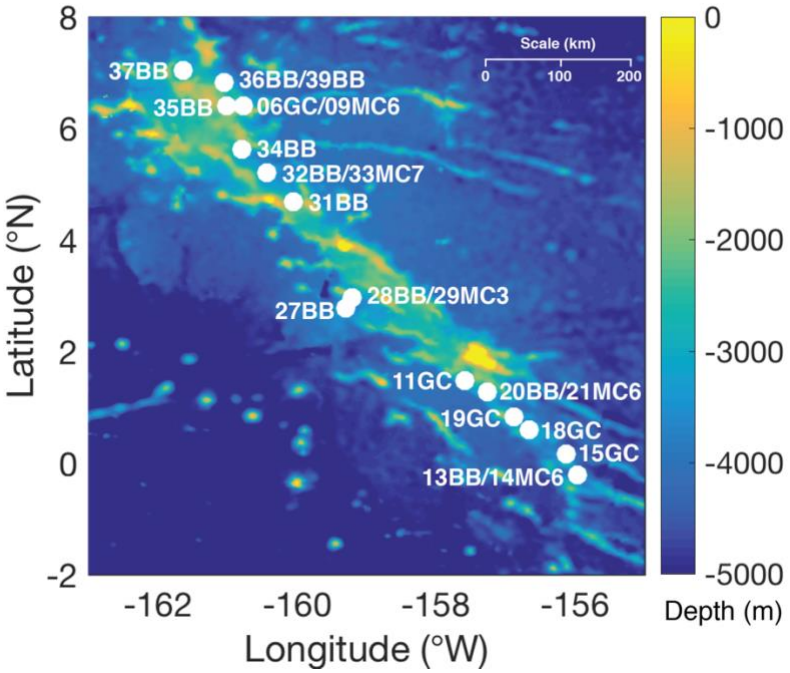

Figure 1 Bathymetric map (Amante & Eakins, 2009) of Line Islands core sites presented in this study (white markers).

1.2.2 Analytical Methods for Line Islands Sediment Cores

G. ruber $\delta^{18}O$ data for all but one of the sediment core sites were published and discussed previously (Lynch-Stieglitz et al., 2015). We generated data for sediment core ML1208-32BB and the multicore tops as part of this study. $\delta^{18}O$ measurements were

conducted on a Thermo MAT253 Stable Isotope Mass Spectrometer coupled to a Kiel IV Carbonate Device at Georgia Tech. 15 *G. ruber* individuals were analyzed from the 250-355 μm size fraction. $\delta^{18}O$ measurements were converted to PDB using an in-house standard and NBS-19. Reproducibility of the in-house standard was 0.045 ‰ for $\delta^{18}O$ and 0.014 ‰ for $\delta^{13}C$ (1 sigma).

For Mg/Ca measurements, approximately 60 individual *G. ruber* were selected from the 250-355 μm size fraction, gently crushed, homogenized, and split into two aliquots for replicate measurements, except where noted (Table 6). *G. ruber* is a symbiont-bearing foraminifera which confines its calcification depth to the upper ~50 (e.g. Schiebel & Hemleben, 2005) or 100 meters (Rippert et al., 2016). *G. ruber* (sensu stricto) was picked whenever possible, though some sensu lato were necessary for sufficient sample masses. Oxygen isotopic measurements have shown no offset between morphotypes at the Line Islands (Lynch-Stieglitz et al., 2015). Mg/Ca samples were cleaned using both reductive and oxidative steps (Boyle & Rosenthal, 1996). The majority of measurements were done at University of Colorado, Boulder on a Thermo Element 2 ICP-MS. As indicated in the data supplement, some samples were cleaned and analyzed at Old Dominion University, with two cores (28BB and 37BB) cleaned and analyzed at Texas A&M University. Cleaning methods were consistent between labs and replicate measurements were used as inter-laboratory comparison (see Appendix A) and show no systematic interlaboratory offset. Internal standards at CU Boulder are validated against powdered community standards BAM RS3, ECRM 752-1, and CMSI 1767 (Greaves et al., 2008). Al/Ca, Mn/Ca and Fe/Ca ratios were monitored for possible contamination and anomalously high values

(>100 μmol/mol) were discarded (n=1). Average reproducibility based on 94 replicate measurements was ±0.22 mmol/mol.

Mg/Ca measurements are converted to SST using the $\Delta[CO_3^{2-}]$-corrected calibration of Dekens et al. (2002), which gives the best match to climatology (see Appendix A). We used modern bottom water $[CO_3^{2-}]$ values computed using World Ocean Circulation Experiment (WOCE) P16N measurements and CO2SysV2.1 for Excel. Sensitivity tests were performed using estimates of LGM Pacific $\Delta[CO_3^{2-}]$ changes, though these are generally believed to be small in magnitude (See Appendix A). Late Holocene SSTs agree with climatological mean annual SSTs (Schmidtko et al., 2013) within the calibration error (Figure 2). It should be noted, however, that *G. ruber* Mg/Ca can also influenced by salinity (e.g. Nürnberg et al., 1996; Lea et al., 1999; Russell et al., 2004), carbonate chemistry conditions during calcification, expressed as either pH or $[CO_3^{2-}]$ (e.g. Evans et al., 2016, Gray et al., 2018). It has also recently been shown that the canonical ~9% sensitivity of Mg/Ca to temperature may overestimate the pure thermal component (Gray and Evans, 2018). Several multivariate calibrations have been published (Gray & Evans, 2019; Khider et al., 2015; Saenger & Evans, 2019; Tierney et al., 2019). The implications of these other Mg/Ca calibrations are discussed in Appendix A, but do not change the main conclusions of this work.

1.2.3 Global G. ruber Mg/Ca compilation

We compiled available LGM Mg/Ca data for *Globigerinoides ruber* (white) from the literature (Table 6). We only compile data from *G. ruber*, as *Trilobatus sacculifer*, the other ubiquitous tropical surface-dwelling foraminifera species, has been shown to add

significant amounts of gametogenic calcite at depth (Spero & Lea, 1993; Wycech et al., 2018), which may complicate the interpretation of *T. sacculifer* Mg/Ca as a purely SST signal. Cores located between 15 °N and 15 °S with radiocarbon dated LGM sections and *G. ruber* (212-355 μm) Mg/Ca data were selected. *G. ruber* (sensu stricto) data were used where available and noted, however some studies did not distinguish which morphotype was used. *G. ruber* (pink) data from the Atlantic was not included except one study which used *G. ruber* pink occasionally to increase sample size (Lea, Pak, Peterson, & Hughen, 2003). Mg/Ca values between 0-4 ka (Late Holocene) and 19-23 ka (LGM) were averaged, as determined by the age models in the original publications. Raw Mg/Ca values were first corrected to account for differing cleaning methods, with a 10% correction applied to cores that omit the reductive cleaning step, as it has been shown that the reductive step reduces Mg/Ca ratios by ~ 10% (Barker et al., 2003). Average Mg/Ca ratios were converted to SST using the Dekens et al., (2002) $\Delta[CO_3^{2-}]$ calibration using modern bottom water $[CO_3^{2-}]$ for all Late Holocene data and the LGM data in the Pacific Ocean. In the Atlantic, LGM $\Delta[CO_3^{2-}]$ values were adjusted by +19 μmol/kg above 2.8 km water depth and -21 μmol/kg below this depth (Appendix A). The magnitude of LGM cooling is calculated by taking the difference between Late Holocene and LGM Mg/Ca SSTs. Where Late Holocene samples are not available, the magnitude of LGM cooling is reported relative to the modern climatology. Mg/Ca temperature estimates for the global compilation are adjusted by +0.6 °C, the mean offset between modern climatological mean annual SST and the Late Holocene Mg/Ca SST found in the global dataset (Appendix A). This prevents the overestimation of the magnitude of LGM cooling for the core sites where cooling is

reported relative to the modern climatological SST. The magnitude of cooling for locations with Late Holocene Mg/Ca are independent of the application of this offset.

1.3 Results and Discussion

1.3.1 LGM Temperature in the Central Equatorial Pacific

The Mid-Holocene (4-8 ka) is the most recent time interval for which data is available at all latitudes along our Line Islands Ridge transect. While there are only three locations for which Late Holocene data are available, there is no indication of significant changes in temperature between the Mid and Late Holocene (Figure 2). While all cores show moderately cooler temperature estimates for the Late and Mid-Holocene relative to the climatological data (Schmidtko et al., 2013), the offset (-0.6 °C) is the same as was found between the Late Holocene and climatological SST in our global tropical data set. The lack of significant change between the Late and Mid Holocene is broadly consistent with PMIP2 and PMIP3 6 ka simulations that show only modest SST changes (0.2-0.4 °C cooling) near the Line Islands (An & Choi, 2014).

Glacial Mg/Ca SST estimates indicate cooling at all Line Islands core locations, between 1.4 to 2.8 °C (mean = 2.0 °C) relative to the Late and Mid Holocene. Cores influenced by equatorial upwelling (-0.22-1.27 °N) show a slightly larger magnitude of LGM cooling (-2.0 ± 0.2 °C, 1 sigma standard error) than more northerly cores influenced by the North Equatorial Counter Current (-1.9 ± 0.2 °C). The glacial-interglacial difference in temperature is reported with the standard error, which approximates our ability to state the mean value in glacial-interglacial Mg/Ca temperature difference using our chosen calibration at this location. The error on the individual SST estimates can be approximated

using the 1.2 °C calibration error from Dekens et al., (2002). The true glacial-interglacial temperature difference in this region may differ due to systematic errors in the proxy and calibration which are difficult to quantify without the consideration of multiple proxies (e.g. Waelbroeck et al., 2009).

Our results do not agree with CLIMAP and MARGO, which suggest little to no SST change near the Line Islands and throughout most of the central Pacific. In contrast, our data are consistent with both model simulations that show ~2.0-2.5 °C cooling near the Line Islands (Brady et al., 2013; DiNezio et al., 2011) as well as proxy records from the eastern and western equatorial Pacific (Benway et al., 2006; Bolliet et al., 2011; de Garidel-Thoron et al., 2005, 2007; Koutavas & Joanides, 2012; Lea et al., 2000; Lea et al., 2006; Leduc et al., 2007; Rosenthal et al., 2003; Steinke et al., 2006; Stott et al., 2002, 2007; Xu, Kuhnt, Holbourn, Regenberg, & Andersen, 2010). The recent LGM data assimilation study of Tierney et al. (2020) shows cooling at our core sites, but of a higher magnitude (-3.9°C) than we find in this study. Central equatorial Pacific cooling is a robust feature of LGM model simulations, but has until now not been corroborated by proxy reconstructions in the region.

The Line Islands meridional SST gradient is sensitive to changes in zonal currents, local equatorial upwelling strength, and thermocline depth and tilt, all of which may reflect changes to Pacific Walker Circulation (DiNezio et al., 2011; Lynch-Stieglitz et al., 2015). Today, Northern Line Islands sites are 0.7 ± 0.2 °C warmer than Southern Line Islands sites. During the Mid-Holocene, the Line Islands meridional SST gradient remained similar (0.8 ± 0.3 °C). During the LGM, the meridional Line Islands SST gradient was increased to 1.1 ± 0.4 °C. While the meridional gradients are not distinguishable within the estimated

errors, it is likely (72%) that the LGM temperature gradient was larger than modern (Appendix A). An earlier study (Lynch-Stieglitz et al., 2015) based on this suite of sediment cores found an enhanced LGM gradient in the $\delta^{18}O$ of *G. ruber* calcite for these sediment cores, and discussed how the enhanced gradient relates to changes in tropical Pacific climate including the Walker Circulation. The Mg/Ca temperature data clarify that the increased gradient in foraminiferal $\delta^{18}O$ is partially due to the increased temperature gradient and partially to an increase in the $\delta^{18}O$ of seawater (Appendix A).

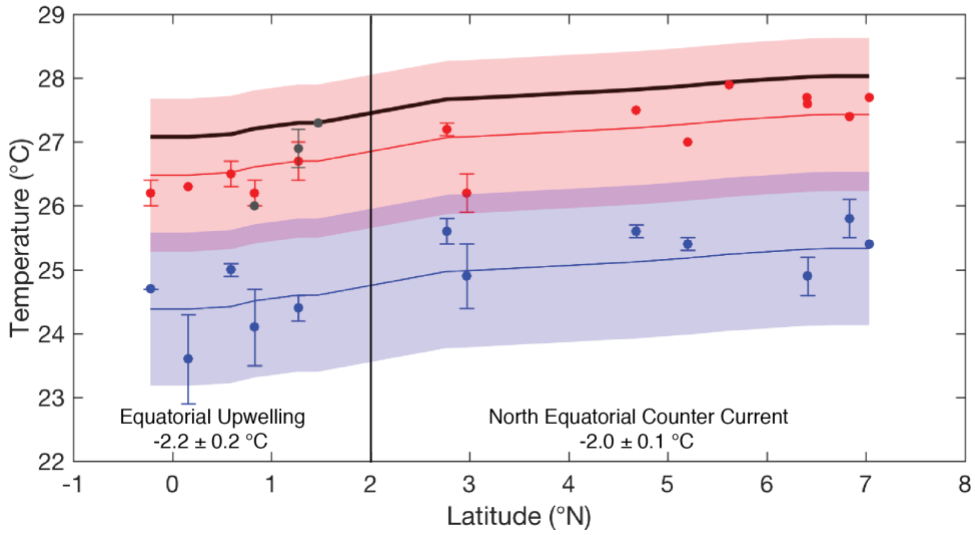

Figure 2 Mean *G. ruber* Mg/Ca-derived SST estimates for the Late Holocene (0-4 ka, gray symbols), Mid-Holocene (4-8 ka, red symbols), and LGM (19-23 ka, blue symbols) compared to modern mean annual SST (black line) (Schmidtko et al., 2013). All temperature estimates are calculated using the Dekens et al. (2002) calibration. Solid lines show the modern climatological SST (black), the modern SST shifted by -0.6 °C (red) and -2.7 °C (blue). The shaded regions denote the 1.2 °C calibration standard error of estimate (Dekens et al., 2002). Error bars show the standard error of the mean for data within a given time slice. A cooling of 2.1 degrees between the Late Holocene and LGM is inferred.

1.3.2 Tropical LGM Cooling from G. ruber Mg/Ca

Coupled ocean-atmosphere models consistently simulate stronger and more uniform LGM ocean cooling than MARGO in the tropical oceans (Braconnot et al., 2007; Brady et al., 2013; DiNezio et al., 2011; Otto-Bliesner et al., 2009). Our compilation of 73 LGM *G. ruber* Mg/Ca SST estimates also shows a larger tropical mean LGM cooling than MARGO, 2.5 ± 0.1 °C (1 sigma standard error on mean) as compared to 1.7 ± 1.0 °C (total error) (Figure 3, Table 1). In the Atlantic, our compilation shows 2.9 ± 0.4 °C cooling, in agreement with 2.9 ± 1.3 °C from MARGO. However, in the Pacific and Indian oceans, our compilation indicates 2.4 ± 0.1 °C and 2.6 ± 0.1 °C cooling, respectively, larger than the 1.2 ± 1.1 °C and 1.4 ± 0.7 °C suggested by MARGO. With the addition of the new central Pacific data, our Mg/Ca based compilation also shows more uniform cooling, without the large meridional gradients suggested in that study. It should be noted that our estimates, while systematically cooler than MARGO, do fall within their estimate of total error which accounts for proxy spread among a number of other factors. Our compilation is also broadly consistent with LGM alkenone compilations (*e.g.* Rosell-Melé et al., 2004), although the magnitude of LGM cooling is sensitive to the choice of calibration (Tierney & Tingley, 2017) and may be affected by different seasonal influences than Mg/Ca (*e.g.* Timmermann, Sachs, & Timm, 2014). Our compilation gives a smaller LGM tropical cooling than a recent data assimilation study which shows 3.4°C of cooling in the 15°S to 15°N latitude band (Tierney et al., 2020). However, the authors of this study note that the spatial average tropical SST change based on the geochemical proxy data alone is 0.9°C smaller than the change based on the data assimilation product, implying that the proxy data average change would be very similar to what we find in our compilation. They

attribute this difference to enhanced cooling throughout the central and eastern tropical Pacific in their assimilated field, cooling which is not corroborated by the new central tropical Pacific Mg/Ca data presented here. The magnitude of glacial cooling estimated here based on *G. ruber* Mg/Ca is in line with model estimates, and provides support for the idea that CLIMAP data from the central Pacific may not be reliable, as has been previously suggested (Mix et al., 1999; Crowley, 2000)

Table 1 Regional estimates of tropical (15 °N-15 °S) LGM Cooling

	Atlantic	Indian	Pacific	Global
MARGO	-2.9 ± 1.3	-1.4 ± 0.7	-1.2 ± 1.1	-1.7 ± 1.0
This study	-2.9 ± 0.4	-2.6 ± 0.1	-2.4 ± 0.1	-2.5 ± 0.1

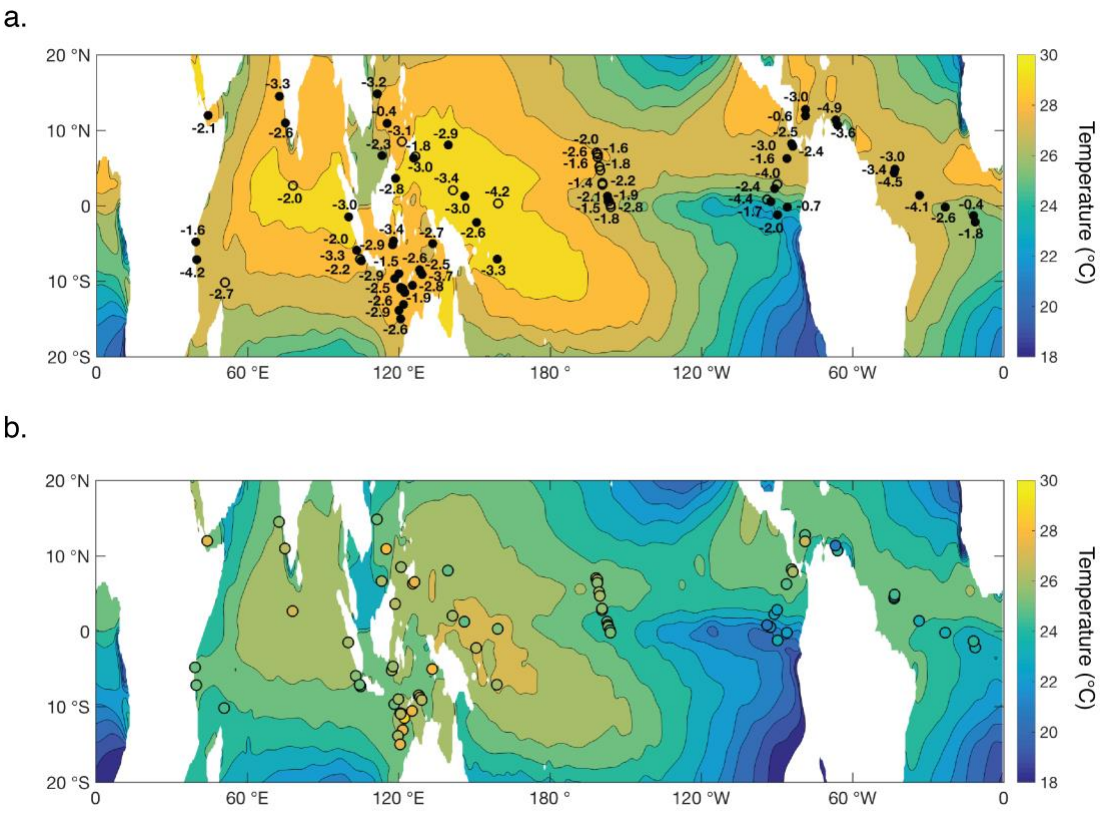

Figure 3 Magnitude of mean LGM SST change (LGM-modern) from equatorial (15 °N to 15 °S) *G. ruber* Mg/Ca studies (references in Table S5). Markers indicate core locations. Negative values indicate cooling relative to the Late Holocene (filled

symbols), or modern climatological SSTs where Late Holocene data are not available (open symbols). Base map is mean annual SST (Schmidtko et al., 2013). b) Base map is the same as 3a, with the mean tropical LGM-modern cooling (-2.5 °C) subtracted in order to better allow for the visual assessment of any systematic changes in the spatial gradients from the modern (base map) to the LGM (markers). Marker color denotes the absolute SST during the LGM based on *G. ruber* Mg/Ca.

It has been suggested that tropical Pacific SST change during the LGM (Lea 2004) and overall tropical temperature change (Hargreaves et al., 2012) provide a constraint on equilibrium climate sensitivity. Studies using MARGO tropical SSTs have estimated equilibrium climate sensitivity at 1.0-3.6 °C (Waelbroeck et al., 2009) and 1.2-2.4 °C (Annan & Hargreaves, 2013) (95% confidence intervals). Alternatively, a model-data analysis that assumed MARGO SST change was underestimated by 1 °C found a climate sensitivity of 1.6 – 4.5 °C (95% confidence interval), consistent with estimates from models run with LGM boundary conditions (*e.g.* Brady et al., 2013). Our compilation results would also suggest a lower climate sensitivity than was estimated using 2.8 °C cooling from a single Eastern Pacific Mg/Ca record (Lea 2004). The recent multi-proxy data assimilation study (Tierney et al., 2020) found climate sensitivity to be 2.4 – 4.5 °C (95% confidence interval) – broadly consistent with the estimate from Schmidt et al., (2014) but with a higher lower bound.

1.4 Conclusions

We have produced the first planktonic foraminiferal Mg/Ca data for the glacial central tropical Pacific, which show, on average ~2.0 °C cooling, in line with model estimates but disagreeing with the CLIMAP and MARGO compilations. These data, together with existing Mg/Ca temperature estimates from the global tropics suggest a tropical cooling of ~2.5 °C, implying that MARGO-based Equilibrium Climate Sensitivity

estimates may be underestimated. Our new central Pacific data underscores the importance of continued work on both proxy development and the value of developing radiocarbon dated and geochemically-based SST records from the open ocean. While the open ocean temperature estimates originating from the faunal counts of the CLIMAP program over forty years ago were revolutionary for their time, these data alone are insufficient for constraining today's state-of-the-art climate models.

1.5 Acknowledgements

The authors acknowledge the US National Science Foundation Grant OCE-1502927 to J.L.-S. We also thank T.-Y. Chang for technical assistance. All radiocarbon, Mg/Ca and oxygen isotope data presented in this study are included in Appendix A and are archived at the National Oceanic and Atmospheric Administration National Centers for Environmental Information database (https://www.ncdc.noaa.gov/paleo/study/29252).

CHAPTER 2. TOWARDS RECONSTRUCTING SOUTHEASTERN TROPICAL PACIFIC SEA SURFACE TEMPERATURES DURING THE LAST GLACIAL MAXIMUM

2.1 Introduction

As described in Chapter 1, reconstructing tropical Pacific SSTs during the LGM has been a focus of paleoceanographic research for decades. Though the 2009 MARGO compilation showed better spatial coverage than the previous CLIMAP synthesis, the southeastern tropical Pacific remains poorly represented. The southeastern tropical Pacific (10-20 °S, 120-150 °W), is a region that the MARGO compilation suggests ranged from 1 °C warmer to 2 °C cooler during the LGM. Near 150 °W the MARGO compilation is unable to reconstruct SSTs at all, due to the lack of proxy records in the area. In this chapter we examine a Mg/Ca record from the southeastern tropical Pacific in order to improve our understanding of LGM SSTs in the region.

2.2 Methods

Core VM19-74 is located in the southeastern tropical Pacific at 15.6 °S, 145.0 °W and 1525 meters water depth. VM19-74 is a 457 cm long, carbonate-rich piston core collected in May 1963. Mean annual sea surface temperature and salinity at this site are 28.0 °C and 36.2 psu, respectively. Seasonal SSTs at this site vary by 1.8 °C while salinity is near-constant, with only a 0.2 psu annual range (Schmidtko et al., 2013).

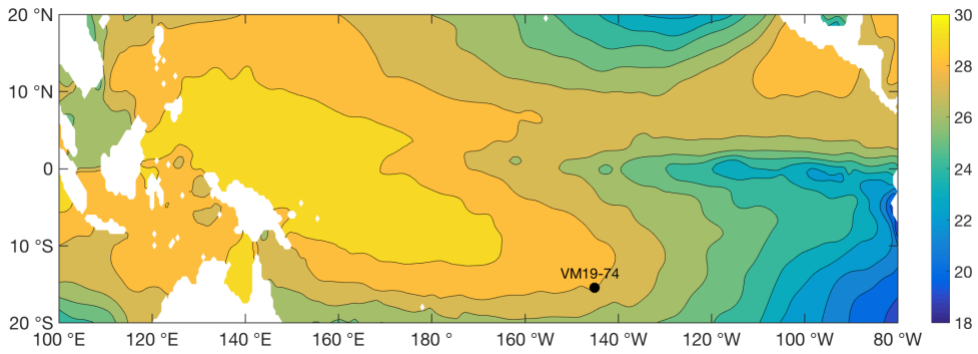

Figure 4 Map of VM19-74 location (15.6 °N, 140 °W, 1525 m water depth). Basemap if mean annual SST from Schmidtko et al., (2013).

VM19-74 oxygen isotope data were generated for both *Globigerinoides ruber* and *Trilobatus sacculifer*. 10 *G. ruber* and 8 *T. sacculifer* individuals were picked from the 250-355 μm size fraction for analysis. Mg/Ca data were generated on *G. ruber* in two labs. First, samples at Lamont (LDEO) were cleaned using the oxidative only cleaning method. The second set of samples were cleaned at Texas A&M University (TAMU) using both oxidative and reductive cleaning steps. Mg/Ca analyses were performed on a Jobin-Yvon inductively coupled plasma atomic emission spectrophotometer (ICP-AES) at LDEO and an Element 2 ICP-MS at Texas A&M University, respectively. Mg/Ca values are converted to SST using the Dekens et al., (2002) calibration with bottom water ΔCO_3^{2-}correction to account for dissolution. Data cleaned at Lamont are corrected to account for the discrepancy in cleaning methods, as it has been shown that the reductive step lowers Mg/Ca by ~10% as compared to cleaning with the oxidative only reagent (e.g. Barker et al., 2003). When the oxidative-only data are corrected by a 10% reduction in Mg/Ca, the two dataset are in agreement (Figure 6). The age model for this site is based on 4 radiocarbon measurements from the NOSAMS Lab at Woods Hole, calibrated to calendar age using the CALIB 7.1 Marine13 curve with standard reservoir correction (Reimer et al., 2009).

2.3 Results

Radiocarbon measurements indicate a core-top age of 4,260 calendar years before present. 3 additional radiocarbon samples at 30.5, 80.5 and 180.5 cm constrain the Last Glacial Maximum to 30.5-40.5 cm depth. Isotope stratigraphies indicate a hiatus below 80.5 cm depth (~26.3 ka based on interpolated radiocarbon dates), where $\delta^{18}O$ data show a steep enrichment, and data below this suspected hiatus are not presented. Isotope and trace element measurements were generated in 5 cm intervals, yielding an average resolution 2,870 years during the Holocene and 600 years during the LGM. Core-top, mid-Holocene calculated SST is 27.7 °C, in good agreement with 28.0 °C mean annual SST in modern climatology (Schmidtko et al., 2013). Calculated SSTs range from 27.4 -28.5 °C through the upper 60.5 cm (25.1 ka) of VM19-74. Most notably, LGM (19-23 ka) calculated SSTs (28.2 °C) remain as warm as the Mid Holocene (4-8 ka, 27.9 °C) at this site. SST data at this site indicate no glacial cooling or significant temperature trend through Marine Isotope Stages 1 and 2. Conversely, *G. ruber* $\delta^{18}O$ measurements show a 1.37 ‰ increase between the Mid Holocene and LGM. Accounting for a 1.05 ‰ whole ocean $\delta^{18}O$ increase during the LGM (Adkins & Schrag, 2001) and the lack of temperature change from Mg/Ca, the 0.32 ‰ residual $\delta^{18}O$ calcite signal suggests an additional ~0.3 psu glacial salinity increase at this site, which is characterized by 36.2 psu mean annual SSS today. If, instead, we consider that the Mg/Ca data indicating no SST change are incorrect, the 0.32 ‰ $\delta^{18}O$ signal could, at most, account for approximately 1.5 °C cooling during the LGM. The nearest available grid cells in the MARGO compilation, 12.5-17.5 °S, 147.5- 143.5 °W do not have reconstructed LGM SSTs due to the lack of nearby proxy

records. More broadly, VM19-74 sits approximately 5 °SE of an area of reconstructed cooling (1-2 °C) but west of an area of projected warming (0-1 °C).

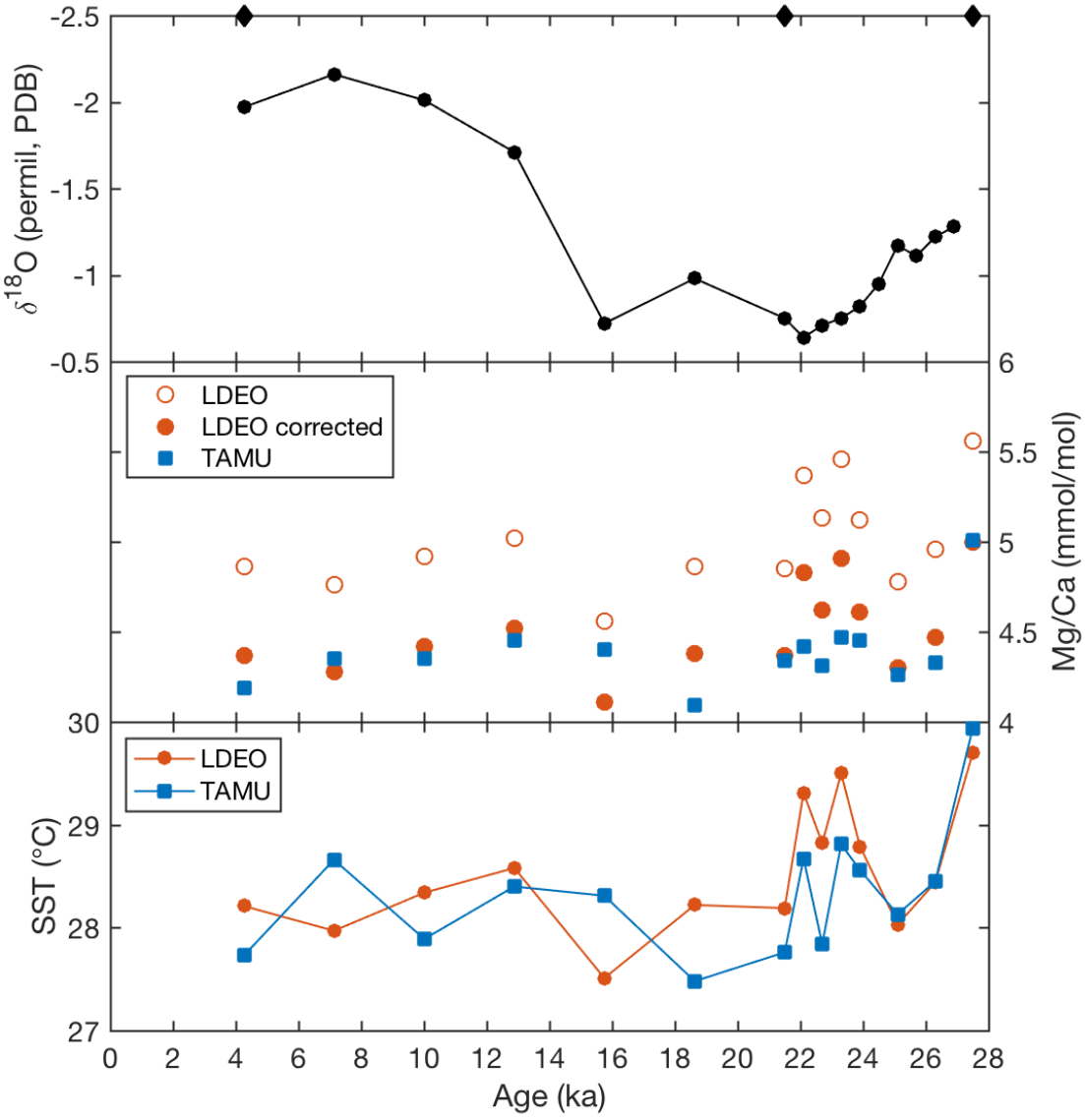

Figure 5 VM19-74 *G. ruber* $\delta^{18}O$ data (top) with radiocarbon age dates denoted (diamond symbols). Mg/Ca data (middle) from LDEO (open orange symbols) and TAMU (blue symbols). LDEO samples cleaned with the oxidative-only procedure are corrected by 10% (filled orange markers) to account for Mg loss during the more rigorous reductive cleaning method. SST records (bottom) from TAMU data (blue) and corrected LDEO data (orange). SSTs are converted to SST using Dekens et al., (2002). Age models developed from linearly interpolating radiocarbon age dates.

2.4 Discussion

Previous work on *G. ruber* Mg/Ca has shown that the magnitude of Late Holocene to LGM SST change in the equatorial (15 °N-15 °S) Pacific was ~2.4 °C (Monteagudo et al., 2021 and references therein), which is also supported by coupled ocean-atmosphere model output (e.g. Brady et al., 2013; Otto-Bleisner et al., 2009). Other available geochemical proxies -- alkenones, TEX86 and clumped isotopes, throughout the tropical ocean also show similar magnitude (~2.7 °C) of glacial cooling (e.g. Tierney et al., 2020). Assuming VM19-74 SSTs remained unchanged during the LGM, the ice volume corrected $\delta^{18}O$ signal implies a 0.3 psu increase in sea surface salinity, inconsistent with Earth System Models like the IPSL-CM5A-MR that suggest a ~0.3 psu LGM salinity decrease (Gray and Evans, 2019).

While we initially assumed VM19-74 Mg/Ca to record a climate signal, it is also possible that sedimentological or geochemical processes may have altered the Mg content in our samples. We can rule out bioturbation as an explanation for VM19-74 Mg/Ca data, since oxygen isotope analyses show a clear 1.37 ‰ glacial enrichment. There are, however, several processes that may only alter Mg/Ca while leaving $\delta^{18}O$ relatively unaffected, which we explore next. High Mg calcite coatings have been shown to form on the inner chamber walls of *G. ruber* in high salinity environments, such as the Mediterranean Sea, which ranges from 36-40 psu (Ferguson et al., 2008). Notably, these high Mg coatings account for ~10 % of shell Mg by weight and were only visible via Scanning Electron Microscopy (SEM), not light microscopy used to pick foraminifera for trace element analysis (Sexton et al., 2006). No SEM analyses have been performed on VM19-74 samples, so we cannot evaluate for the presence of high Mg overgrowths. However, while

sea surface salinity at VM19-74 (36.2 psu) is similar to the Mediterranean, salinity at 1500 meters is only 34.6 psu. 34-35 psu is typical of the deep Pacific, where *G. ruber* shells have been recovered for Mg/Ca studies, showing ~2.5 °C glacial cooling using the same calibration applied here. In the Mediterranean transect from Ferguson et al., (2008), bottom water salinity remains high at depth. Thus, while no SEM imagery has been conducted on VM19-74 samples, it does not appear likely that high Mg overgrowths would formed on these samples.

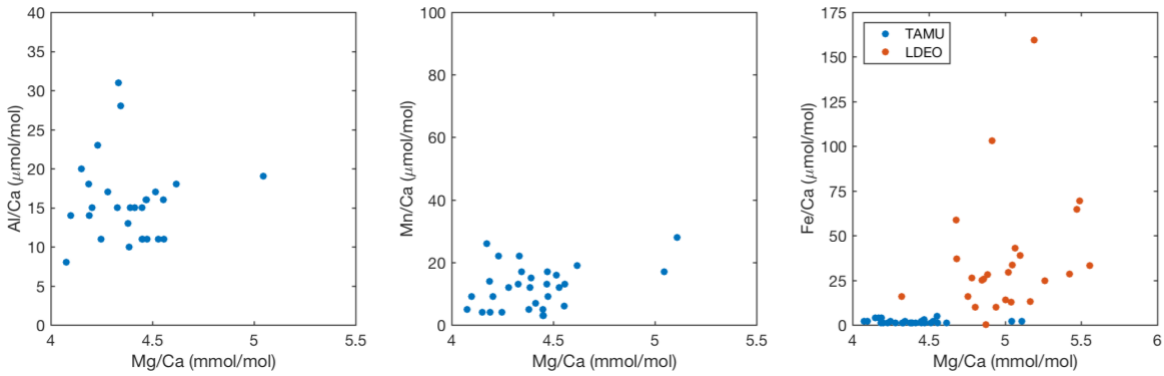

Figure 6 Al/Ca (left), Mn/Ca (middle), and Fe/Ca (right) ratios of VM19-74 samples. All trace element data are available for TAMU samples (blue symbols), compared to Fe/Al only for LDEO samples (orange symbols).

Several other trace metals are analyzed at the same time as Mg, and can be used as indicators of cleaning efficacy or diagenetic alteration. Al/Ca and Fe/Ca ratios may be elevated if aluminosilicate clays remain on a sample after cleaning (Barker et al., 2003; Lea et al., 2005). Thresholds of 175 μmol/mol and 40 μmol/mol for Fe/Ca and Al/Ca, respectively, have been used previously (Lea et al., 2005) to exclude data due to incomplete cleaning. High Mn/Ca ratios are also possible in samples affected by iron-manganese overgrowths. For VM19-74 samples analyzed at LDEO using the less intensive oxidative-

only cleaning method, Fe/Ca ratios range from 13-159 μmol/mol, averaging 37.3 ± 34 (mean ± 1 sigma standard deviation). TAMU samples yield lower Fe/Ca ratios of 3-28 μmol/mol (mean = 12 ± 7) due to the more rigorous reductive cleaning methods. However, data from both labs fall well beneath the 175 μmol/mol threshold used in a previous study from the Eastern Equatorial Pacific (Lea et al., 2005). Al/Ca ratios are generally low for TAMU data (8-31 μmol/mol) with only 1 datapoint exceeding the 40 μmol/mol threshold used by Lea et al., (2005). Al/Ca data from LDEO is not available. Incomplete cleaning is unlikely to explain observed trends in Mg/Ca data, since values are generally low and no relationship exists between Al/Ca and Mg/Ca (Figure 6a). Mn/Ca data is only available for TAMU data but is generally low, from 1-5 μmol/mol. All samples fall well below the 100 μmol/mol threshold generally regarded as the upper limit for data uncontaminated by Mn-rich overgrowths (Boyle, 1983).

A study from the Eastern Equatorial Pacific showed elevated Mg/Ca values due to input from high volcanic activity nearby (Lea et al., 2005), which is not the case at VM19-74. High Mg/Ca data at this site were also accompanied by elevated Al/Ca and Mn/Ca ratios unlike at our location. It has also been suggested that in regions with high organic matter deposition, pore water redox when organic matter is consumed may lead to the mobilization of elements from the sediment which then adhere to the foraminiferal test (Boyle, 1983). Again, if this were the explanation for VM19-74, we would also expect to see high Mn values which we do not.

It has been shown that non-thermal influences affect the Mg/Ca of *G. ruber*, which, if unaccounted for, will lead to erroneous calculated SSTs. Such influences can be divided into two categories: 1) post-depositional dissolution and 2) surface ocean influences as the

foraminifera calcifies, namely salinity and carbonate chemistry (expressed as either pH or $[CO_3^{2-}]$). The calibration we use to convert Mg/Ca to SST accounts for post-depositional dissolution based on estimates of the past bottom water ΔCO_3^{2-} change. However, changes Pacific deepwater ΔCO_3^{2-} from the Holocene to the LGM are generally believe to be small (~5-10 μmol/kg) (Yu et al., 2013) and affect all sites. Thus, bottom water dissolution does not explain the VM19-74 temperature trend. Our calibration does not account for the possible influence of surface ocean pH or salinity which have been shown to affect Mg/Ca ratios as the foraminfera calcifies. During the LGM, it has been shown that whole ocean salinity increased by ~1 psu (Adkins & Schrag, 2001). Estimates of the salinity sensitivity of *G. ruber* Mg/Ca generally converge on ~4% mmol/mol change in Mg/Ca per psu salinity (Gray and Evans, 2019). Thus, increased salinity during the LGM would have increased glacial Mg/Ca values; since the Dekens calibration does not account for salinity, glacial Mg/Ca values would be higher than they would be from temperature alone, reducing the apparent magnitude of glacial cooling if salinity changes are not accounted for. Gray and Evans (2019) argue that *G. ruber* shows a sensitivity to surface pH, not $[CO_3^{2-}]$, which we consider next. pH is negatively related to Mg/Ca, with estimates generally between -5 to -9% mmol/mol change in Mg/Ca per unit pH change. The estimated surface glacial ocean pH increase of ~0.12 units would have lowered glacial Mg/Ca values; since the Dekens calibration does not account for surface pH, glacial Mg/Ca values would be lower than they would be from temperature alone, increasing the apparent magnitude of glacial cooling if pH changes are not accounted for. Taken together, changes to surface salinity and pH during the LGM would in part cancel each other out, resulting in a Mg/Ca bias of less than

0.5 °C in this region (Gray and Evans, 2019), in contrast with the ~1.5 °C cooling suggested by ice volume corrected $\delta^{18}O_c$.

We have also attempted to generate another Mg/Ca record in the southeast tropical Pacific to compare with VM19-74. RC11-34TP is located at 14.8 °S, 140.0 °W, 2950 meters water depth. While foraminiferal preservation throughout the 40 cm multicore is generally good, oxygen isotope analyses suggest that sediments have been disturbed and is not suitable for further use. $\delta^{18}O$ values range from -1.8 to -1.2 ‰, but do not show the expected glacial enrichment necessary to continue working on this material (Figure 7).

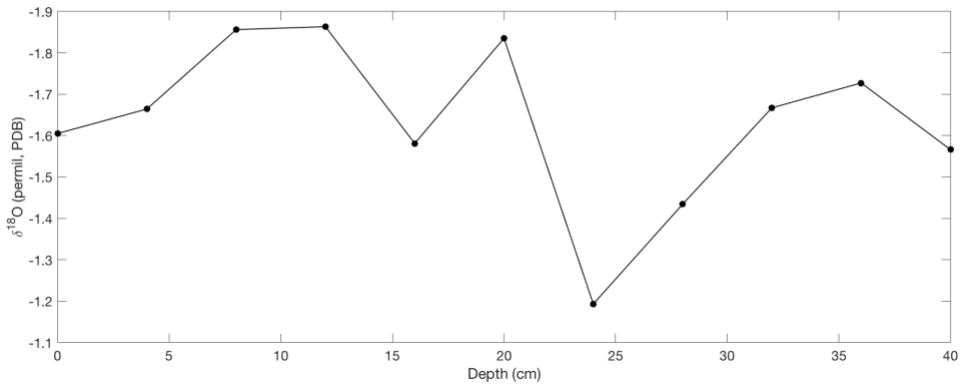

Figure 7 RC11-34TP *G. ruber* $\delta^{18}O$ data. Note the lack of deglacial enrichment.

2.5 Conclusions

The southeastern tropical Pacific is a region of significant uncertainty in global compilations of LGM ocean temperature. In this study we attempted to fill the data gap by presenting a new Mg/Ca record from VM19-74, which showed no glacial SST change. Using co-occurring trace elements, we explored alternate explanations for our Mg/Ca data but were unable to identify one. Nearby core RC11-34TRI was examined for possible use, but oxygen isotopes revealed evidence of significant sediment disturbance. Recovering

good quality marine sediment cores from the open ocean Pacific is difficult, but would greatly improve our understating of the glacial surface ocean.

CHAPTER 3. LAST INTERGLACIAL SEA SURFACE TEMPERATURES IN THE CENTRAL EQUATORIAL PACIFIC

3.1 Introduction

Understanding the magnitude of tropical sea surface temperature (SST) change in response to elevated CO_2 levels is an area of ongoing focus for future climate change. One method used to better constrain the relationship between temperature and CO_2 is to reconstruct past temperature during intervals of varying CO_2. Over the last 800,000 years, during which atmospheric CO_2 records are available from ice cores, it is then possible to link SST change to CO_2 more precisely. Marine Isotope Stage (MIS) 5, ~115-130 ka, also known as the Last Interglacial (LIG) is the most recent interglacial period before the Holocene. While Stage 5 atmospheric CO_2 levels were similar to the Pre Industrial (PI), there is evidence for sea level being as much as 6-9 meters higher than modern (Hearty et al., 2007; Kopp et al., 2009). Proxy reconstructions suggest that MIS 5 global mean surface sea surface temperatures (SSTs) peaked anywhere from 0 to 2 °C warmer than the Pre Industrial (Turney and Jones, 2010; McKay et al., 2011). For these reasons, MIS 5 has been referred to as a "super interglacial" (Turney and Jones, 2010) and has garnered attention as a possible analogue for future climate change. MIS 5 is also a time period of focus for proxy-model intercomparison. In contrast to proxy records, climate models generally show more modest (~0.5 °C) warming relative to the PI (Otto-Bliesner et al., 2021). This proxy-model disagreement has important implications for future climate change, as the LIG used to study Equilibrium Climate Sensitivity, the temperature response associated with a doubling of atmospheric CO_2. Warmer LIG temperatures as indicated by some proxy records correspond with larger ECS values, given that LIG and PI atmospheric CO_2 are

similar and the other radiative forcings indicate only a small increase relative to the PI (Friedrich et al., 2016). It has been suggested that because the tropical oceans are far-removed from the direct influence of high latitude ice sheets, they may better reflect an equilibrium climate response to atmospheric CO_2 (Hargreaves et al., 2012) which makes reconstructing tropical SSTs of particular importance.

A number of hypotheses have been suggested to reconcile the proxy-model disagreement and explains peak MIS 5 warming. It has been suggested that temperature proxies are biased towards the warm season, thus leading to erroneously warm temperatures if interpreted as mean annual values (e.g. Bova et al., 2021). Larger seasonal contrasts in temperature result from the other major climate forcing for the Last Interglacial – changes to the amount of incoming solar radiation. On timescales of tens to hundreds of thousands of years, small changes in Earth's orbital configuration changes in the amount of incoming solar radiation (insolation) as a function of time and latitude. Eccentricity, the measure of Earth's elliptic orbit, causes small changes in global mean annual insolation, with dominant periodicities of 100 and 413 ka. Precession alters the seasonal distribution of insolation in the tropics with a periodicity of 23 ka. The effect of precession is also modulated by eccentricity, leading to amplified insolation seasonality when eccentricity is high. Obliquity, the Earth's axial tilt, affects the seasonal contrast in insolation at a given latitude, with highest effect at the high latitudes. In the tropics, seasonal insolation changes over time are due mostly to precession. However, some tropical temperature records show 41 ka cyclicity which may be due to orbital forcing at the mid or high latitudes, which are then translated to the tropics via the thermocline or teleconnections.

Differences between the Holocene and LIG have been explained by higher warm season insolation during MIS 5, since greenhouse gas forcing during both interglacials was relatively similar. Given these constraints, the Last Interglacial is a period of interest for studying the climate system's response to both greenhouse gas (GHG) and insolation-driven forcing. SST reconstructions in the tropical Pacific are sparse in global LIG compilations (Turney & Jones, 2010; McKay et al., 2011) with no geochemical proxy data in the central equatorial Pacific (Hoffman et al., 2017). In this study we present 4 new central equatorial Pacific SST reconstructions based on the Mg/Ca ratio of the planktonic foraminifera *Globigerinoides ruber* over the last 150,000 years. We also compile existing tropical Pacific *G. ruber* Mg/Ca records through MIS 6, and standardize their age models and paleotemperature calibrations in order to create a tropical Pacific SST stack over the last glacial cycle.

3.2 Materials and Methods

3.2.1 Site Description and Age Models

The cores presented in this study (Figure 8) were collected along the Line Islands Ridge in the central equatorial Pacific (Lynch-Stieglitz et al., 2015). These cores span -0.2 to 7 °N, 155-162 °W and 2798-3050 meters water depth. Today, the Line Islands is characterized by a ~1 °C meridional gradient in mean annual SST, as cores north of 2 °N are supplied with warm (~28 °C) waters from the western Pacific by the North Equatorial Counter Current (NECC). Core sites south of 2 °N are ~27 °C due to upwelling along the equator and cool waters from the Eastern Pacific via the South Equatorial Current.

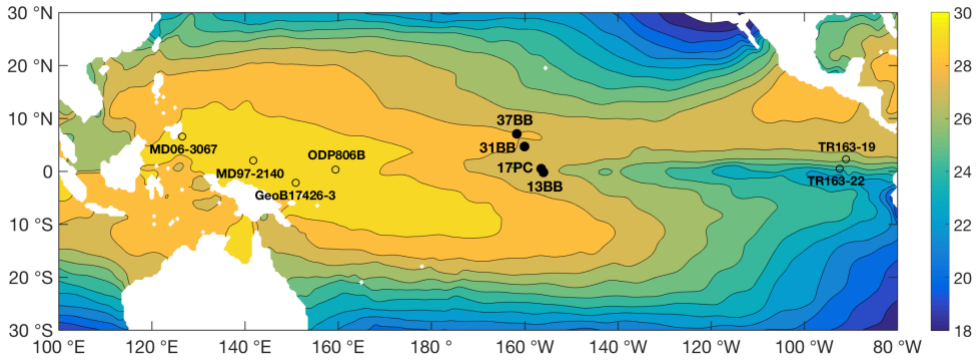

Figure 8 Map of *G. ruber* Mg/Ca records from the Line Islands (0-7 °N, 155-162 °W, solid symbols). Open symbols show the locations of eastern and western Pacific *G. ruber* Mg/Ca records (Bolliet et al., 2011; de-Garidel-Thoron et al., 2005, Lea et al., 2000; Lea et al., 2006; Hollstein et al., 2019). Base map is climatological mean annual sea surface temperature from Schmidtko et al., (2013).

Age models for each core are developed by linearly interpolating between radiocarbon dates originally published in Lynch-Stieglitz et al., (2015) and are shown in Figure 9. Beyond the range of radiocarbon, *G. ruber* $\delta^{18}O$ stratigraphies are aligned to the LR04 benthic stack using the HMM Match algorithm from Lin et al., (2014). The age models developed here are not significantly different than previously developed by Lynch-Stieglitz et al., (2015). Analyses for $\delta^{18}O$ and Mg/Ca were run in 2-4 cm intervals, resulting in an average resolution of ~2.0 kyr during MIS 5 and 6.

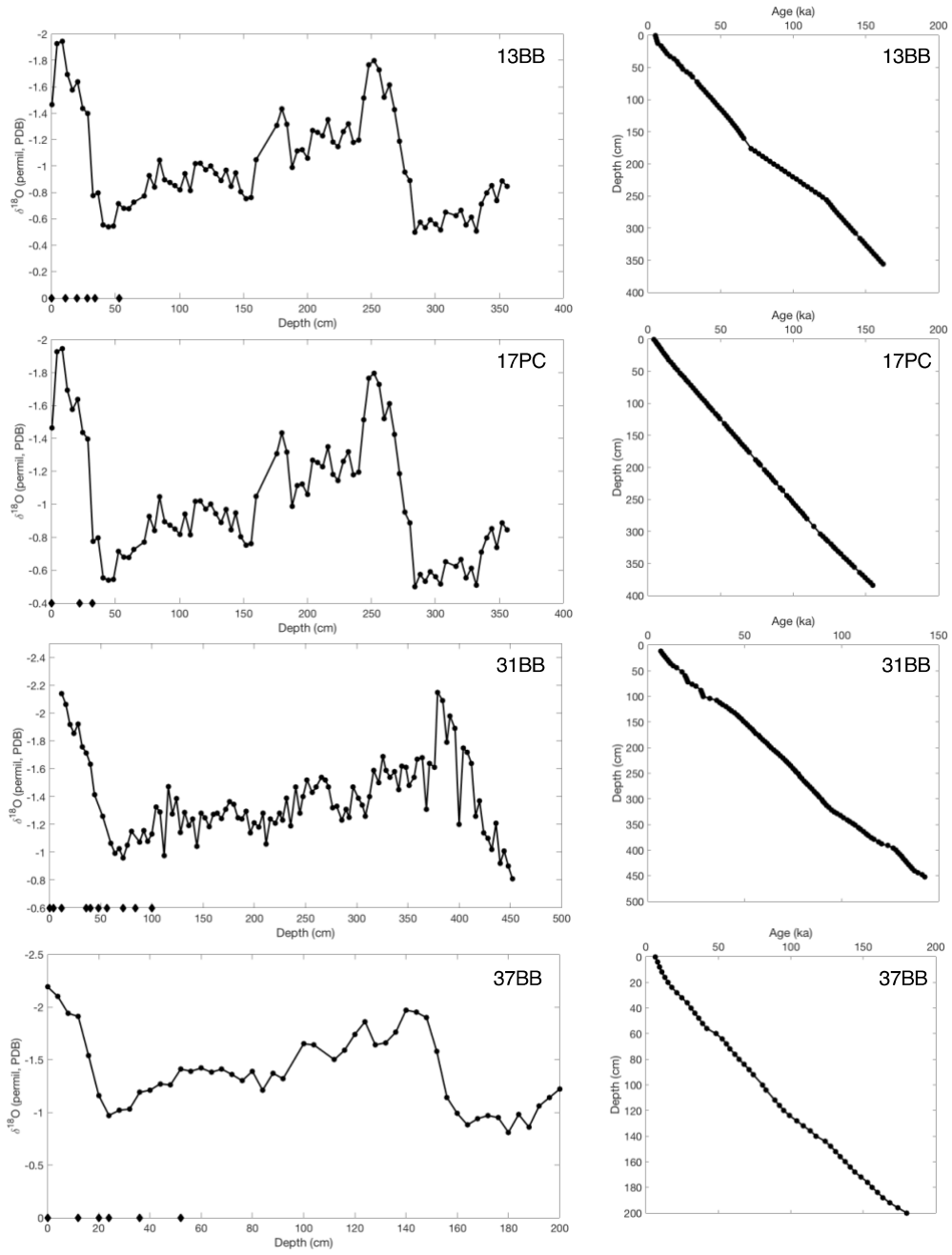

Figure 9 ML1208 Age Models. Left panels show *G. ruber* oxygen isotope stratigraphy (black line) with the depths of radiocarbon age dates shown (diamond symbols). Right panels show age-depth relationships for each core based on interpolated radiocarbon age dates and tuning to LR04 using the HMM Match algorithm (Lin et al., 2014).

3.2.2 Analytical Methods

Holocene and LGM sections of these cores were previously presented in Monteagudo et al., (2021). New Line Islands data presented here were generated using the same methods, summarized as follows: 60 individual *Globigerinoides ruber* were picked from the 250-355 um size fraction, split in 2 aliquots for replicate analysis. Samples were cleaned using both reductive and oxidative steps. Samples from 13BB and 31BB were analyzed on a Thermo Element 2 at University of Colorado, Boulder. Samples from 37BB were analyzed on a Thermo Element 2 at Texas A&M University. 17PC data are from Yuan (2018), and were analyzed on an ICP-OES at UC Santa Cruz.

We apply the Dekens et al., (2002) calibration that converts raw Mg/Ca values to SST using a correction term for post-depositional dissolution as a function of bottom water ΔCO_3^{2-}. Modern bottom water ΔCO_3^{2-} values are calculated using data from nearby World Ocean Circulation Experiment (WOCE) P16N station data and CO_2Sys for Excel version 2.1. Equilibrium constants for carbonic acid, K_1 and K_2, are from Mehrbach et al. (1973) refit by Dickson and Millero (1987) and KSO_4^{2-} from Dickson 1990. Estimates of past bottom water ΔCO_3^{2-} changes are taken from B/Ca based estimates from Western Equatorial Pacific site MW91-9 (0 °N, 158 °E, 2300 km depth) (Yu et al., 2013) and incorporated into the correction term in the SST calibration. These quantitative estimates of Pacific bottom water saturation state over the last 140,000 years are broadly consistent with a compilation of qualitative dissolution proxies from Gwizd and Lea (2021). Bottom water ΔCO_3^{2-} remains similar during the Mid Holocene and LGM (3.9 and 3.1 μmol/kg, respectively). During our Stage 5 and 6 time slices, bottom water ΔCO_3^{2-} is 1.0 and 6.5 μmol/kg, respectively. The minimum in the MW91-9 record (-11 μmol/kg) occurs at 112

ka, along the transition from MIS 4 to MIS 5. Even at 112 ka, when bottom water ΔCO_3^{2-} change is largest, this correction accounts for only ~0.4 °C in the Mg/Ca record, thus our dissolution correction does not explain the larger features we interpret in Section 3.4.

Several calibrations exist for converting *G. ruber* Mg/Ca to temperature and were considered. We did not use the recent multivariate Bayesian BAYMAG calibration (Tierney et al. 2019) because it has been observed that this calibration exaggerates spatial SST gradients by a factor of 1.6, based on a Late Holocene (0-4 ka) coretop *G. ruber* dataset. The Dekens et al., (2002) calibration with carbonate ion correction we use instead only exaggerates SST gradients by 1.05 when applied to that same Late Holocene coretop data (Monteagudo et al., 2021). It has also been shown that non-thermal influences in the surface ocean (*i.e.* salinity and carbonate chemistry, described by either pH or ΔCO_3^{2-} influence *G. ruber* Mg/Ca (*e.g.* Gray et al., 2018) but are often difficult to account for in the past. The largest change in whole ocean salinity during the last glacial cycle is estimated to be 1 psu (during the LGM), even then the glacial salinity temperature bias near the Line Islands is predicted to be ~0.5 °C or less (Gray and Evans, 2019).

3.2.3 Compilation Methods

We also compile tropical Pacific (15 °N- 15 °S) *G. ruber* Mg/Ca records that extend to Marine Isotope Stage 6. All cores used in this compilation are shown in Figure 8. For studies where samples were cleaned with an oxidative only treatment, we apply a 10% reduction in Mg/Ca, as the reductive cleaning step has been shown to reduce Mg/Ca values (*e.g.* Barker et al., 2003) and the Dekens et al., (2002) temperature calibration was developed using the reductive cleaning step. Age models for all sites are developed as described above for Line Islands cores: calibrated calendar ages are taken from the original

publication and linearly interpolated. After the last available calendar age, *G. ruber* $\delta^{18}O$ is aligned to LR04 benthic stack using the HMM Match algorithm from Lin et al., (2014). Where the morphotype of *G. ruber* (white) used was noted, we have included the sensu stricto data as it has been show to calcify higher in the water column (refs), though most studies do not note which morphotype is used, and morphotypes may occupy the same calcification depth based on upper water column conditions. As described in Section 2.3, estimates of bottom water ΔCO_3^{2-} changes are incorporated into the dissolution correction term in the SST calibration, with estimates from Yu et al., (2013). 8 of the 10 cores in our compilation are located between 2.5-3.1 km depth, with the other 2 cores in the Western Equatorial Pacific at 1.3 and 1.6 km depth. Although additional Mg/Ca records from *T. sacculifer* also exist, we have excluded them since there is evidence they add significant amounts of gametogenic calcite at depth (Spero and Lea, 1993; Wycech et al., 2018).

3.3 Results

3.3.1 Line Islands results

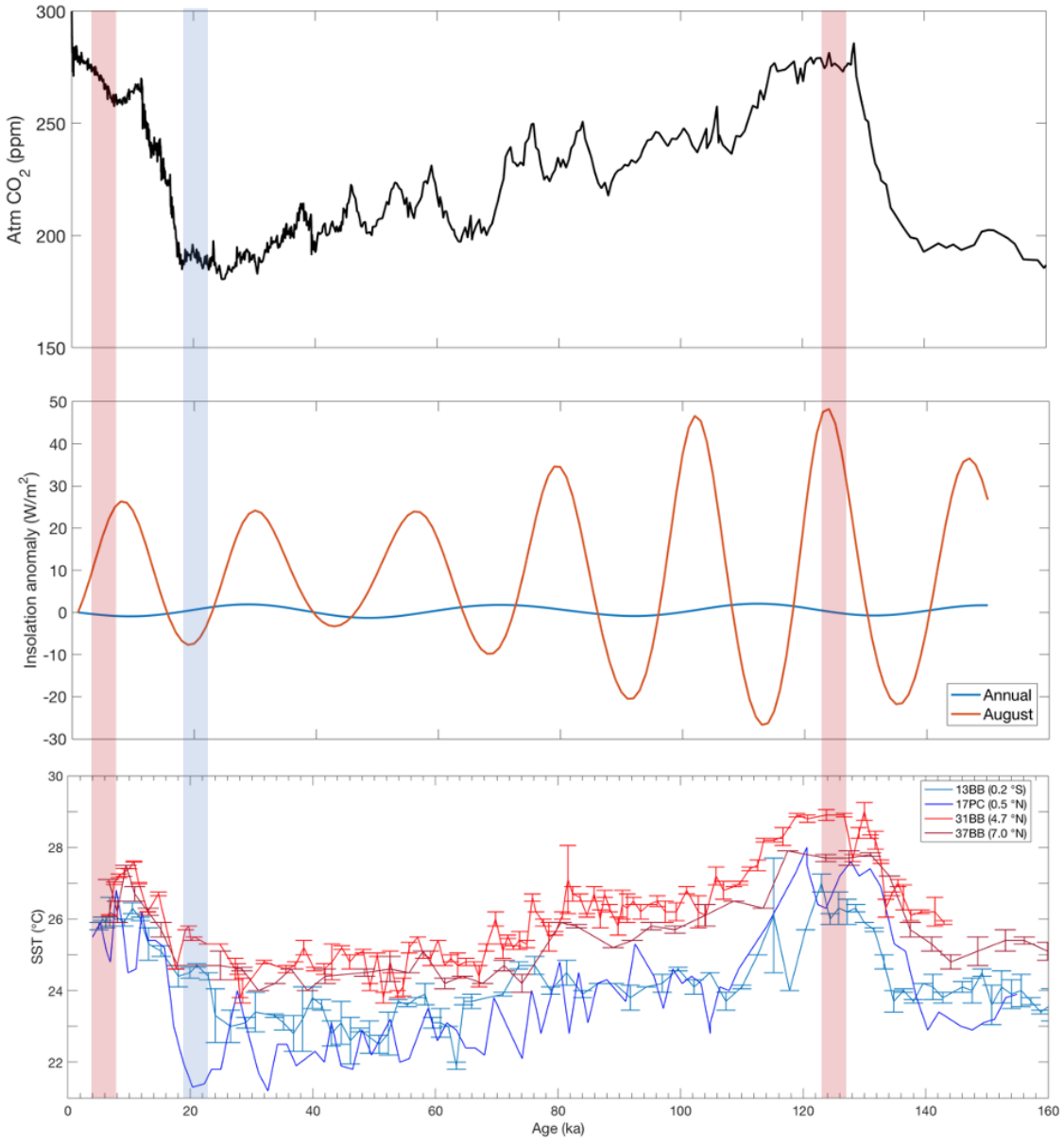

Figure 10 Line Islands SST timeseries. A) Antarctic atmospheric CO_2 record from Lüthi et al., (2008). B) August (orange) and mean annual (blue) insolation changes (relative to modern) at 7 °N, calculated using the Climate Data Toolbox from Greene et al., (2019). C) Line Islands Mg/Ca values converted to SST using the Dekens et al., (2002) calibration with bottom water ΔCO_3^{2-} correction. Error bars show the spread from replicate Mg/Ca measurements. Mid Holocene and LIG time slice intervals and shown with red vertical bars, LGM time slice is shown with blue vertical bars.

Line Islands *G. ruber* Mg/Ca ratios range from 2.37 to 4.48 mmol/mol or ~21.2 to 29.0 °C. The Mid Holocene (4-8 ka) is the most recent time interval for which Mg/Ca are

available at all Line Islands sites and we use it to compare with the LIG. The Mid Holocene is also a focus of proxy-modern intercomparison studies, which allows for comparison of trends in both proxies and model output over the last glacial cycle. Line Islands SSTs range from 27.1-26.0 °C during Mid Holocene compared to 21.3-25.5 °C during the Last Glacial Maximum (Figure 10). SSTs generally peak during Stage 5e near 125 ka and show a cooling trend until around 70 ka, with the exception of site 13BB where Stage 5 cooling 105 ka. Stage 5e SSTs range from 28.9-26.5 °C, warmer than the Mid Holocene at all core sites. The magnitude of peak LIG warming is higher at our highest resolution core locations. In the southern Line Islands region (-0.2 to 0.5 °N), higher resolution core 17PC indicates that Stage 5e was 1.2 °C warmer than the MH, as compared to 0.5 °C at nearby lower resolution core 13BB. Similarly in the Northern Line Islands (4.7-7.0 °N), higher resolution core 31BB shows a 2.3 °C warming (5e-Mid Holocene) as compared to 0.6 °C at lower sedimentation rate site 37BB. During Stage 6 (138-142 ka), Line Islands SSTs are 26.2-23.2 °C. At 3 of our 4 Line Islands sites, Stage 6 SSTs are warmer than the LGM by 0.6-1.9 °C. At Site 13BB, Stage 6 SSTs are 0.5 °C cooler than the LGM. The magnitude of SST change across TI ranges from 1.1 to 4.3 °C in Line Islands. Across TII, there is a more narrow range, from 2.4-3.6 °C. The lower estimates of TI SST change (1.1 and 1.4 °C) come from sites 13BB and 31BB, respectively, which both show cooler SSTs earlier in Stage 2 that miss our LGM (19-23 ka) time slice.

Spatial gradients in tropical Pacific SST change may also elucidate changes to surface currents and atmospheric circulation. Northern Line Islands sites (4.8 to 7.0 °N) are influenced by the North Equatorial Counter Current (NECC), which brings warm waters east from the Western Pacific. Southern Line Islands sites (-0.2 to 0.5 °N)

experience cooler mean annual SSTs as a result of upwelling along the equator and the South Equatorial Current (SEC), which brings cool waters from the Eastern Pacific to these sites. In the modern, the SST gradient between northern and southern Line Islands core sites is ~0.7 °C (Schmidtko et al, 2013). If Pacific Walker Circulation were stronger in the past, we would expect to see an increase in the meridional Line Islands SST gradient due to the strengthened equatorial current systems bringing warm water to our northern sites and cool water to the southern sites, and stronger upwelling along the equator. Conversely, in the case of weaker Walker circulation, we would expect to see a reduction in the meridional Line Islands SST gradient as a result of weaker zonal currents. During the LIG, the meridional SST gradient is 1.7 ± 0.4 °C, increased from the Mid Holocene when it is 1.0 ± 0.1 °C.

3.3.2 Compilation Results

Our compilation includes 10 records from the equatorial Pacific: 4 from the Western Pacific Warm Pool, 2 from the Eastern Pacific Cold Tongue, and our 4 new Line Islands records (Figure 8). All records span through our MIS 6 time slice (142 ka) with the exception of TR163-22 in the Eastern Pacific. In order to compare the magnitude of SST change across Terminations I and II, we define 4 kyr time slices centered on the peak of MIS 5e (123-127 ka) and MIS 6 (138-142 ka) in the LR04 benthic stack for comparison with the Mid Holocene (4-8 ka) and Last Glacial Maximum (19-23 ka). While some cores contain Late Holocene (0-4 ka) sediment, all sites contain at least Mid Holocene sections as the most recent. We create a tropical Pacific Mg/Ca SST stack by averaging our 10 compiled records in 3 kyr, non-overlapping bins between 0 and 142 ka. Our compilation

shows that MIS 5e equatorial Pacific SSTs are 1.2 °C warmer than Mid Holocene (Figure 11). Regionally, we group our compilation into Western Pacific (n=4), Eastern Pacific (n=2), Northern Line Islands (n=2) and Southern Line Islands (n=2). The magnitude of MIS 5e warming is smaller in the Western Pacific Warm Pool 0.9 ± 0.1 as compared to the Eastern Pacific 2.1 ± 0.1 (mean ± 1 sigma standard error). In the Southern Line Islands, MIS 5e is 0.8 ± 0.3 °C warmer than the Mid Holocene, as compared to 1.5 ± 0.8 °C in the Northern Line Islands.

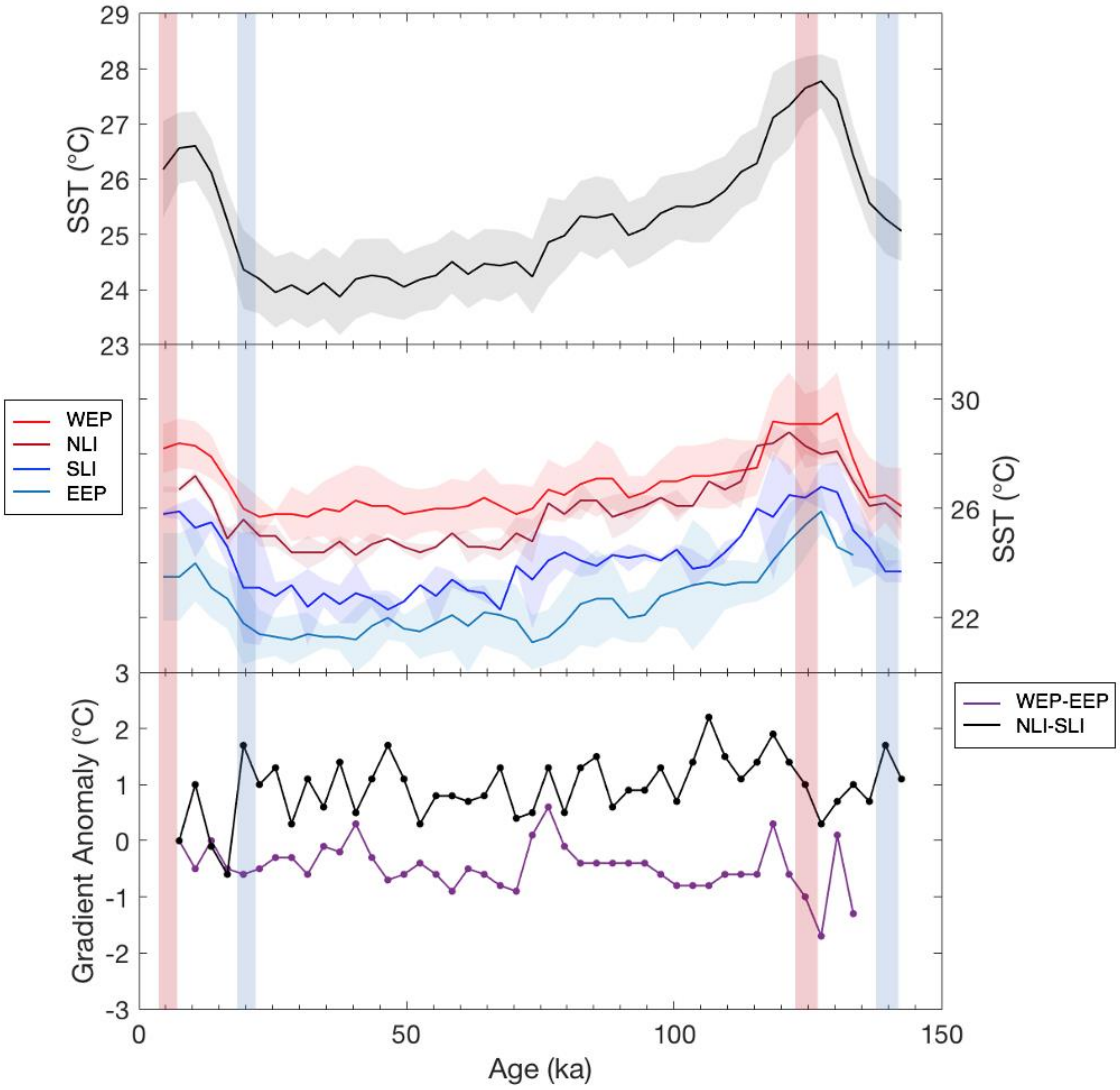

Figure 11 Compilation of equatorial (15 °N - 15 °S) Pacific Mg/Ca records. 3 kyr-binned compilation of 10 equatorial records (top). 3 kyr-binned regional averages of

SST from the Western Equatorial Pacific (light red, n=4), Northern Line Islands (dark red, n=2), Southern Line Islands (light blue, n=2) and Eastern Equatorial Pacific (dark blue, n=2) (middle). Shaded curves denote ±1 sigma standard deviation. Computed zonal (WEP-EEP, purple) Pacific and Line Islands meridional (NLI-SLI, black) gradients. Gradients are reported as anomaly from the Mid Holocene where positive values indicate a larger gradient than the Mid Holocene. Mid Holocene and LIG time slice intervals denoted by red vertical bars. LGM and Stage 6 time slices shown by blue vertical bars.

Spatial temperature gradients between different equatorial Pacific regions may also elucidate changes to atmospheric circulation (*i.e* Walker Circulation). Throughout our record, the meridional SST gradient between Northern and Southern Line Islands sites varies from 0 to 2 °C larger than modern. This gradient shows peaks during the LGM (19.5 ka), Late Stage 2 (46.5 ka), Stage 5c (106.5 ka) and just before Stage 5e (118.5 ka). During MIS 5e, the Line Islands meridional SST gradient is 1.7 °C , larger than 1.0 °C during the Mid Holocene, driven by the larger magnitude of LIG warming at the already warmer Northern Line Islands sites. Zonally, the Western-Eastern equatorial Pacific SST gradient is 0.8 °C smaller during MIS 5e. A smaller tropical Pacific zonal SST gradient should reflect weakened Walker Circulation, the opposite implication of larger Line Islands meridional However, given the scatter of the records and the lack of clear glacial-to-interglacial signal in the computed gradients (Figure 11) it remains unclear what mechanism is driving this variability. A student's t test shows that the magnitude of LIG warming in the WEP is significantly different than the EEP ($p<0.05$), however, the meridional LIG temperature gradient is not ($p=0.3$). It has also been shown in models that changes to Pacific Walker Circulation will be more clearly reflected in the thermocline temperatures than at the surface (DiNezio et al., 2011).

3.4 Discussion

3.4.1 Stage 5 (Last Interglacial)

During MIS 5e (123-127 ka), eccentricity and obliquity are higher than during the Mid Holocene, leading to changes in mean annual and seasonal insolation. Obliquity at 125 ka was larger than modern (23.8 ° compared to 23.4 °), which caused higher insolation at the high latitudes in both hemispheres, and slightly lower insolation in the tropics. Eccentricity was also higher at 125 ka (0.040 compared to 0.017). At the high latitudes, higher LIG seasonal insolation during is driven by higher obliquity, whereas in the tropics, higher seasonal insolation contrasts are mostly driven by precession, which is, in turn, modulated by eccentricity. At the equator, mean annual insolation at 125 ka was barely higher than modern (~2 W/m^2) due to eccentricity, but seasonal insolation peaked at nearly 55 W/m^2 higher than modern during summer (June) and 50 W/m^2 lower during winter (February) (Otto-Bleisner et al., 2013).

In previous tropical Pacific cores where a warmer MIS 5 has been observed, several mechanisms have been invoked to explain the observation, these include: warming of equatorial thermocline source waters, changes in the position of the Intertropical Convergence Zone (ITCZ) and/or changes to the El Niño Southern Oscillation. Spectral analysis of late Pleistocene SST records has shown variability at not only 100 kyr, but also 41 and 23 kyr, which supports a larger role for insolation in tropical Pacific SSTs (Lea et al., 2000; Dyez and Ravelo 2013, 2014). A multivariate model found that the best fit to the observed Eastern Pacific (TR163-19) data includes GHG forcing, July 65 °N insolation lagged 2 kyr as an ice volume proxy and local (7 °N) fall insolation. Though it should be noted that even then, modeled MIS 5e SSTs do not fully capture the peak warming

observed in tropical Pacific records. The inclusion of boreal fall insolation reflects the influence of ITCZ migration on tropical SST patterns. In the modern climate, the ITCZ migrates north during boreal summer and autumn due to increased warming in the Northern Hemisphere. These changes in seasonal ITCZ position are largest in the in the Eastern Pacific, where a more northerly (summer/fall) position is also linked to stronger trade winds and enhanced upwelling. Since summer insolation is as much as 55 W/m^2 higher during the LIG, it has been suggested that enhanced EEP cooling may result from local insolation changes causing the ITCZ to retain its more northerly position. Our compilation does not show strong evidence for this mechanism. LIG warming is larger in the Eastern Pacific than the West, which, all else equal, is in inconsistent with enhanced upwelling bringing cool waters to the surface in the EEP. Although it has been suggested that during the LIG upwelled waters were warmed at their source, it remains difficult to test this hypothesis due to the lack of extra tropical SST records. Evidence for LIG ITCZ position from the Line Islands remains unclear from available dust flux records (Jacobel et al., 2016).

We also compile equatorial (15 °N-S) Pacific alkenone ($U_{37}^{k\prime}$) records to compare with Mg/Ca. Alkenone-based SSTs are taken from their original publications, based on age models and calibrations. Available $U_{37}^{k\prime}$ records (n=5) also show Stage 5 SSTs that are 0.8-1.9 °C warmer than the Mid-Holocene (Pelejero et al., 1999; Liu & Herbert, 2004; Rincón-Martínez et al., 2010), further supporting that a warm tropical Pacific Stage 5 is not an artefact of the Mg/Ca proxy. It should be noted that Western Pacific Warm Pool SSTs (>27 °C) exist at or exceeding the upper limit of the $U_{37}^{k\prime}$ calibration range, and thus carry a larger uncertainty as the alkenone proxy may not work well above 27 °C (e.g. Prahl et al., 1988).

Even so, looking only at the two available Eastern Pacific Cold Tongue records that are well within the reliable range of the $U_{37}^{k'}$ proxy range, MIS 5e SSTs are 1.7-1.9 °C warmer than the Mid Holocene. The global compilations of LIG SSTs that are used to validate climate model experiments for the LIG however, are based largely on microfossil assemblages and fewer geochemical records. One such compilation noted that $U_{37}^{k'}$ records during MIS 5 are warmer than Mg/Ca, which they suggest may reflect a strong warm season bias (Hoffman et al., 2017). Looking at this compilation more closely, microfossils generally show more moderate tropical cooling than Mg/Ca and $U_{37}^{k'}$. In the equatorial Pacific, the two available microfossil records in the Hoffman et al., (2017) compilation suggest the LIG was 1.3 and 1.7 °C cooler than coretop (presumed Holocene) SSTs, in sharp contrast to Mg/Ca and $U_{37}^{k'}$which both suggest 1.2-1.3 °C warming. Since over half of the records used in the Hoffman compilation come from microfossil assemblages, the magnitude of LIG cooling overall is dampened which may explain why these compilations more closely match model results. Additional evidence for LIG tropical warming also comes from terrestrial temperature proxies, which indicate 0.71 °C higher temperatures in the 30 °N to 30 °S band (Otto-Bleisner et al., 2013).

In contrast to geochemical proxy records, climate models generally show LIG tropical SSTs that are very similar to the Mid Holocene. The PMIP4/CMIP6 multi-model mean shows -0.01 ± 0.28 °C (mean ± 1 standard deviation) surface ocean temperature change during lig127k experiments, with individual models ranging from -0.44 to 0.49 °C (Otto-Bliesner et al., 2021). The PMIP4/CMIP6 mean annual cooling signal is driven by ~1-2 °C winter (DJF) cooling and mixed sign summer (JJA) trend – ~0.5 °C cooling over much of the southeastern and central Pacific, and ~1 °C warming over the western and

northeastern equatorial Pacific. While microfossil estimates agree with model output, our Mg/Ca data and available tropical $U_{37}^{k'}$ records show a larger LIG warming signal that does not agree with model output. In this study we have attempted use the most similar records – the same proxy in the same species -- to reduce the amount of inter-proxy noise in estimating LIG temperature. The disadvantage of our approach is that it limits the number of core sites available for comparison. However, if microfossil assemblages struggle to capture peak LIG warming, our work lends support for generating new geochemical reconstructions of LIG temperature.

Towards resolving this proxy-model disagreement, is has been suggested that seasonal bias in Mg/Ca and alkenone records combined with higher seasonal insolation may explain the apparent peak LIG warming. Proxy records generally peak during MIS 5e when seasonal insolation is highest, whereas models tend to show near-constant SST throughout Stage 5, more closely resembling CO_2 and mean annual insolation. Looking at our 3 kyr binned regional and tropical Pacific stacks, we see an increasing trend from 115.5-127.5 ka, consistent with previous studies, until SSTs peak ~1.2 °C warmer than the Mid Holocene. The Bova et al., (2021) compilation shows that both proxy and CCSM3 output suggest the magnitude of seasonal SST bias driven by LIG insolation is ~1 °C at its peak near 124 ka. For this seasonal bias to be a full explanation of the LIG proxy SST trend would require the foraminifera flux to the sediment to be almost completely warm season individuals. Any contribution of non-warm season foraminifera would act to reduce peak LIG warming, so 1 °C appears to be the upper limit of possible seasonal influence. It should be noted that numerical models show that seasonal insolation changes may generate a mean annual temperature response in the tropical Pacific due to changes in ENSO, despite near-

constant mean annual insolation (Clement et al., 1999). So while seasonal bias in the proxy records may explain some of the 1.2 °C peak LIG warming, there is also evidence that seasonal insolation changes in this region can result in mean annual temperature changes as well.

3.4.2 Potential Dissolution Bias

The calibration we use to convert Mg/Ca to SST (Dekens et al., 2002) also includes a term for bottom water ΔCO_3^{2-} to account for potential dissolution. To account for past changes in bottom water ΔCO_3^{2-} quantitatively, we use B/Ca-based estimates from Yu et al (2013). Less preserving conditions (lower ΔCO_3^{2-}) than modern during Stages 5 and 6 from Yu et al (2013) B/Ca is also consistent with more qualitative dissolution proxies in the tropical Pacific. Gwizd and Lea (2020) showed that the percent coarse fraction (%CF) during our Stage 5e timeslice (123-127 ka) was lower than the Holocene in both the eastern and western equatorial Pacific. Since low ΔCO_3^{2-} reduces Mg/Ca ratios and Stage 5 ΔCO_3^{2-} was lower than modern, the dissolution correction does not explain why Stage 5e Mg/Ca and SSTs are higher than Mid Holocene.

3.4.3 Stage 6 (Penultimate Glacial Maximum)

Though not as well studied as the LGM and LIG, our data also extend to the Penultimate Glacial Maximum (PGM, Marine Isotope Stage 6). We have used the isotopic maximum at 140 ka in the LR04 benthic stack to establish a timeslice for the PGM, consistent with other literature which places the PGM near 140 ka (e.g. Colleoni et al., 2016; Wekerle et al., 2016). Climate conditions during the PGM are more poorly constrained than the LGM. Sea level recontructions range from 92-150 meters, averaging

near 120 meters of sea level drop during the PGM (Rabineau et al., 2006; Lambeck et al., 2001). While ice volume is generally thought to be similar to the LGM, geological evidence for a PGM Laurentide Ice Sheet was destroyed by LGM glaciation (Dyke et al., 2002) and there is evidence that the Eurasian Ice Sheet may have been as much as double its LGM size (Svendsen et al., 2004). During this timeslice (138-142 ka) atmospheric CO_2 was 196 ppm (compared to 189 ppm during the 19-23 ka LGM timeslice). At the Line Islands, Stage 6 SSTs range from 0.5 cooler to 1.9 °C warmer than the LGM, with no latitudinal trend. For the 1 EEP site with MIS 6 Mg/Ca data, it is 0.2 °C cooler than MIS 2. In the Western Pacific, PGM SSTs were 0.6-1.4 °C warmer than the LGM. A warmer tropical Pacific PGM than LGM is also seen in alkenone records which range from 0.6-1.6 °C (PGM-LGM). Stage 6 results from the Line Islands are consistent with model output showing a slightly warmer tropics during the PGM than LGM (Colleoni et al., 2016).

3.5 Conclusions

Here we have presented 4 new central equatorial Pacific sea surface temperature records that span the last ~140,000 years. We show that as reported in other tropical Pacific Mg/Ca records, all 4 Line Islands sites record peak warmth during MIS 5 that exceeds that of the Mid Holocene by 0.5-2.3 °C. In the tropical Pacific overall, our Mg/Ca compilation shows 1.2 °C warmer LIG than the Mid Holocene, which is also supported by alkenones that show 1.3 °C warmer LIG in tropical Pacific. While warm season bias in both Mg/Ca and $U_{37}^{k'}$ has been invoked to explain as much as 1 °C of peak LIG warmth, seasonal proxy bias is unlikely to fully explain our results.

The magnitude of LIG SST change also has important implications for ECS estimates. Our tropical Pacific Mg/Ca compilation shows 2.4 °C SST change across TI and

2.9 °C across TII, both in response to an 82 ppm change in atmospheric CO_2. Taken at face value, the larger magnitude of SST change across TII would support a larger ECS, however, it is not clear what component of the temperature change may be driven by non-CO_2 (i.e. orbital) forcing or seasonal proxy bias. Studies that use the warm LIG SSTs to constrain climate sensitivity result in larger ECS estimates than the CMIP5 multimodel mean (Friedrich et al., 2016) . Though there is evidence that climate sensitivity is larger in a warmer mean state (*e.g.* Knütti et al., 2017), it is still important to disentangle the components of LIG warming forced by CO_2 and insolation.

Our data also show that within global proxy compilations, there is a discrepancy between geochemical and microfossil reconstructions of tropical LIG SSTs – with Mg/Ca and alkenones showing a larger magnitude LIG warming than microfossil records. This finding underscores the importance of generating new geochemical SST records and conducting inter-proxy comparisons.

CHAPTER 4. IMPLICATIONS OF CMIP6 AND SUGGESTIONS FOR FUTURE RESEARCH

4.1 CMIP6 Equilibrium Climate Sensitivity

Since the publication of Chapter 1, newer estimates of Equilibrium Climate Sensitivity from PMIP4/CMIP6 ensemble members have become available. While the likely range of ECS remained fairly constant at ~2-4.5 K from the IPCC Second Assessment Report (CMIP1) in 2001 until the Fifth Assessment Report (CMIP5) in 2013, ECS estimates from CMIP6 used in the Sixth Assessment Report in 2021 increased to ~2-5.5 K (Meehl et al., 2020). Out of 52 CMIP6 models analyzed, 16 produced an ECS greater than 4.5 K, which has largely been attributed to strong shortwave cloud feedbacks (Zelinka et al., 2020). High ECS models, like the CESM2, also overestimate LGM cooling when run under glacial boundary conditions. The CESM2 produces 11 and 7 °C of global and tropical LGM cooling, respectively (Zhu et al., 2021). In contrast, our Mg/Ca compilation suggests only 2.6 °C of tropical cooling. Our results, as well as other LGM proxy syntheses, suggest that models such as the CESM2 simulate an unrealistic magnitude of LGM cooling, and thus ECS estimates from these models are likely overestimates (Zhu et al., 2021). This observation shows that proxy reconstructions of the LGM continue to serve as important constraints on model-based ECS estimates.

Additionally, a new multi-proxy data assimilation study for the LGM was also published recently and used in IPCC's The Sixth Assessment Report (AR6). This compilation included geochemical proxy records but did not include our Line Islands data as the two studies were in publication at the same time. In the Tierney et al., (2020) data

assimilation study, geochemical records from the tropical Pacific are once again concentrated along the eastern and western margins like CLIMAP and MARGO. In the Tierney data assimilation, the Line Islands are estimated to have cooled by 3.9 °C, almost double the 2.0 °C suggested by Chapter 1. Overall, in the equatorial band (15 °N-15 °S), this LGM data assimilation estimates 3.4 °C cooling, as compared to 2.6 °C by *G. ruber* Mg/Ca in Chapter 1. Our Mg/Ca data show more modest cooling at both the Line Islands and global equatorial band than the Tierney data assimilation.

AR6 also includes information on our current understanding of the Last Interglacial (LIG) Period. While the Multi-model mean of CMIP6 models showed `-0.01 ± 0.28 °C (mean ± 1 standard deviation) ocean surface temperature change (Otto-Bliesner et al., 2021), AR6 states that proxy-based estimates of global LIG temperature change are 0.5-1.5 °C warmer than the 1850-1900 baseline (medium confidence) (IPCC, 2021). AR6 also states that there is now high confidence that ECS increases with temperature, suggesting that cool period (e.g. LGM) ECS estimates will be lower than warm periods (LIG). While AR6 provides both proxy and model-based estimates of ECS from the LGM, warm period ECS discussion is generally limited to the Mid-Pliocene Warm Period rather than the LIG.

4.2 Suggestions for Future Research

This thesis has improved our understanding of central Pacific SST change throughout the last glacial cycle, in particular during the LGM and LIG. However, many questions remain which highlight possible avenues for continued work.

Chapter 2 showed that large spatial gaps still remain in our understanding of the glacial surface ocean. The southeast equatorial Pacific, near site VM19-74, in one region that is particularly poorly sampled, as evidenced by the lack of records for comparison with our data or inclusion in MARGO. Additional marine sediment cores in this region may help with the interpretation of VM19-74 data as well as providing a new data in a region that MARGO was not able to provide an LGM SST estimate for.

In Chapter 3, the largest questions center on whether tropical LIG warming is driven by CO_2 or seasonal insolation. It remains unclear as to whether mean annual temperature is responding to seasonal insolation forcing or a non-linear response to CO_2, or, if instead Mg/Ca and alkenones are significantly seasonally biased and record a warm season skew. As discussed in Chapter 3, the argument that LIG Mg/Ca records are seasonally biased so much that this alone explains the 1.2 °C warming signal would require the flux of *G. ruber* to be dominated by warm season individuals. While modern sediment traps have shown higher *G. ruber* flux during boreal summer and fall (e.g. Anand et al., 2003), it is unlikely that seasonal fluxes are large enough to fully explain LIG warming. However, one method to test the role of possible warm season bias on LIG SST records is to measure the $\delta^{18}O$ and/or Mg/Ca of individual tests to reconstruct past changes in seasonality. *G. ruber* live for approximately 2 weeks in the upper ocean (e.g. Schiebel and Hemleben, 2005). In this thesis, we picked 60 individual foraminifera per core interval, then crushed, cleaned and analyzed aliquots of the homogenous mixture. This method is thought to lead to the reconstruction of mean annual temperature, since foraminifera live for short periods of time all throughout the year, and the sediment in a given core interval represents hundreds to thousands of years. Conversely, by measuring

the $\delta^{18}O$ or Mg/Ca composition of individual foraminifera it is possible to reconstruct many 2 week snapshots of upper water column conditions. By measuring many (i.e. 50-100) individuals in a given core interval, it is possible to plot a distribution of those $\delta^{18}O$ and/or SSTs, and observe how this distribution may change downcore. Individual Foraminifera Analysis (IFA) will show not only changes in the mean (a shift of the distribution to higher or lower values), but also changes in the range (a wider or narrower distribution) which may reflect seasonality. In the tropical Indo-Pacific, studies of *G. ruber* and *T. sacculifer* IFA have been to reconstruct changes in past seasonality and ENSO variability over the late Pleistocene (e.g. White et al., 2018; Thirumalai et al., 2019; Rustic et al., 2020). Line Islands samples have previously been used in both core-top (Rongstad et al., 2019) and downcore (Rustic et al., 2020; White et al., 2018) IFA studies. Rustic et al., (2020) includes a Stage 5e datapoint from ML1208-17PC, which they interpret as increased ENSO amplitude during the LIG. However, to date there has been no equatorial Pacific IFA study with a particular focus on the LIG. Such a study may allow us to disentangle whether observed IFA trends are driven by an altered seasonal cycle, ENSO frequency and/or ENSO amplitude (Rustic et al., 2020). Given our understanding of the LIG, I would expect IFA data to show evidence for a larger seasonal SST cycle given the large amplitude of tropical seasonal insolation during Stage 5. Such an observation, along with the data presented in Chapter 3, would support the interpretation that seasonal insolation changes manifest in a mean annual temperature signal. Graduate student Celeste Pallone at Columbia University is generating new $\delta^{18}O$ IFA data from a core in the eastern equatorial Pacific, including the Last Interglacial.

These data, in conjunction with the growing number of IFA studies, may offer insight into the potential role of increased seasonality in explaining observed LIG trends.

APPENDIX A. SUPPLEMENTARY INFORMATION TO "CENTRAL EQUATORIAL PACIFIC COOLING DURING THE LAST GLACIAL MAXIMUM"

The following supplemental information includes text and figures with additional information on age model development, analytical methods, sensitivity tests, and statistics.

A.1 Mg/Ca Inter-laboratory comparison

Samples were first cleaned at Old Dominion University and analyzed on a Thermo Finnigan Element Inductively Coupled Plasma Mass Spectrometer (ICP-MS) there using isotope dilution. Another subset of samples was cleaned at the Georgia Institute of Technology and analyzed on an Element 2 magnetic sector ICP-MS at the University of Colorado, Boulder. Cleaning methods were consistent between labs. 12 samples were used as inter-laboratory comparison (Figure 12). The offset between data run at Old Dominion University and University of Colorado, Boulder ranges from -0.16 to 0.17 mmol/mol Mg/Ca (average = 0.002 mmol/mol). 29MC3, 20BB 16 cm and 20BB 20 cm samples were re-run due to the large spread between replicate measurements of the original Old Dominion data. The new data for these 3 samples fall within the range of original data, suggesting the original samples were not homogenized. Cores 28BB and 37BB were analyzed on a Thermo Scientific High Resolution ICP-MS using isotope dilution at Texas A&M University in Fall 2014. A comparison of in-house standards indicates no offset between data run at Texas A&M and Old Dominion University. Overall, no systematic interlaboratory offset is observed. Average reproducibility based on 94 replicate measurements was 0.22 mmol/mol.

A.2 Mg/Ca Inter-laboratory comparison

In this study we use the core top calibration of Dekens et al. (2002), using their equation for *G. ruber* using $\Delta[CO_3^{2-}]$ as a dissolution correction. Several calibrations exist for converting measured *G. ruber* Mg/Ca ratios to SST based on laboratory cultures (Lea et al., 1999; Nürnberg, et al., 1996), core-top calibrations (Dekens et al., 2002), and sediment trap samples (Anand et al., 2003). These calibrations generally converge on a temperature sensitivity of 9.0 ± 1.0 % mmol/mol change in Mg/Ca per °C.

It has also been shown that dissolution lowers Mg/Ca ratios and, if unaccounted for, would result in lower than observed temperature estimates. Recent results from the Ontong Java Plateau support a percentage loss model for *G. ruber* Mg/Ca (Rongstad et al., 2017) due to seafloor dissolution, in contrast to a molar loss (Regenberg et al., 2014). Dissolution of foraminiferal calcite depends on the calcite saturation state of deep waters, which is often expressed as $\Delta[CO_3^{2-}] = [CO_3^{2-}]_{\text{in situ}} - [CO_3^{2-}]_{\text{saturation.}}$ A widely-applied core-top *G. ruber* Mg/Ca calibration includes a term to correct for the Mg/Ca lost to dissolution, using either core depth or modern bottom water $\Delta[CO_3^{2-}]$ (Dekens et al., 2002). Core depth is often used to correct for dissolution since water depth is relatively constant over recent geologic time, and past changes in bottom-water $[CO_3^{2-}]$ are poorly constrained. However, the depth-corrected calibration (Dekens et al., 2002) yields calculated SSTs ~2.0 °C warmer than modern mean annual SST at this location (Figure 13). Instead, the equation that corrects for dissolution using modern $\Delta[CO_3^{2-}]$ provides a better match between Late Holocene multicore-top Mg/Ca and modern climatology. The depth-dependent calibration is equivalent to a vertical change in $\Delta[CO_3^{2-}]$ of ~-14 µmol/kg per km depth, however, the observed decrease near the Line Islands is ~-6 µmol/kg per km depth. It appears that the

depth-corrected calibration underestimates in situ $\Delta[CO_3^{2-}]$, over-correcting for Mg/Ca loss due to dissolution, and resulting in warmer than observed SSTs. For this reason, and because bottom water $[CO_3^{2-}]$ is more directly linked to the mechanism causing calcite dissolution, we use the $\Delta[CO_3^{2-}]$-corrected calibration.

Line Islands carbonate chemistry calculations were made using pH and alkalinity data from nearby World Ocean Circulation Experiment (WOCE) transect P16N and CO_2Sys for Excel version 2.1 (Lewis & Wallace, 1998). Equilibrium constants for carbonic acid K_1 and K_2 are from (Mehrbach et al., 1973) refit by (Dickson & Millero, 1987), and K_{SO4} from (Dickson, 1990). $[CO_3^{2-}]_{sat}$ is calculated as:

$$[CO_3^{2-}]_{sat} = \frac{[CO_3^{2-}]_{in\ situ}}{\Omega} \quad (1)$$

where Ω is the saturation state of calcite.

Modern Line Islands $\Delta[CO_3^{2-}]$ ranges from -7.3 µmol/kg (2.77 °N, 3,331 m depth) to 5.8 µmol/kg (6.41 °N, 2,371 m depth) (Table 3). The temperature calculated for different time slices is sensitive to the assumed downcore changes in bottom water $\Delta[CO_3^{2-}]$, explored below.

The multi-species calibration from Anand et al., (2003) has a 9% temperature sensitivity, with no correction for secondary influences or dissolution but is commonly applied to convert from Mg/Ca to SST. The Anand calibration yields coretop SSTs that are ~1.5 °C cooler than climatological SSTs at the Line Islands today. This suggests the need for a calibration with a correction term to add back Mg/Ca lost from dissolution, such as the Dekens calibration we used for this study. However, use of the Anand calibration would

not change the magnitude of the LH-LGM SST change since they both feature 9% temperature sensitivities.

A.3 Sensitivity to changes in bottom water [ΔCO_3^{2-}]

Given the narrow range of Line Islands core depths used in this study, past changes in bottom water [CO_3^{2-}] are expected to affect all cores equally. Thus, the meridional SST gradient for a given time period will not be sensitive to changes in bottom water [CO_3^{2-}]; however, the magnitude of glacial cooling may be affected, if changes to bottom water [CO_3^{2-}] are sufficiently large. Calcite preservation cycles have long been observed in tropical Pacific cores (Arrhenius, 1952); however, geochemical estimates of tropical Pacific glacial-interglacial bottom water [CO_3^{2-}] changes vary greatly: ~5 µmol/kg higher (Anderson & Archer, 2002; Farrell & Prell, 1989), little to no change (Marchitto et al., 2005; Qin et al., 2017; Yu et al., 2010), or ~30 µmol/kg lower during the LGM (Fehrenbacher & Martin, 2011). If glacial bottom water [CO_3^{2-}] was ~5 µmol/kg higher than modern, the magnitude of LGM SST change is not significantly changed from assuming constant bottom water [CO_3^{2-}] conditions. If, however, glacial bottom water [CO_3^{2-}] was 30 µmol/kg lower than modern (Fehrenbacher & Martin, 2011), the magnitude of glacial cooling would be reduced to 0.2-1.6 °C (mean = 0.7 °C), LGM-LH or LGM-Modern where Late Holocene data are not available (Figure 14). It should be noted, however, that higher or similar to modern [CO_3^{2-}] is supported both qualitatively by dissolution proxies such as percent weight carbonate (Arrhenius, 1952; Lalicata & Lea, 2011) and quantitatively by most geochemical estimates (Anderson & Archer, 2002; Farrell & Prell, 1989; Marchitto et al., 2005; Qin et al., 2017), whereas lower bottom water

$[CO_3^{2-}]$ is only suggested by one study (Fehrenbacher & Martin, 2011) and not supported by the physical sediment properties that indicate the extent of dissolution. The coarse fraction and shell weight data from the ML1208 sediment cores are in agreement with the Pacific-wide sedimentary data suggesting similar or slightly enhanced preservation during the LGM (Lynch-Stieglitz et al., 2015).

A.4 Nonthermal Influences on Mg/Ca

It has been shown that as foraminifera calcify, salinity and carbonate chemistry, expressed as either $[CO_3^{2-}]$ or pH, also influence Mg/Ca. Laboratory cultures generally converge on a sensitivity of ~4-8% change in Mg/Ca per salinity unit (Gray & Evans, 2019; Kisakürek et al., 2008; Lea et al., 1999; Nürnberg et al., 1996). Some core-top studies suggest an increase of Mg/Ca between 15 and 59% per salinity unit change (Arbuszewski et al., 2010; Ferguson et al., 2008; Mathien-Blard & Bassinot, 2009), though subsequent studies have shown that such large values are likely overestimates (Hertzberg & Schmidt, 2013). The secondary influences of salinity and pH on *G. ruber* Mg/Ca have recently been supported by a global sediment trap study (Gray et al., 2018). The influence of pH on planktic foraminiferal Mg/Ca has been quantified as ~5-10% per 0.1 unit pH change (Evans et al., 2016; Kisakürek et al., 2008; Lea et al., 1999; Russell et al., 2004).

Here we consider the impacts of non-thermal influences on Mg/Ca, such as salinity and pH on foraminiferal Mg/Ca, and the sensitivity of our conclusions to the proposed influences of these factors. We find that these alternative approaches would result in a range of Late Holocene to LGM temperature change for our Line Islands transect from -1.9°C to -2.1°C for the global calibration equations that either don't account for dissolution or use a fixed percentage loss on dissolution (Gray & Evans, 2019; Gray et al., 2018;

Tierney et al., 2019) For all estimates we assume an LGM to Late Holocene salinity increase of 1.1 psu and pH increase of 0.13 consistent with Tierney et al. (2019).

We first consider the equations in Gray et al. (2018, 2019). These calibrations were developed using laboratory culture (Gray & Evans, 2019) and net tow and sediment trap (Gray et al., 2018) data, and have not yet been extended to core-top sediment samples. Laboratory culture, net tow, and sediment trap samples differ from core-top samples in two significant ways with respect to dissolution, and thus Mg/Ca ratios. First, sample preparation for these samples omit the reductive cleaning step, which has been shown to reduce Mg/Ca ratios by ~10% (Barker et al., 2003). Second, sediment samples are subject to seafloor dissolution, unlike net tow and sediment trap samples. However, assuming that dissolution has removed a similar percentage of Mg/Ca from both the Late Holocene and LGM foraminifera in our sediment samples, we can apply these equations and determine the implied Late Holocene to LGM temperature difference. Using the locations where we have Late Holocene (0-4 ka) data (19GC, 20BB/21MC, 11GC), we find that the temperature difference is quite similar to that inferred using the Dekens et al. (2002) $\Delta[CO_3^{2-}]$-corrected calibration (no change for Gray et al., 2018 and 0.2 °C smaller change for Gray & Evans, 2019).

We then consider the approach of (Tierney et al., 2019) (BAYMAG), using the seasonal, group specific model for *G. ruber*. This approach uses Bayesian statistics to provide a range of paleotemperature estimates, but the median value yields a Late Holocene to LGM temperature change at the Line Island Ridge core sites that differs from the Dekens et al. calibration by less than 0.1 °C. Similarly, applying this calibration to our global tropical data set gives a Late Holocene to LGM temperature difference that is only 0.1 °C

greater than what is inferred using the Dekens calibration. However, this calibration produces exaggerated (1.5x) spatial temperature gradients in the global tropics (15 °S to 15 °N) for both the Late Holocene and LGM relative to the modern observed climatology (Figure 15). This is not surprising, given that Tierney et al. (2019) report a strong correlation of the residuals for the *G. ruber* model with temperature. They are not able to fully explain or correct for this, and propose that either the Mg/Ca may respond non-linearly to temperature, or there is a missing environmental control that scales nonlinearly to temperature. It is also possible that foraminifera in the natural environment do not respond in the same way as they did in the laboratory experiments. Applying the Dekens et al. (2002) calibration to the same core top data used in the Tierney et al. (2019) study more accurately captures the spatial gradients in the tropical ocean (1.05x exaggeration of the Late Holocene spatial gradients relative to the climatology), with smaller residuals (even before applying the 0.6 °C core-top/climatology offset discussed below) that are less correlated to temperature relative to the BAYMAG estimates.

The core top calibration of (Dai et al., 2019) only considers Atlantic Ocean data and lacks a term related to the saturation state of bottom water, so is not appropriate for use here. However, using that calibration would increase the magnitude of the estimated Late Holocene to LGM temperature change at the Line Islands by 0.7 °C. The calibrations of (Khider et al. , 2015) and (Saenger & Evans, 2019) incorporate a fixed molar amount of Mg/Ca rather than a percentage loss on dissolution. It is not clear why the Mg would be lost in this manner and this will tend to exaggerate cooling since foraminifera that initially calcify in colder waters have a lower Mg/Ca ratio. Recent results from the Ontong Java Plateau support a percentage loss model for *G. ruber* Mg/Ca (Rongstad et al., 2017) due to

seafloor dissolution. Using the Saenger & Evans, 2019 calibration on the Line Islands data increases the magnitude of the inferred cooling by 3 °C.

A.5 Global Tropical G. ruber Mg/Ca Compilation

Existing Mg/Ca records from the equatorial region (15 °N to 15 °S) were compiled in Table 6. For the most direct comparison, our compilation includes only Mg/Ca measurements on *G. ruber*. LGM Mg/Ca values for each core location are the average Mg/Ca value for all measurements between 19-23 ka, as indicated by the age models in individual studies. To correct for different cleaning methods, a 10% correction was applied to Mg/Ca values for studies that used only the oxidative cleaning step, as studies have shown the reductive step to reduce Mg/Ca values by ~10% (Barker et al., 2003). Modern $\Delta[CO_3^{2-}]$ values were taken from existing studies when possible, or calculated using nearby WOCE transect data and CO_2sys for Excel version 2.1 (Lewis & Wallace, 1998).

Glacial $\Delta[CO_3^{2-}]$ values for the Pacific and Indian Ocean are assumed to be the same as today (see Text S3). To estimate glacial changes in Atlantic deepwater $\Delta[CO_3^{2-}]$, we compiled available records of B/Ca-based estimates of $[CO_3^{2-}]$ throughout modern NADW (Chalk et al., 2019). We used these 11 records to calculate the relative changes in upper (<2800 m) and lower (>2800 m) NADW between the Late Holocene (0-4 ka) and LGM (19-23 ka). All cores located in upper NADW indicate increased LGM $[CO_3^{2-}]$, with an average of 19 μmol/kg. All cores located in lower NADW show decreased LGM $[CO_3^{2-}]$, on average 21 μmol/kg lower than the Late Holocene. KNR110-82 (2.816 km depth) was included in upper NADW. These values are consistent with other tracers of glacial Atlantic circulation, which show that higher $[CO_3^{2-}]$ Glacial North Atlantic Intermediate Water

(GNAIW) was shoaled relative to the modern, while lower [CO_3^{2-}] Southern Sourced Waters (SSW) filled in more of the deep Atlantic.

SST is calculated using the core top calibration of Dekens et al. (2002), using their equation for *G. ruber* using $\Delta[CO_3^{2-}]$ as a dissolution correction. The 53 Late Holocene SST estimates are on average 0.6 degrees cooler than climatological values. Applying this same calibration to the larger (154 location) core top tropical (15 °S to 15 °N) dataset of Tierney et al (2019), also yields an offset from the WOA13 climatology (Boyer et al., 2013) of -0.6 ± 0.1 °C (mean ± standard error). While Dekens et al. (2002) used an earlier climatology (Levitus & Boyer, 1994), the difference between the two climatologies was small at the core locations (mean = 0.1 °C). The offset may result from random error introduced by the smaller set of cores used in the Dekens et al. (2002) calibration. Also, the Dekens calibration included some higher latitude core sites where the seasonal preferences of *G. ruber* can complicate the use of mean annual climatological SST for the calibration. Another possibility is that the core top samples used here are more biased than those used in the Dekens et al. (2002) study towards older time periods that could have in actuality been cooler. In order to avoid overestimating the LGM to Late Holocene temperature change when comparing to the climatological values, we adjust the paleotemperature estimates from the Dekens et al. (2002) calibration by +0.6 °C for the global compilation (Figures 2,3 and Table 6), and consider the adjusted values presented in Table 6 to be our current best estimate for LGM temperature. However, the true temperature change may be up to 0.6°C larger if core top age is the main source for the discrepancy.

A.6 Global Tropical *G. ruber* Mg/Ca Compilation

We find greater temperature change at our southern Line Islands sites in the South Equatorial Current (south of 2°S) than the sites in the North Equatorial Counter Current (north of 2°S). To compute the likelihood that Central Tropical Pacific SST North-South difference increased between the modern and LGM, we treat North-South difference for each time period as a population described by its mean (X) and variance (σ^2). We then compute the z-score as:

$$Z = \frac{X_1 - X_2}{\sqrt{(\sigma_{x1}^2 + \sigma_{x2}^2)}} \quad (2)$$

The likelihood that the glacial North-South difference is greater than modern (72%) reported in the main body of the paper is the value taken from a z-table.

A.7 Global Tropical *G. ruber* Mg/Ca Compilation

Previously published *G. ruber* $\delta^{18}O$ ($\delta^{18}O_c$) data showed that the meridional Line Islands $\delta^{18}O_c$ gradient during the LGM was enhanced relative to the Holocene (Lynch-Stieglitz et al., 2015). Incorporating the new data published here yields a Mid Holocene meridional $\delta^{18}O_c$ gradient (northern-southern sites) of -0.20 ‰ as compared to -0.32 ‰ during the LGM (Table 5, Figure 16). Using Mg/Ca-derived temperature estimates from the same cores, we calculate seawater $\delta^{18}O$ ($\delta^{18}O_{sw}$) for *G. ruber* records in the tropical Pacific using the low-light paleotemperature equation (Bemis et al., 1998), though observed trends are insensitive to the use of Kim & O'Neil, 1997. This indicates that

temperature and $\delta^{18}O_{sw}$ contribute in roughly equal proportions to the increased N-S $\delta^{18}O_c$ gradient at the Line Islands.

We also compute $\delta^{18}O_{sw}$ for the tropical Pacific cores in our global compilation in the same way, and calculate the Late Holocene to LGM difference (Figure 17). To correct for the influence of continental ice sheets, glacial $\delta^{18}O_{sw}$ values are corrected by +1.05 ‰ (Adkins & Schrag, 2001). Ice volume-corrected (IVC) reconstructions of $\delta^{18}O_{sw}$ change ($\Delta\delta^{18}O_{sw}$) from the Western Pacific Warm Pool generally show a modest isotopic depletion, which has previously been interpreted as a slight freshening of Western Pacific surface waters (Rosenthal et al., 2003) consistent with increased convection and strengthened Pacific Walker Circulation. Eastern Pacific IVC $\Delta\delta^{18}O_{sw}$ reconstructions show little to no change. Line Islands IVC $\Delta\delta^{18}O_{sw}$ (LGM-Late Holocene or LGM-Modern where Late Holocene data is not available) range from -0.15 to -0.55 ‰ (mean = -0.37 ‰). The magnitude of IVC $\Delta\delta^{18}O_{sw}$ is slightly larger in Line Islands cores north of 2 °N (-0.41 ± 0.04 compared to -0.32 ± 0.07). Overall, negative IVC $\delta^{18}O_{sw}$ values at the Line Islands are consistent in sign with Western Pacific records and indicate slight freshening of glacial Central Pacific surface waters.

A.8 Additional Mg/Ca records

Previously unpublished *G. ruber* Mg/Ca data for core V28-234 (Western Pacific) are included in the compilation of tropical SSTs (Table 6) and in the data supplement (Table 7). These additional samples were cleaned using standard cleaning protocol, both

reductive and oxidative steps, and analyzed on an Element 2 at the University of South Carolina.

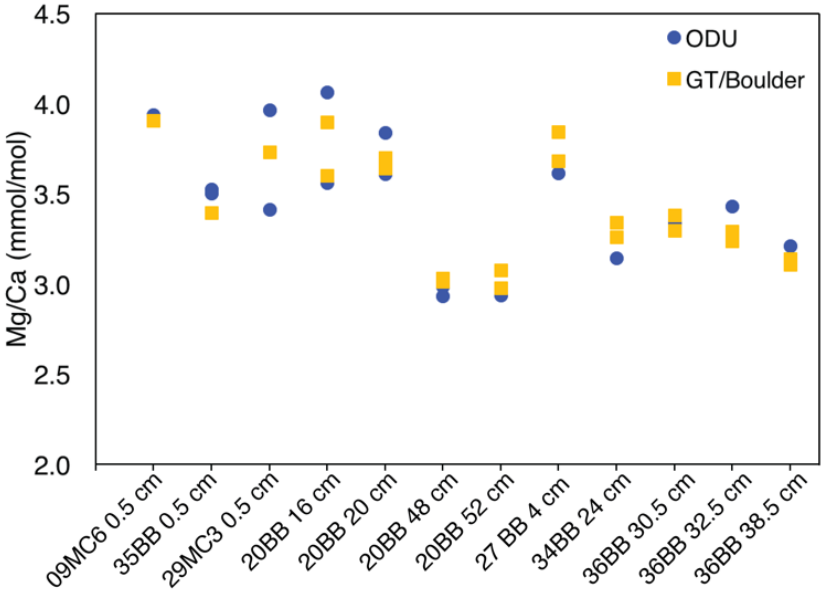

Figure 12 Interlaboratory comparison of replicate Mg/Ca measurements cleaned and analyzed at Old Dominion University (blue) with samples cleaned at Georgia Tech, analyzed at University of Colorado, Boulder (yellow).

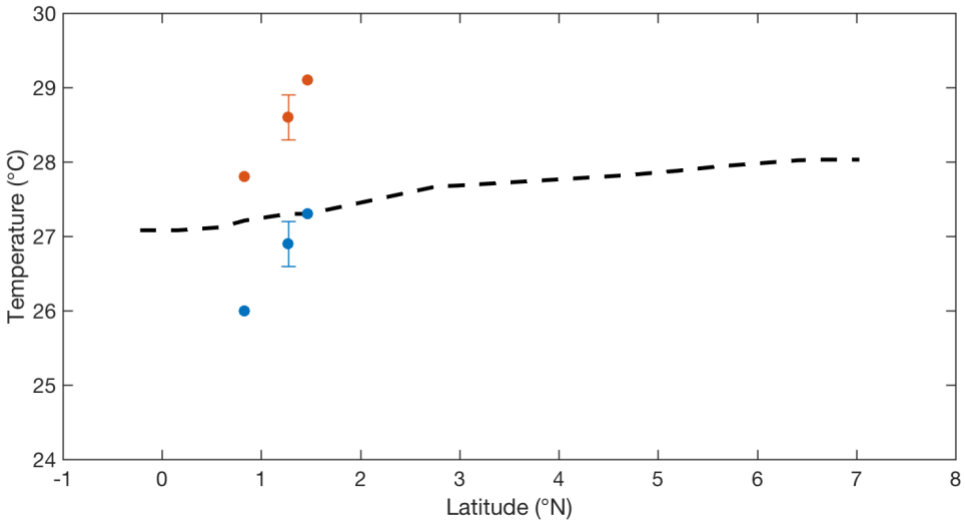

Figure 13 Estimated Late Holocene SSTs using the Dekens calibration with depth (orange) and ΔCO_3^{2-} (blue) corrections, compared to modern mean annual SST (Schmidtko, Johnson, & Lyman, 2013) (black line).

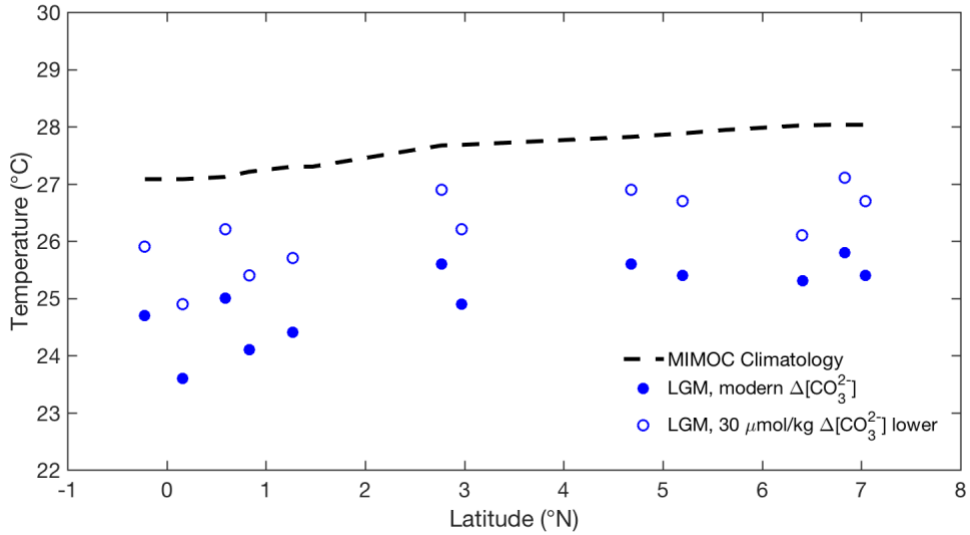

Figure 14 Comparison of calculated LGM (19-23 ka) SSTs from *G. ruber* Mg/Ca using the $\Delta[CO_3^{2-}]$ equation (Dekens et al., 2002) with modern bottom water $\Delta[CO_3^{2-}]$ (blue filled symbols) and 30 µmol/kg lower $[CO_3^{2-}]$ (Fehrenbacher & Martin, 2011) (open blue symbols), as compared to modern climatology (Schmidtko et al., 2013) (black line).

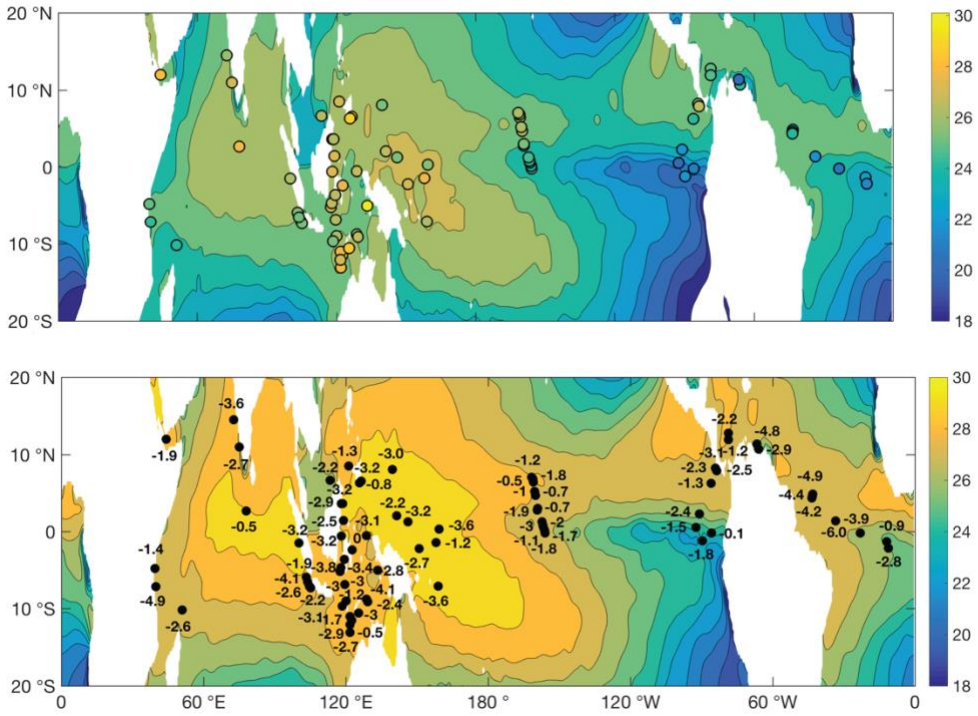

Figure 15 LGM cooling suing BAYMAG calibration. a) LGM SST for equatorial Pacific *G. ruber* Mg/Ca, base map is modern climatology (Schmidtko et al., 2013) with the mean tropical Pacific LGM cooling (-2.6 °C) subtracted. Color denotes the absolute SST during the LGM based on *G. ruber* Mg/Ca and the Tierney et al., (2019) calibration. b) Magnitude of mean LGM SST change (LGM-Modern) from our global

compilation of tropical (15 °N-15 °S) *G. ruber* Mg/Ca records. Markers indicate core locations and labels denote the magnitude of cooling, LGM-Late Holocene or LGM-Modern where Late Holocene data are not available.

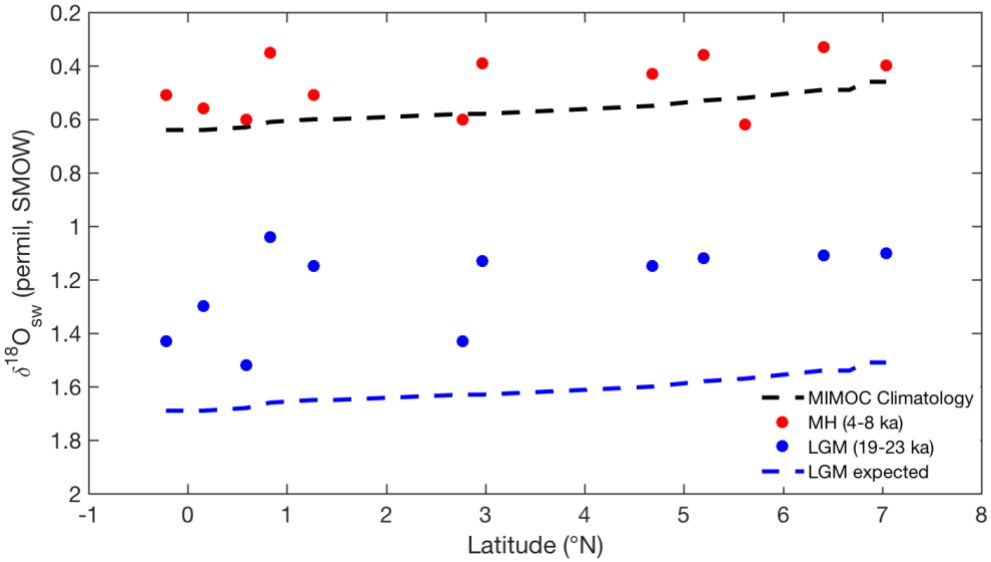

Figure 16 Reconstructed Mid Holocene (red symbols) and LGM (blue symbols) $\delta^{18}O_{sw}$ based on $\delta^{18}O_c$ measurements and Mg/Ca temperatures, compared to modern expected values (black line). $\delta^{18}O_{sw}$ is calculated using the Dekens et al. (2002) calibration without an offset applied. The blue line denotes the modern gradient shifted by 1.05 ‰, the whole ocean ice volume correction (Adkins & Schrag, 2001).

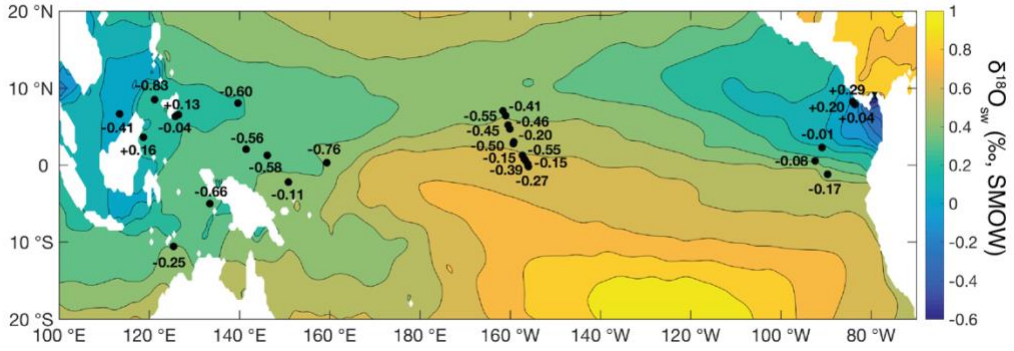

Figure 17 Ice Volume Corrected $\Delta\delta^{18}$Osw (LGM-Late Holocene) from *G. ruber* Mg/Ca and $\delta^{18}O_c$ records. For cores missing Late Holocene (0-4 ka) data, modern $\delta^{18}O_{sw}$ calculated from climatological salinity (Schmidtko et al., 2013) and the tropical SSS-$\delta^{18}O_{sw}$ relationship (LeGrande & Schmidt, 2006) is used. Negative values indicate a relative isotopic depletion during the LGM. Records in the Western Equatorial Pacific (WEP) and Central Equatorial Pacific show relative depletion (freshening), whereas cores in the Eastern Equatorial Pacific generally show a smaller magnitude of change.

APPENDIX B. DATA TABLES

Table 2 Radiocarbon dates for ML1208 Cores

Core	Depth (cm)	14C Age	Error	Calendar Age (yr BP)	Species	Source
06BB	8.5	6030	25	6443	*G. sacculifer*	This study
06BB	28.5	15700	85	18566	*G. ruber*	This study
06BB	44.5	21200	170	25059	*G. ruber*	This study
09MC	0.5	6210	25	6657	*G. sacculifer*	This study
11GC	0.5	2850	20	2635	*G. sacculifer*	This study
13BB	0	4780	45	5049	*G. ruber*	Lynch-Stieglitz et al. (2015)
13BB	11	5960	20	6365	*G. ruber*	Costa et al., (2017)
13BB	20	9640	30	10533	*G. ruber*	Costa et al., (2017)
13BB	28	11650	30	13149	*G. ruber*	Costa et al., (2017)
13BB	34	14580	40	17261	*G. ruber*	Costa et al., (2016)
13BB	53	20760	70	24437	*G. ruber*	Costa et al., (2016)
14MC	0.5	4700	20	4916	*G. sacculifer*	This study
15GC	0	7150	45	7618	*G. ruber*	Lynch-Stieglitz et al. (2015)
15GC	24	11300	30	12761	*G. ruber*	This study
15GC	40	17700	65	20855	*G. sacculifer*	This study
15GC	76	26800	230	30667	*G. sacculifer*	This study
15GC	212	6210	20	6657	*G. sacculifer*	This study
18GC	0	3320	45	3167	*G. sacculifer*	Lynch-Stieglitz et al. (2015)
18GC	16	5530	60	5916	*G. ruber*	Lynch-Stieglitz et al. (2015)

18GC	32	8900	55	9552	*G. ruber*	Lynch-Stieglitz et al. (2015)
18GC	48	9800	40	10713	*G. ruber*	Lynch-Stieglitz et al. (2015)
18GC	60	13750	90	16053	*G. ruber*	Lynch-Stieglitz et al. (2015)
18GC	68	15250	60	18052	*G. ruber*	Lynch-Stieglitz et al. (2015)
18GC	92	22500	130	26304	*G. sacculifer*	This study
18GC	112	28500	130	31844	*G. ruber*	Lynch-Stieglitz et al. (2015)
18GC	140	33200	250	36795	*G. ruber*	Lynch-Stieglitz et al. (2015)
19GC	0	3120	35	2895	*G. ruber*	Lynch-Stieglitz et al. (2015)
19GC	28.5	8510	35	9134	*G. sacculifer*	This study
19GC	48.5	14550	70	17220	*G. ruber*	This study
19GC	60.5	20400	150	24054	*G. sacculifer*	This study
20BB	0	3860	30	3823	*G. ruber*	Lynch-Stieglitz et al. (2015)
20BB	7	5380	20	5747	*G. ruber*	Costa et al., (2017)
20BB	27	11400	30	12851	*G. ruber*	Costa et al., (2017)
20BB	34	13050	30	15057	*G. ruber*	Costa et al., (2017)
20BB	40	14685	40	17400	*G. ruber*	Costa et al., (2016)
20BB	55	19100	70	22540	*G. ruber*	Costa et al., (2016)
21MC	0.5	2330	25	1945	*G. ruber*	Costa et al., (2016)
27BB	0	5550	45	5937	*G. ruber*	Lynch-Stieglitz et al., (2015)
27BB	0.5	6780	25	7307	*G. sacculifer*	This study
27BB	8	7540	25	7990	*G. ruber*	This study

27BB	15.5	10050	35	11062	*G. ruber*	This study
27BB	43.5	18400	85	21797	*G. ruber*	This study
27BB	68.5	27200	250	30941	*G. ruber*	This study
28BB	0	4420	20	4578	*G. sacculifer*	This study
28BB	8	5950	25	6356	*G. ruber*	Costa et al., (2017)
28BB	24	8460	25	9062	*G. ruber*	Costa et al., (2017)
28BB	34	10550	30	11824	*G. ruber*	Costa et al., (2017)
28BB	46	13550	40	15794	*G. ruber*	Costa et al., (2017)
28BB	54	16600	60	19550	*G. ruber*	Costa et al., (2016)
28BB	76	25400	160	29033	*G. ruber*	Costa et al., (2016)
29MC	0.5	4770	20	5018	*G. ruber*	Costa et al., (2016)
31BB	0	11200	60	12689	*G. ruber*	Lynch-Stieglitz et al., (2015)
31BB	4	6700	45	7213	*G. ruber*	Lynch-Stieglitz et al., (2015)
31BB	12	6280	50	6735	*G. ruber*	Lynch-Stieglitz et al., (2015)
31BB	36	10450	30	11573	*G. ruber*	Jacobel et al., (2016)
31BB	40	11550	45	13030	*G. ruber*	Lynch-Stieglitz et al., (2015)
31BB	48	14100	35	16520	*G. ruber*	Jacobel et al., (2016)
31BB	56	16100	45	18806	*G. ruber*	Jacobel et al., (2016)
31BB	72	17450	75	20560	*G. ruber*	Lynch-Stieglitz et al., (2015)
31BB	84	23000	120	26919	*G. ruber*	This study
32BB	8	8870	25	9513	*G. ruber*	Costa et al., (2017)
32BB	17	11000	30	12564	*G. ruber*	Costa et al., (2017)
32BB	20	12800	30	14443	*G. ruber*	Costa et al., (2017)

32BB	25	15350	75	18170	*G. ruber*	Costa et al., (2016)
32BB	35	19300	75	22750	*G. ruber*	Costa et al., (2016)
33MC	0.5	4930	35	5272	*G. ruber*	Costa et al., (2016)
34BB	0	8540	45	9173	*G. ruber*	Lynch-Stieglitz et al., (2015)
34BB	8	6090	20	6514	*G. ruber*	This study
34BB	20	20700	110	24375	*G. ruber*	This study
34BB	44	23400	150	27324	*G. ruber*	This study
35BB	0.5	12450	40	13931	*G. sacculifer*	This study
36BB	0.5	7950	25	8403	*G. ruber*	This study
36BB	5	7920	25	8378	*G. ruber*	Costa et al., (2017)
36BB	15	11650	40	13148	*G. ruber*	Costa et al., (2016)
36BB	19	13950	35	16310	*G. ruber*	Costa et al., (2017)
36BB	25	16700	65	19674	*G. ruber*	Costa et al., (2016)
36BB	28.5	19050	90	22506	*G. ruber*	This study
36BB	36.5	25700	290	29372	*G. sacculifer*	This study
37BB	0	6180	35	6619	*G. ruber*	Lynch-Stieglitz et al., (2015)
37BB	12	9940	30	10911	*G. ruber*	Jacobel et al., (2016)
37BB	20	13200	45	15242	*G. ruber*	Jacobel et al., (2016)
37BB	24	15100	55	17887	*G. ruber*	Jacobel et al., (2016)
37BB	36	24800	200	28423	*G. ruber*	Jacobel et al., (2016)
39MC	0.5	6870	25	7388	*G. sacculifer*	This study

Table 3 ML1208 Chapter 1 Mg/Ca Data

Core	Lat (°N)	Long (°E)	Δ[CO32-] (μmol/kg)	Depth (cm)	Age (yr BP)	Mg/Ca (mmol/mol)	Lab	Mg/Ca (mmol/mol)	Lab	Mg/Ca (mmol/mol)	Lab	δ18Oc (permil)	δ13C (permil)	Timeslice
13BB	-0.22	-155.96	-0.8	0.5	5049	3.37	B	3.31	B			-1.46	1.23	MH
13BB	-0.22	-155.96	-0.8	4.5	5645	3.46	B	3.44	B			-1.93	1.43	MH
13BB	-0.22	-155.96	-0.8	8.5	6171	3.47	B	3.39	B			-1.94	1.61	MH
13BB	-0.22	-155.96	-0.8	12.5	6828	3.62	B	3.38	B			-1.69	1.39	MH
13BB	-0.22	-155.96	-0.8	16.5	9144	3.33	B	3.40	B			-1.58	1.37	-
13BB	-0.22	-155.96	-0.8	40.5	19905	2.99	B	3.06	B			-0.55	0.99	LGM
13BB	-0.22	-155.96	-0.8	44.5	21038	3.06	B	3.04	B			-0.54	1.25	LGM
13BB	-0.22	-155.96	-0.8	48.5	22926	3.04	B	2.99	B			-0.54	1.24	LGM
14MC	-0.22	-155.96	-0.8	0.5	4916	3.69	B	3.66	B			-1.88	1.50	MH
15GC	0.16	-156.12	-5.0	0	7618	3.44	B	3.48	B			-1.76	1.39	MH
15GC	0.16	-156.12	-5.0	4	8475	3.26	B	3.24	B			-1.64	1.38	-
15GC	0.16	-156.12	-5.0	8	9332	3.20	B	3.53	B			-1.56	1.20	-
15GC	0.16	-156.12	-5.0	12	10190	3.56	B	3.58	B			-1.58	1.18	-
15GC	0.16	-156.12	-5.0	16	11047	3.45	B	3.48	B			-1.51	1.38	-
15GC	0.16	-156.12	-5.0	20	11904	3.51	B	3.51	B			-1.36	1.19	-
15GC	0.16	-156.12	-5.0	40	20855	2.54	B					-0.38	1.07	LGM
15GC	0.16	-156.12	-5.0	44	21945	2.97	B	2.81	B			-0.53	1.22	LGM
15GC	0.16	-156.12	-5.0	48	23035	2.98	B					-0.61	1.00	-
15GC	0.16	-156.12	-5.0	52	24126	2.87	B	2.85	B			-0.58	1.15	-
15GC	0.16	-156.12	-5.0	56	25216	2.84	B					-0.52	1.12	-
18GC	0.59	-156.66	-3.2	16	5916	3.40	B	3.52	B			-1.76	1.37	MH
18GC	0.59	-156.66	-3.2	20	6825	3.65	B	3.62	B			-1.76	1.37	MH

18GC	0.59	-156.66	-3.2	24	7734	3.62	B	3.53	B	-1.76	1.37	MH
18GC	0.59	-156.66	-3.2	28	8643	3.68	B	3.63	B	-1.74	1.39	-
18GC	0.59	-156.66	-3.2	32	9552	3.70	B	3.40	B	-1.64	1.31	-
18GC	0.59	-156.66	-3.2	36	9842	3.74	B	3.43	B	-1.35	1.11	-
18GC	0.59	-156.66	-3.2	40	10133	3.72	B	3.60	B	-1.25	1.15	-
18GC	0.59	-156.66	-3.2	72	19427	3.13	B	3.03	B	-0.42	1.22	LGM
18GC	0.59	-156.66	-3.2	76	20803	3.15	B	3.12	B	-0.64	1.25	LGM
18GC	0.59	-156.66	-3.2	80	22178	3.08	B	3.00	B	-0.48	1.07	LGM
18GC	0.59	-156.66	-0.1	84	23553	2.73	B	2.62	B	-0.66	1.07	-
19GC	0.83	-156.87	-0.1	4.5	3786	3.49	B	3.37	B	-1.71	1.71	LH
19GC	0.83	-156.87	-0.1	8.5	4678	3.46	B	3.43	B	-2.10	1.67	MH
19GC	0.83	-156.87	-0.1	12.5	5569	3.58	B	3.59	B	-1.91	1.72	MH
19GC	0.83	-156.87	-0.1	16.5	6460	3.58	B	3.57	B	-1.76	1.43	MH
19GC	0.83	-156.87	-0.1	20.5	7351	3.33	B	3.32	B	-1.99	1.4	MH
19GC	0.83	-156.87	-0.1	24.5	8243	3.69	B	3.72	B			-
19GC	0.83	-156.87	-0.1	28.5	9134	3.68	B	3.67	B	-1.56	1.58	-
19GC	0.83	-156.87	-0.1	32.5	10751	3.20	B	3.35	B	-1.52	1.310	-
19GC	0.83	-156.87	-0.1	40.5	13986	3.23	B	3.18	B	-1.42	1.35	-
19GC	0.83	-156.87	-0.1	44.5	15603	3.13	B	3.10	B	-0.88	1.23	-
19GC	0.83	-156.87	-0.1	48.5	17220	3.00	B	3.14	B	-0.44	1.45	-
19GC	0.83	-156.87	-0.1	52.5	19498	2.70	B	2.79	B	-1.08	1.22	LGM
19GC	0.83	-156.87	-0.1	56.5	21776	2.98	B	3.13	B	-0.57	1.14	LGM
19GC	0.83	-156.87	-0.1	60.5	24054	3.06	B	3.02	B	-0.63	1.37	-
20BB	1.27	-157.26	-0.3	0	3823	3.60	B	3.57	B	-2.10	1.47	LH
20BB	1.27	-157.26	-0.3	4	4922	3.49	O	3.51	O	-1.98	1.55	MH
20BB	1.27	-157.26	-0.3	8	6102	3.70	O	3.66	O	-1.99	1.44	MH
20BB	1.27	-157.26	-0.3	12	7523	3.80	O			-1.71	1.28	MH

20BB	1.27	-157.26	-0.3	16	8944	3.90	B	3.60	B			-1.76	1.28	-
20BB	1.27	-157.26	-0.3	20	10365	3.84	O	3.64	B	3.70	B	-1.61	1.18	-
20BB	1.27	-157.26	-0.3	24	11785	3.42	O	3.45	O			-1.21	0.93	-
20BB	1.27	-157.26	-0.3	28	13166	3.46	O	3.38	O			-1.31	1.02	-
20BB	1.27	-157.26	-0.3	40	17402	3.21	O	3.25	O			-0.70	1.07	-
20BB	1.27	-157.26	-0.3	44	18773	2.79	O					-0.67	1.12	-
20BB	1.27	-157.26	-0.3	48	20144	3.01	B	3.03	B			-0.74	1.06	LGM
20BB	1.27	-157.26	-0.3	52	21516	3.08	B	2.98	B			-0.76	1.09	LGM
20BB	1.27	-157.26	-0.3	56	22887	2.75	O	2.95	O			-0.81	1.15	LGM
21MC	1.27	-157.26	-0.3	0.5	1945	3.81	O					-2.11	1.55	LH
11GC	1.47	-157.58	-1.2	0.5	2635	3.83	O					-2.06	1.92	LH
27BB	2.77	-159.29	-7.3	4	7600	3.62	O	3.84	B			-1.85	1.42	MH
27BB	2.77	-159.29	-7.3	8	7990	3.67	B	3.69	B			-1.93	1.34	MH
27BB	2.77	-159.29	-7.3	12	9526	3.75	B	3.82	B			-1.84	1.44	-
27BB	2.77	-159.29	-7.3	15.5	11062	3.90	B	3.93	B			-1.89	1.26	-
27BB	2.77	-159.29	-7.3	39.5	20263	3.15	B	3.20	B			-0.77	1.25	LGM
27BB	2.77	-159.29	-7.3	43.5	21797	3.29	O	3.29	O			-0.72	1.45	LGM
27BB	2.77	-159.29	-7.3	47.8	23260	3.22	B	3.18	B			-0.84	1.35	-
27BB	2.77	-159.29	-7.3	52.5	25089	3.15	B	3.35	B			-0.90	1.62	-
27BB	2.77	-159.29	-7.3	56.5	26552	3.23	O	3.36	O			-0.81	1.25	-
28BB	2.97	-159.20	-5.1	4	5467			3.67	T			-1.77	1.39	MH
28BB	2.97	-159.20	-5.1	8	6356	3.27	T	3.46	B			-1.93	1.57	MH
28BB	2.97	-159.20	-5.1	12	7033	3.27	T	3.33	T			-1.92	1.51	MH
28BB	2.97	-159.20	-5.1	16	7709	3.25	T	3.38	T			-1.94	1.56	MH
28BB	2.97	-159.20	-5.1	20	8386	3.50	T	3.45	T			-1.79	1.54	-
28BB	2.97	-159.20	-5.1	24	9062	3.64	T	3.59	T			-1.82	1.32	-
28BB	2.97	-159.20	-5.1	28	9983	3.47	T	3.53	T			-1.85	1.27	-

28BB	2.97	-159.20	-5.1	32	10903	3.42	T	3.91	T			-1.53	1.21	-
28BB	2.97	-159.20	-5.1	56	20412	3.18	T					-0.92	1.39	LGM
28BB	2.97	-159.20	-5.1	60	22136	2.92	T					-0.87	1.14	LGM
29MC	2.97	-160.77	-5.1	0.5	5018	3.41	O	3.96	O	3.73	B	-1.69	1.29	MH
31BB	4.68	-160.05	-1.0	12	6735	3.98	B	3.86	B			-2.14	1.60	MH
31BB	4.68	-160.05	-1.0	60	19245	3.34	B	3.32	B			-1.06	1.27	LGM
31BB	4.68	-160.05	-1.0	64	19683	3.43	B	3.32	B			-0.99	1.22	LGM
31BB	4.68	-160.05	-1.0	68	20122	3.20	B	3.31	B			-1.03	1.31	LGM
31BB	4.68	-160.05	-1.0	72	20560	3.31	B	3.21	B			-0.96	1.32	LGM
31BB	4.68	-160.05	-1.0	76	22680	3.28	B	3.19	B			-1.05	1.18	LGM
31BB	4.68	-160.05	-1.0	80	24799	3.29	B	3.05	B			-1.15	1.18	-
32BB	5.20	-160.43	-1.9	0		3.72	B					-2.07	1.44	
32BB	5.20	-160.43	-1.9	4		3.86	B					-2.07	1.35	
32BB	5.20	-160.43	-1.9	8	9513	3.94	B					-1.93	1.25	-
32BB	5.20	-160.43	-1.9	12	10869	4.00	B					-1.72	1.21	-
32BB	5.20	-160.43	-1.9	24	17421	3.42	B							-
32BB	5.20	-160.43	-1.9	28	19541	3.26	B					-1.02	1.26	LGM
32BB	5.20	-160.43	-1.9	32	21375	3.20	B					-1.00	1.22	LGM
32BB	5.20	-160.43	-1.9	36	23210	3.31	B	3.36	B			-0.99	1.29	-
33MC	5.20	-160.43	-1.9	0.5	5272	3.74	B					-2.10	1.45	MH
34BB	5.62	-160.79	-2.4	0		3.99	O	4.34	O			-1.84	1.28	-
34BB	5.62	-160.79	-2.4	4		3.90	O	4.12	O			-1.78	1.43	-
34BB	5.62	-160.79	-2.4	8	6514	4.01	O	4.09	O			-2.04	1.04	MH
34BB	5.62	-160.79	-2.4	12	12468	3.89	O	4.29	O			-1.92	1.44	-
34BB	5.62	-160.79	-2.4	16	18421	3.49	B	3.50	B			-1.50	1.35	-
34BB	5.62	-160.79	-2.4	20	24375	3.26	O	3.36	O			-1.06	1.24	-
34BB	5.62	-160.79	-2.4	24	24867	3.34	B	3.26	B			-1.18	1.04	-

34BB	5.62	-160.79	-2.4	28	25358	3.32	O			-1.35	1.29	-
34BB	5.62	-160.79	-2.4	32	25850	3.83	O	3.99	O	-1.29	1.18	-
09MC	6.40	-160.77	-4.6	0.5	6657	3.91	B	3.94	O	-1.82	1.29	MH
06BB	6.41	-161.01	5.8	8.5	6443	4.03	B	4.04	B	-2.18	1.30	MH
06BB	6.41	-161.01	5.8	12.5	8868	3.79	B	4.05	B	-1.35	1.61	-
06BB	6.41	-161.01	5.8	16.5	11292	3.86	B	3.87	B	-1.41	1.30	-
06BB	6.41	-161.01	5.8	24.5	16141	3.38	B	3.45	B	-1.01	1.46	-
06BB	6.41	-161.01	5.8	28.5	18566	3.46	B			-1.00	1.44	-
06BB	6.41	-161.01	5.8	32.5	20189	3.08	B			-1.01	1.32	LGM
06BB	6.41	-161.01	5.8	36.5	21813	3.24	B			-1.04	1.40	LGM
06BB	6.41	-161.01	5.8	40.5	23436	3.34	B	3.38	B	-0.96	1.40	-
35BB	6.67	-160.73		0.5	13931	3.40	B					-
36BB	6.83	-161.04	-0.6	0.5		3.80	O	3.86	O	-2.08	1.11	-
36BB	6.83	-161.04	-0.6	2.5		3.81	O			-2.15	1.23	-
36BB	6.83	-161.04	-0.6	4.5	8378	4.00	O			-2.21	1.30	-
36BB	6.83	-161.04	-0.6	6.5	9332	3.97	O	4.12	O	-2.22	1.10	-
36BB	6.83	-161.04	-0.6	8.5	10286	4.08	O			-2.10	1.25	-
36BB	6.83	-161.04	-0.6	10.5	11240	3.93	O	3.74	O	-1.91	1.28	-
36BB	6.83	-161.04	-0.6	12.5	12194	3.90	O	3.74	O	-1.80	1.25	-
36BB	6.83	-161.04	-0.6	14.5	13148	3.57	O			-1.75	1.04	-
36BB	6.83	-161.04	-0.6	24.5	19674	3.25	O			-1.05	1.24	LGM
36BB	6.83	-161.04	-0.6	26.5	21090	3.33	O			-1.23	1.19	LGM
36BB	6.83	-161.04	-0.6	28.5	22506	3.38	O	3.67	O	-1.13	1.04	LGM
39MC	6.83	-161.04	-0.6	0.5	7833	3.88	O	3.87	O			MH
37BB	7.04	-161.63	-0.6	0	6619	3.76	T	4.19	B	-2.19	1.29	MH
37BB	7.04	-161.63	-0.6	4	8050	3.42	T	3.94	B	-2.10	1.15	-
37BB	7.04	-161.63	-0.6	8	9480	3.85	T	4.11	B	-1.94	1.11	-

37BB	7.04	-161.63	-0.6	12	10911	3.72	T	3.60	T	-1.91	1.19	-	
37BB	7.04	-161.63	-0.6	28	21399	3.43	B	3.04	T	-1.02	1.18	LGM	

B=CU Boulder, O=Old Dominion University, T=Texas A&M University

Table 4 ML1208 LGM and Holocene Time Slice Data

	Late Holocene (0-4 kyr BP)					Mid Holocene (4-8 kyr BP)					LGM (19-23 kyr BP)				
Core	Mg/Ca (mmol/mol)	s.e.	Dekens SST (°C)	s.e.	n	Mg/Ca (mmol/mol)	s.e.	Dekens SST (°C)	s.e.	n	Mg/Ca (mmol/mol)	s.e.	Dekens SST (°C)	s.e.	n
13BB/ 14MC	NaN	NaN	NaN	NaN	NaN	3.48	0.1	26.2	0.2	5	3.03	0.0	24.7	0.0	3
15GC	NaN	NaN	NaN	NaN	NaN	3.46	NaN	26.3	NaN	1	2.72	0.2	23.6	0.7	2
18GC	NaN	NaN	NaN	NaN	NaN	3.56	0.1	26.5	0.2	3	3.09	0.0	25.0	0.1	3
19GC	3.43	NaN	26.0	NaN	1	3.48	0.1	26.2	0.2	4	2.90	0.2	24.1	0.6	2
20BB/ 21MC	3.70	NaN	26.9	0.3	2	3.66	0.1	26.7	0.3	3	2.97	0.1	24.4	0.2	3
11GC	3.83	NaN	27.3	NaN	1	NaN	NaN	NaN	NaN	NaN	NaN	NaN	NaN	NaN	NaN
27BB	NaN	NaN	NaN	NaN	NaN	3.71	0.0	27.2	0.1	2	3.23	0.1	25.6	0.2	2
28BB	NaN	NaN	NaN	NaN	NaN	3.41	0.1	26.2	0.3	4	3.05	0.1	24.9	0.5	2
31BB	NaN	NaN	NaN	NaN	NaN	3.92	NaN	27.5	NaN	1	3.29	0.0	25.6	0.1	5
32BB/ 33MC	NaN	NaN	NaN	NaN	NaN	3.74	NaN	27.0	NaN	1	3.23	0.0	25.4	0.1	2
34BB	NaN	NaN	NaN	NaN	NaN	4.05	NaN	27.9	NaN	1	NaN	NaN	NaN	NaN	NaN
09MC	NaN	NaN	NaN	NaN	NaN	3.92	NaN	27.7	NaN	1	NaN	NaN	NaN	NaN	NaN

06BB	NaN	NaN	NaN	NaN	NaN	4.04	NaN	27.6	NaN	1	3.16	0.1	24.9	0.3	2
36BB/ 39MC	NaN	NaN	NaN	NaN	NaN	3.87	NaN	27.4	NaN	1	3.37	0.1	25.8	0.3	3
37BB	NaN	NaN	NaN	NaN	NaN	3.98	NaN	27.7	NaN	1	3.24	NaN	25.4	NaN	1

s.e.= standard error

Table 5 ML1208 Oxygen Isotope Time Slice Data

		Modern	Modern	Late Holocene (0-4 ka)			Mid Holocene (4-8 ka)			LGM (19-23 ka)		
	Lat (°N)	SSS (psu)	δ18Osw (permil, SMOW)	δ18Oc (permil, PDB)	Dekens SST (°C)	δ18Osw (permil, SMOW)	δ18Oc (permil, PDB)	Dekens SST (°C)	δ18Osw (permil, SMOW)	δ18Oc (permil, PDB)	Dekens SST (°C)	δ18Osw (permil, SMOW)
13BB/ 14MC	-0.22	35.26	0.64	NaN	NaN	NaN	-1.78	26.2	0.51	-0.55	24.7	1.43
15GC	0.16	35.26	0.64	NaN	NaN	NaN	-1.76	26.3	0.56	-0.46	23.6	1.30
18GC	0.59	35.21	0.63	NaN	NaN	NaN	-1.76	26.5	0.60	-0.51	25.0	1.52
19GC	0.83	35.16	0.61	-1.71	26.0	0.54	-1.94	26.2	0.35	-0.82	24.1	1.04
20BB/ 21MC	1.27	35.12	0.60	-2.10	26.9	0.32	-1.89	26.7	0.51	-0.77	24.4	1.15
11GC	1.47	35.12	0.60	-2.06	27.3	0.46	NaN	NaN	NaN	NaN	NaN	NaN
27BB	2.77	35.05	0.58	NaN	NaN	NaN	-1.89	27.2	0.60	-0.74	25.6	1.43
28BB	2.97	35.04	0.58	NaN	NaN	NaN	-1.89	26.2	0.39	-0.89	24.9	1.13
31BB	4.68	34.92	0.55	NaN	NaN	NaN	-2.14	27.5	0.43	-1.02	25.6	1.15

32BB/ 33MC	5.20	34.87	0.53	NaN	NaN	NaN	-2.10	27.0	0.36	-1.01	25.4	1.12
34BB	5.62	34.82	0.52	NaN	NaN	NaN	-2.04	27.9	0.62	NaN	NaN	NaN
09MC	6.40	34.69	0.49	NaN	NaN	NaN	-1.82	27.7	NaN	NaN	NaN	NaN
06BB	6.41	34.69	0.49	NaN	NaN	NaN	-2.18	27.6	0.40	-1.02	24.9	0.99
36BB/ 39MC	6.83	34.61	0.46	NaN	NaN	NaN	NaN	27.4	NaN	NaN	25.8	NaN
37BB	7.04	34.61	0.46	NaN	NaN	NaN	-2.19	27.7	0.40	-1.02	25.4	1.10

Table 6 Tropical (15 °N-15 °S) LGM *G. ruber* Data

Core	Lat (°N)	Lon (°E)	Depth (km)	SST (°C)	Modern ΔCO3 deep	LH Mg/Ca (mmol/mol)	LH Dekens + 0.6 °C	LGM estimated ΔCO3 deep	LGM Mg/Ca (mmol/mol)	LGM Dekens + 0.6 °C	Best estimate SST change	Cleaning Method	Ocean	Reference
KNR110-50	4.87	-43.21	3.995	27.82	20.5	3.96	27.3	-0.5	2.80	24.4	-3.0	R	A	Fehrenbacher et al., (2006)
KNR110-66	4.56	-43.38	3.547	27.82	30.5	4.00	27.0	9.5	2.73	23.7	-3.4	R	A	Fehrenbacher et al., (2006)
KNR110-82	4.33	-43.49	2.816	27.82	44.0	4.43	27.6	63.0	3.18	23.1	-4.5	R	A	Fehrenbacher et al., (2006)
ODP-999A	12.75	-78.73	2.827	28.08	23.1	4.15	27.8	42.1	3.39	24.7	-3.0	R	A	Schmidt et al., (2006)
PL07-39PC	10.70	-65.94	0.790	25.69	30.3	4.21	27.6	49.3	3.27	24.0	-3.6	R	A	Lea et al., (2003)
RC24-08	-1.34	-11.90	3.882	25.92	15.9	2.98	24.4	-5.1	2.66	24.0	-0.4	R	A	Arbuszewski et al., (2013)
RC24-11	-2.18	-11.25	3.445	25.96	21.2	3.24	25.1	0.2	2.55	23.3	-1.8	R	A	Arbuszewski et al., (2013)

VM12-107	11.33	-66.63	1.079	26.76	42.2	3.73	25.8	61.2	2.57	20.8	-4.9	R	A	Schmidt et al., (2012)
VM25-59	1.37	-33.48	3.824	27.66	22.5	3.97	27.3	1.5	2.53	23.2	-4.1	R	A	Arbuszewski et al., (2013)
VM28-122	11.93	-78.68	3.623	27.90	8.6	3.83	27.5	-12.4	3.34	26.8	-0.6	R	A	Schmidt et al., (2004)
VM30-40	-0.20	-23.15	3.706	26.78	15.6	3.35	25.7	-5.4	2.45	23.1	-2.6	R	A	Arbuszewski et al., (2013)
AAS9/21	14.51	72.65	1.807	28.54	13.7	4.94	28.9	13.7	3.67	25.6	-3.3	O	I	Govil et al., (2010)
GeoB10029-4	-1.49	100.13	0.964	29.33	18.5	5.07	29.0	18.5	3.87	26.0	-3.0	O	I	Mohtadi et al., (2010)
GeoB10038-4	-5.94	103.25	1.819	28.54	15.6	4.33	27.4	15.6	3.61	25.4	-2.0	O	I	Mohtadi et al., (2010)
GeoB10042-1	-7.11	104.64	2.454	28.36	11.5			11.5	3.45	25.0	-3.3	O	I	Setiawan et al., (2015)
GeoB10043-3	-7.31	105.06	2.171	28.30	13.6	4.32	27.4	13.6	3.53	25.2	-2.2	O	I	Setiawan et al., (2015)
GeoB10069-3	-9.01	120.02	1.250	28.47	17.2	4.01	27.6	17.2	3.49	26.1	-1.5	R	I	Gibbons et al., (2014)
GeoB12610-2	-4.82	39.42	0.399	27.61	50.0	4.63	26.7	50.0	3.99	25.0	-1.6	O	I	Rippert et al., (2015)
GeoB12615-4	-7.14	39.84	0.446	27.66	41.1	5.63	29.2	41.1	3.84	25.0	-4.2	O	I	Romahn et al., (2014)
GIK18459-3	-8.50	128.17	1.744	28.48	11.0	4.59	29.4	11.0	3.64	26.8	-2.6	R	I	Xu et al., (2010)
GIK18460-3	-8.79	128.64	1.875	28.50	9.8	4.67	29.6	9.8	3.35	25.9	-3.7	R	I	Xu et al., (2010)
GIK18462-3	-9.09	129.24	1.421	28.46	13.3	4.48	29.0	13.3	3.59	26.6	-2.5	R	I	Xu et al., (2010)
GIK18473-2	-11.52	122.42	2.468	28.67	8.1	4.67	29.7	8.1	4.27	28.7	-1.0	R	I	Xu et al., (2010)
GIK18475-3	-11.03	121.70	1.774	28.72	13.7	4.35	28.7	13.7	3.66	26.8	-1.9	R	I	Xu et al., (2010)
GIK18476-2	-10.95	120.99	0.986	28.73	20.3			20.3	3.59	26.3	-2.5	R	I	Xu et al., (2010)
GIK18477-4	-10.83	120.67	1.478	28.73	15.3	4.38	28.7	15.3	3.69	26.8	-1.9	R	I	Xu et al., (2010)
GIK18500-3	-14.98	120.70	1.167	28.12	18.5	5.20	30.5	18.5	4.00	27.5	-2.9	R	I	Xu et al., (2010)

GIK18507-3	-13.85	120.00	2.450	28.44	9.1	4.32	28.8	9.1	3.42	26.2	-2.6	R	I	Xu et al., (2010)
MD01-2378	-13.08	121.79	1.783	28.55	-0.7	4.63	30.0	-0.7	3.67	27.4	-2.6	R	I	Xu et al., (2008)
MD98-2161	-5.21	117.48	1.185	28.51	23.2	4.64	29.0	23.2	3.59	26.1	-2.9	R	I	Fan et al., (2018)
MD98-2162	-4.69	117.90	1.855	28.75	17.8	5.11	29.1	17.8	3.75	25.7	-3.4	O	I	Visser et al., (2003)
MD98-2165	-9.65	118.40	2.100	28.28	11.9	4.49	27.9	11.9	3.47	25.1	-2.9	O	I	Levi et al., (2007)
P178-15P	11.96	44.30	0.869	28.44	54.0	5.40	29.4	54.0	4.49	27.3	-2.1	R	I	Tierney et al., (2016)
SK157-4	2.67	78.00	3.500	29.07	1.9			1.9	3.61	27.1	-2.0	R	I	Saraswat et al., (2005)
SK237-GC04	10.98	75.00	1.245	27.87	15.4	4.54	29.1	15.4	3.58	26.4	-2.6	R	I	Saraswat et al., (2013)
SO139-74KL	-6.54	103.83	1.690	28.41	16.6	4.40	28.7	16.6	3.16	25.0	-3.4	R	I	Wang et al., (2018)
SO217-18515	-3.63	119.36	0.688	28.80	33.8	4.77	28.9	33.8	3.59	25.7	-3.2	R	I	Schröder et al., (2016)
SO217-18519	-0.57	118.11	1.658	29.06	18.2	4.67	29.3	18.2	3.58	26.3	-3.0	R	I	Schröder et al., (2018)
SO217-18522	1.40	119.08	0.975	29.08	16.4	4.68	29.4	16.4	3.75	26.9	-2.5	R	I	Schröder et al., (2018)
SO217-18526	3.61	118.17	1.524	29.57	18.2	4.72	29.4	18.2	3.60	26.4	-3.0	R	I	Schröder et al., (2018)
SO217-18540	-6.87	119.58	1.189	28.45	23.4	4.50	28.6	23.4	3.48	25.8	-2.9	R	I	Schröder et al., (2018)
TGS931	-2.41	122.62	1.912	28.22	16.7			16.7	3.62	26.5	-1.7	R	I	Schröder et al., (2018)
WIND28k	-10.15	51.01	4.157	27.26	-13.1			-13.1	3.01	24.5	-2.7	O	I	Kiefer et al., (2006)
3cBX	8.02	139.64	2.829	29.35	1.7	4.23	27.7	1.7	3.26	24.8	-2.9	O	P	Sagawa et al., (2012)
GeoB17426-3	-2.19	150.86	1.367	29.58	16.9	5.14	29.2	16.9	4.06	26.6	-2.6	O	P	Hollstein et al., (2018)
GIK17954-3	14.80	111.53	1.515	27.64	8.5	4.09	28.2	8.5	3.07	25.0	-3.2	R	P	Xu et al., (2010)
GIK17957-2	10.90	115.31	2.195	28.24	5.4	4.13	28.5	5.4	3.98	28.0	-0.4	R	P	Xu et al., (2010)

KX973-21-2	-1.42	157.98	1.897	29.50	11.0			11.0	3.73	27.1	-2.4	R	P	Dang et al., (2020)
MD01-2390	6.64	113.41	1.545	26.60	7.5	4.61	28.4	7.5	3.76	26.1	-2.3	O	P	Steinke et al., (2006)
MD02-2529	8.21	-84.12	1.619	27.81	2.1	3.80	27.7	2.1	3.03	25.1	-2.5	R	P	Leduc et al., (2007)
MD06-3067	6.51	126.50	1.575	29.20	7.6			7.6	3.78	27.4	-1.8	R	P	Bolliet et al., (2011)
MD10-3340	-0.52	128.72	1.094	28.51	14.6	4.66	29.4	14.6	3.59	26.5	-2.9	R	P	Dang et al., (2020)
MD97-2138	1.25	146.14	1.960	29.55	18.3	4.60	27.9	18.3	3.51	24.9	-3.0	O	P	de Garidel-Thoron et al., (2007)
MD97-2140	2.02	141.46	2.547	29.41	7.8			7.8	3.70	26.0	-3.4	O	P	de Garidel-Thoron et al., (2005)
MD97-2141	8.47	121.17	3.633	28.82	0.4			0.4	3.51	25.7	-3.1	O	P	Rosenthal et al., (2003)
MD98-2170	-10.59	125.39	0.832	28.89	24.0	5.35	30.5	24.0	4.14	27.7	-2.8	R	P	Stott et al., (2007)
MD98-2176	-5.00	133.44	2.382	27.77	7.8	5.08	30.6	7.8	3.99	28.0	-2.7	R	P	Stott et al., (2007)
MD98-2178	3.62	118.70	1.194	29.51	12.0	4.49	29.1	12.0	3.48	26.3	-2.8	R	P	Fan et al., (2018)
MD98-2181	6.30	125.83	2.114	29.21	9.3	5.19	30.8	9.3	3.96	27.8	-3.0	R	P	Stott et al., (2002)
ME005A-43JC	7.86	-83.61	1.368	27.79	2.9	4.12	27.3	2.9	3.33	25.0	-2.4	O	P	Benway et al., (2006)
ML1208-06GC	6.41	-161.01	2.371	28.02	5.8			5.8	3.16	25.5	-2.6	R	P	This study
ML1208-13BB	-0.22	-155.96	3.050	27.08	-0.8			-0.8	3.03	25.3	-1.8	R	P	This study
ML1208-15GC	0.16	-156.12	3.597	27.08	-5.0			-5.0	2.72	24.2	-2.8	R	P	This study
ML1208-18GC	0.59	-156.66	3.362	27.12	-3.2			-3.2	3.09	25.6	-1.5	R	P	This study
ML1208-19GC	0.83	-156.87	2.956	27.21	-0.1	3.43	26.6	-0.1	2.90	24.7	-1.9	R	P	This study
ML1208-20BB/21MC	1.27	-157.26	2.850	27.30	-0.3	3.58	27.1	-0.3	2.97	25.0	-2.1	R	P	This study

ML1208-27BB	2.77	-159.29	3.331	27.67	-7.3			-7.3	3.23	26.2	-1.4	R	P	This study
ML1208-28BB	2.97	-159.20	3.153	27.68	-5.1			-5.1	3.05	25.5	-2.2	R	P	This study
ML1208-31BB	4.68	-160.05	2.857	27.82	-1.0			-1.0	3.29	26.2	-1.6	R	P	This study
ML1208-32BB	5.20	-160.43	2.926	27.88	-1.9			-1.9	3.23	26.0	-1.8	R	P	This study
ML1208-36BB	6.83	-161.04	2.855	28.03	-0.6			-0.6	3.37	26.4	-1.6	R	P	This study
ML1208-37BB	7.04	-161.63	2.798	28.03	-0.6			-0.6	3.24	26.0	-2.0	R	P	This study
MV1014-08JC/07MC	6.23	-86.04	1.993	27.78	0.7	3.32	26.2	0.7	2.88	24.6	-1.6	R	P	Hertzberg et al., (2016)
MV1014-17JC/09MC	-0.18	-85.87	2.868	24.73	-3.0	2.46	23.0	-3.0	2.31	22.3	-0.7	R	P	Hertzberg et al., (2016)
ODP-1242	7.86	-83.61	1.364	27.79	2.9	4.33	29.1	2.9	3.32	26.1	-3.0	R	P	Lea et al., (2000)
ODP-806B	0.32	159.36	2.520	29.65	3.6			3.6	3.13	25.4	-4.2	R	P	Lea et al., (2000)
SO18480-3	-12.06	121.65	2.299	28.74	10.3	4.46	29.1	10.3	3.47	26.3	-2.4	R	P	Dang et al., (2020)
TR163-18	2.81	-89.85	2.030	26.61	0.7			0.7	2.39	22.6	-4.0	R	P	Lea et al., (2000)
TR163-19	2.26	-90.95	2.348	26.31	-0.8	2.99	25.1	-0.8	2.40	22.7	-2.4	R	P	Lea et al., (2000)
TR163-20B	0.79	-93.84	3.200	25.11	-6.1			-6.1	1.97	20.7	-4.4	R	P	Lea et al., (2000)
TR163-22	0.52	-92.40	2.830	24.41	-3.0	2.48	23.1	-3.0	2.12	21.4	-1.7	R	P	Lea et al., (2006)
V21-30	-1.22	-89.68	0.617	23.64	5.0	3.12	25.3	5.0	2.61	23.4	-2.0	R	P	Koutavas and Joanides, (2012)
VM28-234	-7.10	159.00	2.719	29.63	0.8	4.38	29.3	0.8	3.26	26.0	-3.3	R	P	This study

R= Reductive, O=Oxidative cleaning method
A=Atlantic, P=Pacific, I=Indian Ocean

Table 7 VM28-234 *G. ruber* Data

Depth (cm)	Mg/Ca (mmol/mol)	$\delta^{18}O$ (permil, PDB)	$\delta^{13}C$ (permil, PDB)
0	4.08	-2.30	
2	4.34	-2.55	
4	4.62	-2.67	1.50
6	4.49	-2.63	1.35
14	4.05	-2.77	1.63
16	4.27	-2.54	1.47
18	4.28	-2.57	1.50
20	4.31	-2.53	1.58
22	4.35	-2.62	1.55
24	4.17	-2.36	1.59
26	4.38	-2.57	1.38
28	4.42	-2.47	1.43
30	4.37	-2.46	1.51
32	3.69	-2.25	1.63
34	4.35	-2.49	1.21
36	4.52	-2.23	1.54
38	4.32	-2.31	1.34
40	4.39	-2.17	1.06
42	4.66	-2.48	1.28
44	4.24	-2.16	1.22
46	4.18	-2.30	1.17
48	4.65	-2.05	1.21
50	4.36	-2.35	0.92
52	4.28	-2.07	1.27
54	4.14	-2.04	1.04
56	4.04	-1.72	1.35
58	4.13	-2.08	1.07
60	3.97	-1.66	1.22
62	4.12	-2.00	1.39
64	4.07	-1.95	0.88
66	3.94	-1.97	1.03
68	4.04	-2.20	1.06
72	3.88	-1.87	1.14
74	3.82	-1.74	1.02
76	3.73	-2.09	1.08

78	3.92	-1.76	1.16
80	3.98	-1.81	1.00
82	4.16	-1.95	1.17
84	3.84	-1.93	0.95
86	3.98	-1.68	1.09
88	3.80	-1.94	0.93
90	3.36	-1.53	0.98
92	3.41	-1.41	0.84
94	3.47	-1.39	0.80
96	3.53	-1.27	1.16
98	3.44	-1.46	1.03
100	3.39	-1.16	1.49
102	3.31	-1.34	1.22
104	3.17	-1.24	1.23
106	3.08	-1.07	1.42
108	3.27	-1.10	1.07
110	3.11	-1.04	1.33
112	3.10	-1.20	1.44
114	3.02	-1.35	1.25
116	3.18	-1.49	1.22
118	3.04	-1.33	1.07
120	3.27	-1.05	1.32
122	3.22	-1.24	1.17
124	3.01	-1.27	1.17
126	3.10	-1.25	1.39
128	3.02	-1.39	0.99
136	3.36	-1.34	
138	3.43	-1.40	
140	3.30	-1.37	
144	3.39	-1.24	
146	3.08	-1.33	
148	3.37	-1.27	
150	3.11	-1.28	
152	3.25	-1.37	
154	3.03	-1.33	
156	3.20	-1.30	
158	3.16	-1.46	
160	3.21	-1.28	0.96
162	3.07	-1.42	
164	3.00	-1.71	

176	3.53	-1.37	
178	3.54	-1.38	
180	3.39	-1.40	1.02
182	3.38	-1.44	1.13
184	3.28	-1.37	1.31
186	3.42	-1.38	1.47
188	3.44	-1.42	1.23
190	3.25	-1.43	1.05
192	3.32	-1.52	1.40
194	3.35	-1.36	1.54
196	3.40	-1.54	1.38

Table 8 VM19-74 Isotope Data

Core	Depth (cm)	$\delta^{18}O$ (permil, PDB)	$\delta^{13}C$ (permil, PDB)	# Individuals	Species
VM19-74	0.5	-1.97	1.65	10	*G. ruber*
VM19-74	5.5	-2.16	1.54	10	*G. ruber*
VM19-74	10.5	-2.01	1.61	10	*G. ruber*
VM19-74	15.5	-1.71	1.36	10	*G. ruber*
VM19-74	20.5	-0.72	1.03	10	*G. ruber*
VM19-74	25.5	-0.98	1.11	10	*G. ruber*
VM19-74	30.5	-0.75	1.25	10	*G. ruber*
VM19-74	35.5	-0.64	1.53	10	*G. ruber*
VM19-74	40.5	-0.71	1.34	10	*G. ruber*
VM19-74	45.5	-0.75	1.50	10	*G. ruber*
VM19-74	50.5	-0.82	1.21	10	*G. ruber*
VM19-74	55.5	-0.95	1.25	10	*G. ruber*
VM19-74	60.5	-1.17	1.36	10	*G. ruber*
VM19-74	65.5	-1.11	1.38	10	*G. ruber*
VM19-74	70.5	-1.22	1.33	10	*G. ruber*
VM19-74	75.5	-1.28	1.19	10	*G. ruber*

Table 9 VM19-74 Trace Element Data

Core	Depth (cm)	Mg/Ca (mmol/mol)	Fe/Ca (mmol/mol)	Al/Ca (mmol/mol)	Mn/Ca (mmol/mol)	Lab
VM19-74	0	4.87	0			LDEO
VM19-74	0	4.85	25			LDEO
VM19-74	5	4.76	16			LDEO
VM19-74	10	4.92	103			LDEO
VM19-74	15	5.00	14			LDEO
VM19-74	15	5.04	13			LDEO
VM19-74	20	4.80	10			LDEO
VM19-74	20	4.32	16			LDEO
VM19-74	25	4.94	10			LDEO
VM19-74	25	4.78	26			LDEO
VM19-74	30	5.02	29			LDEO
VM19-74	30	4.68	37			LDEO
VM19-74	35	5.47	65			LDEO
VM19-74	35	5.26	25			LDEO
VM19-74	40	5.10	39			LDEO
VM19-74	40	5.16	13			LDEO
VM19-74	45	5.42	29			LDEO
VM19-74	45	5.49	69			LDEO
VM19-74	50	5.05	33			LDEO
VM19-74	50	5.19	159			LDEO
VM19-74	60	4.88	28			LDEO
VM19-74	60	4.68	59			LDEO
VM19-74	70	4.86	26			LDEO
VM19-74	70	5.07	43			LDEO
VM19-74	80	5.56	33			LDEO
VM19-74	0	4.19	4	14	4	TAMU
VM19-74	5	4.55	6	16	5	TAMU
VM19-74	5	4.15	4	20	4	TAMU
VM19-74	10	4.25	4	11	2	TAMU
VM19-74	10	4.45	3	11	2	TAMU
VM19-74	15	4.45	5	15	1	TAMU
VM19-74	15	4.45	3	11	1	TAMU
VM19-74	20	4.41	7	15	1	TAMU
VM19-74	20	4.38	5	13	1	TAMU
VM19-74	25	4.10	9	14	2	TAMU
VM19-74	25	4.08	5	8	2	TAMU

VM19-74	30	4.20	9	15	1	TAMU
VM19-74	30	4.47	9	11	1	TAMU
VM19-74	35	4.56	13	11	1	TAMU
VM19-74	35	4.28	12	17	1	TAMU
VM19-74	40	4.23	22	23	1	TAMU
VM19-74	40	4.38	12	10	1	TAMU
VM19-74	45	4.62	19	18	1	TAMU
VM19-74	45	4.33	22	31	1	TAMU
VM19-74	50	4.51	16	17	1	TAMU
VM19-74	50	4.39	15	15	1	TAMU
VM19-74	55	4.17	26	911	4	TAMU
VM19-74	55	4.33	13	15	1	TAMU
VM19-74	60	4.34	17	28	2	TAMU
VM19-74	60	4.19	14	18	1	TAMU
VM19-74	65	4.47	13	16	2	TAMU
VM19-74	65	4.53	12	11	2	TAMU
VM19-74	70	4.47	17	16	3	TAMU
VM19-74	75	5.05	17	19	2	TAMU
VM19-74	80	5.11	28	56	2	TAMU

Table 10 RC11-34TRI Isotope Data

Core	Depth (cm)	$\delta^{18}O$ (permil, PDB)	$\delta^{13}C$ (permil, PDB)	# Individuals	Species
RC11-34TRI	0	-1.61	1.34	15	*G. ruber*
RC11-34TRI	4	-1.66	1.35	15	*G. ruber*
RC11-34TRI	8	-1.86	1.38	15	*G. ruber*
RC11-34TRI	12	-1.86	1.03	15	*G. ruber*
RC11-34TRI	16	-1.58	1.11	15	*G. ruber*
RC11-34TRI	20	-1.84	1.37	15	*G. ruber*
RC11-34TRI	24	-1.19	1.09	15	*G. ruber*
RC11-34TRI	28	-1.43	1.15	15	*G. ruber*
RC11-34TRI	32	-1.67	1.24	15	*G. ruber*
RC11-34TRI	36	-1.73	1.23	15	*G. ruber*
RC11-34TRI	40	-1.57	1.22	15	*G. ruber*

Table 11 ML1208 Downcore Isotope and Trace Element Data

Core	Depth (cm)	$\delta^{18}O$ (permil, PDB)	Age (ka)	Mg/Ca (mmol/mol)	SST (°C)	Reproducibility (°C)
13BB	0.5	-1.46	5.0	3.34	25.7	0.2
13BB	4.5	-1.93	5.6	3.45	26.1	0.1
13BB	8.5	-1.94	6.2	3.43	26.0	0.3
13BB	12.5	-1.69	6.8	3.50	26.2	0.8
13BB	16.5	-1.58	9.1	3.37	25.8	0.2
13BB	20.5	-1.64	10.5	3.57	26.5	0.3
13BB	24.5	-1.44	11.8	3.45	26.1	0.1
13BB	28.5	-1.40	13.1	3.22	25.3	0.9
13BB	32.5	-0.78	15.2	3.15	25.1	0.3
13BB	36.5	-0.80	18.0	2.99	24.5	0.6
13BB	40.5	-0.55	19.9	3.03	24.6	0.3
13BB	44.5	-0.54	21.0	3.05	24.7	0.1
13BB	48.5	-0.54	22.9	3.02	24.6	0.2
13BB	52.5	-0.71	24.1	2.69	23.3	1.5
13BB	56.5	-0.68	26.6	2.61	23.0	0.9
13BB	60.5	-0.68	29.0	2.65	23.2	0.3
13BB	64.5	-0.73	30.6	2.74	23.5	1.1
13BB	72.5	-0.77	33.7	2.66	23.2	0.1
13BB	76.5	-0.93	35.2	2.66	23.2	0.4
13BB	80.5	-0.84	36.8	2.58	22.9	1.0
13BB	84.5	-1.05	38.3	2.66	23.2	1.8
13BB	88.5	-0.89	39.9	2.81	23.8	0.6
13BB	92.5	-0.87	41.4	2.79	23.7	0.3
13BB	96.5	-0.85	43.0	2.61	23.0	0.7
13BB	100.5	-0.82	44.6	2.67	23.2	1.2
13BB	104.5	-0.94	46.1	2.52	22.6	1.3
13BB	108.5	-0.81	47.7	2.59	22.9	0.1
13BB	112.5	-1.02	49.2	2.57	22.8	0.9
13BB	116.5	-1.02	50.8	2.55	22.7	0.5
13BB	120.5	-0.97	52.3	2.62	23.0	1.2
13BB	124.5	-1.00	53.9	2.82	23.9	0.1
13BB	128.5	-0.94	55.4	2.79	23.7	0.1
13BB	132.5	-0.89	57.0	2.80	23.7	0.0
13BB	136.5	-0.97	58.3	2.83	23.9	0.6
13BB	140.5	-0.85	59.5	2.66	23.2	0.3

13BB	144	-0.95	60.8	2.67	23.2	0.8
13BB	148		62.1	2.64	23.1	0.0
13BB	152	-0.75	63.4	2.37	21.9	0.2
13BB	156	-0.76	64.6	2.74	23.5	0.2
13BB	160	-1.05	65.9	2.69	23.3	0.4
13BB	176	-1.31	71.0	2.82	23.8	0.1
13BB	180	-1.43	73.6	3.09	24.9	0.2
13BB	184	-1.32	76.2	3.01	24.6	0.5
13BB	188	-0.99	78.8	2.84	23.9	0.2
13BB	192	-1.11	81.4	2.92	24.2	0.7
13BB	196	-1.12	84.0	2.78	23.7	0.2
13BB	200	-1.06	86.6	2.83	23.9	0.0
13BB	204	-1.27	89.2	2.86	24.0	0.0
13BB	208	-1.25	91.8	2.76	23.6	0.7
13BB	212	-1.23	94.4	2.83	23.9	0.0
13BB	216	-1.35	97.0	2.88	24.1	0.5
13BB	220	-1.18	99.6	2.98	24.5	0.1
13BB	224	-1.15	102.2	2.86	24.0	0.4
13BB	228	-1.26	104.8	2.87	24.0	0.0
13BB	232	-1.32	107.4	2.73	23.5	0.5
13BB	236	-1.18	110.0	2.81	23.8	0.1
13BB	240	-1.20	112.6	2.98	24.4	0.0
13BB	244	-1.51	115.2	3.32	25.6	3.2
13BB	248		117.8	2.77	23.6	0.0
13BB	252		120.4	3.26	25.5	0.0
13BB	256		123.0	3.66	26.7	0.5
13BB	260		124.4	3.41	26.0	0.3
13BB	264		125.8	3.45	26.1	0.9
13BB	268		127.2	3.45	26.1	0.7
13BB	272		128.6	3.55	26.4	0.2
13BB	276		130.0	3.42	26.0	0.0
13BB	280		131.6	3.32	25.6	0.1
13BB	284		133.2	3.07	24.8	0.4
13BB	288		134.8	2.82	23.9	0.6
13BB	292		136.4	2.88	24.1	0.1
13BB	296		138.0	2.83	23.9	0.1
13BB	300		139.6	2.96	24.4	0.0
13BB	304		141.2	2.91	24.2	0.7
13BB	308		142.8	2.82	23.9	0.3
13BB	316		146.0	2.90	24.2	0.3

13BB	320		147.6	2.88	24.1	0.7
13BB	324		149.2	2.99	24.5	0.2
13BB	328		150.8	2.78	23.7	1.1
13BB	332		152.4	2.89	24.1	0.9
13BB	336		154.0	2.84	23.9	0.8
13BB	340		155.6	2.88	24.1	0.9
13BB	344		157.2	2.80	23.8	0.2
13BB	348		158.8	2.71	23.4	0.1
13BB	352		160.4	2.77	23.6	0.9
13BB	356		162.0	2.73	23.5	0.5
31BB	12	-2.14	6.7	3.45	26.1	0.0
31BB	16	-2.06	7.5	3.74	27.0	0.1
31BB	20	-1.92	8.3	3.86	27.3	0.1
31BB	24	-1.86	9.2	3.81	27.2	0.2
31BB	28	-1.92	10.0	3.84	27.3	0.0
31BB	32	-1.76	10.8	3.97	27.6	0.0
31BB	36	-1.71	11.6	3.75	27.0	0.0
31BB	40	-1.63	13.0	3.49	26.2	0.0
31BB	44	-1.41	14.8	3.61	26.6	0.1
31BB	52	-1.26	17.7	3.00	24.5	0.0
31BB	60	-1.06	19.2	3.33	25.7	0.0
31BB	64	-0.99	19.7	3.38	25.8	0.0
31BB	68	-1.03	20.1	3.26	25.4	0.0
31BB	72	-0.96	20.6	3.26	25.4	0.0
31BB	76	-1.05	22.7	3.24	25.4	0.0
31BB	80	-1.15	24.8	3.17	25.1	0.0
31BB	88	-1.07	27.3	2.99	24.5	0.6
31BB	92	-1.16	27.7	2.99	24.5	0.3
31BB	96	-1.08	28.1	2.77	23.6	0.0
31BB	100	-1.13	28.5	2.84	23.9	0.7
31BB	104	-1.33	32.0	3.09	24.8	0.1
31BB	108	-1.29	35.6	3.02	24.6	0.2
31BB	112	-0.97	37.1	3.04	24.7	0.2
31BB	116	-1.47	38.5	3.14	25.0	0.4
31BB	120	-1.28	40.2	2.98	24.5	0.1
31BB	124	-1.39	41.8	3.01	24.6	0.3
31BB	128	-1.14	43.1	3.08	24.8	1.0
31BB	132	-1.29	44.7	3.19	25.2	0.1
31BB	136	-1.19	46.0	3.05	24.7	0.4
31BB	140	-1.24	47.0	3.07	24.8	0.0

31BB	144	-1.04	48.2	3.12	25.0	0.1
31BB	148	-1.28	49.3	2.90	24.1	0.2
31BB	152	-1.25	50.5	3.17	25.1	0.1
31BB	156	-1.18	51.5	2.86	24.0	0.3
31BB	160	-1.27	52.6	3.10	24.9	0.6
31BB	164	-1.28	53.8	2.85	23.9	0.2
31BB	168	-1.24	54.7	2.88	24.1	0.5
31BB	172	-1.31	55.7	3.19	25.2	0.3
31BB	176	-1.36	57.1	3.23	25.3	0.0
31BB	180	-1.35	58.0	3.10	24.9	0.2
31BB	184	-1.25	59.2	3.08	24.8	0.4
31BB	188	-1.24	60.4	3.24	25.4	0.0
31BB	192	-1.30	61.5	3.04	24.7	0.0
31BB	196	-1.14	62.5	3.10	24.9	0.2
31BB	200	-1.21	63.6	2.99	24.5	0.7
31BB	204.5	-1.18	65.0	2.97	24.4	0.2
31BB	208.5	-1.28	66.2	2.98	24.4	0.0
31BB	211.5	-1.06	67.1	2.88	24.1	0.6
31BB	215.5	-1.24	68.3	3.09	24.8	0.2
31BB	220.5	-1.21	69.8	3.35	25.7	0.4
31BB	224.5	-1.28	71.0	3.10	24.9	0.4
31BB	227.5	-1.23	71.8	3.25	25.4	0.1
31BB	231.5	-1.39	72.7	3.19	25.2	0.1
31BB	235.5	-1.19	73.7	3.26	25.4	0.5
31BB	240.5	-1.47	74.9	3.22	25.3	0.2
31BB	244.5	-1.28	75.8	3.57	26.5	0.2
31BB	247.5	-1.40	76.4	3.43	26.0	0.0
31BB	251.5	-1.52	77.6	3.32	25.7	0.2
31BB	256.5	-1.43	78.5	3.22	25.3	0.8
31BB	260.5	-1.47	79.5	3.27	25.5	0.1
31BB	265.5	-1.54	80.7	3.37	25.8	0.2
31BB	269.5	-1.52	81.6	3.68	26.8	1.9
31BB	272.5	-1.47	82.4	3.55	26.4	0.4
31BB	276.5	-1.32	83.6	3.51	26.3	0.2
31BB	280.5	-1.33	84.7	3.36	25.8	0.1
31BB	285.5	-1.23	85.9	3.51	26.3	0.4
31BB	289.5	-1.31	86.9	3.30	25.6	0.5
31BB	292.5	-1.25	87.6	3.51	26.3	0.2
31BB	296.5	-1.47	88.4	3.42	26.0	0.2
31BB	301.5	-1.39	89.8	3.27	25.5	0.5

31BB	305.5	-1.34	90.5	3.46	26.1	0.8
31BB	308.5	-1.26	91.3	3.44	26.0	0.8
31BB	312.5	-1.40	92.3	3.51	26.3	0.2
31BB	316.5	-1.59	93.5	3.40	25.9	0.4
31BB	321.5	-1.50	94.8	3.46	26.1	0.0
31BB	325.5	-1.69	96.2	3.51	26.3	0.3
31BB	328.5	-1.59	97.5	3.41	26.0	0.6
31BB	332.5	-1.54	99.3	3.43	26.0	0.5
31BB	337	-1.58	101.0	3.61	26.6	0.2
31BB	341	-1.45	102.9	3.40	25.9	0.9
31BB	344	-1.62	104.1	3.29	25.5	0.6
31BB	348	-1.61	105.8	3.65	26.7	0.5
31BB	351	-1.48	107.0	3.57	26.4	0.5
31BB	356	-1.54	108.7	3.55	26.4	0.0
31BB	359	-1.67	109.7	3.63	26.6	0.1
31BB	364	-1.68	111.3	3.69	26.8	0.1
31BB	368	-1.31	112.6	3.70	26.9	0.3
31BB	371	-1.64	113.6	3.97	27.6	0.1
31BB	376	-1.61	115.3	3.98	27.7	0.1
31BB	379	-2.15	116.7	3.98	27.7	0.5
31BB	384	-2.09	119.0	4.32	28.6	0.1
31BB	388	-1.79	120.7	4.26	28.4	0.2
31BB	391	-1.98	123.8	4.39	28.7	0.3
31BB	396	-1.89	126.7	4.34	28.6	0.1
31BB	400	-1.20	128.1	3.92	27.5	0.2
31BB	404	-1.75	129.1	4.28	28.5	0.3
31BB	408	-1.72	130.0	4.48	29.0	0.5
31BB	412	-1.64	131.0	4.16	28.2	0.1
31BB	416	-1.26	131.8	4.10	28.0	0.5
31BB	420	-1.37	132.7	3.87	27.4	0.1
31BB	424	-1.14	133.5	3.50	26.2	0.5
31BB	428	-1.10	134.5	3.65	26.7	0.1
31BB	432	-1.02	135.5	3.74	27.0	0.2
31BB	436	-1.21	136.4	3.60	26.6	0.7
31BB	440	-0.92	137.6	3.52	26.3	0.3
31BB	444	-1.01	139.3	3.48	26.2	0.1
31BB	448	-0.90	141.5	3.46	26.1	0.8
31BB	452	-0.81	143.0	3.39	25.9	0.1
37BB	0	-2.19	6.6	3.76	27.1	0.0
37BB	4	-2.10	8.1	3.50	26.2	0.6

37BB	8	-1.94	9.5	3.84	27.5	0.0
37BB	12	-1.91	10.9	3.66	26.7	0.4
37BB	16	-1.54	13.1	3.49	26.2	0.2
37BB	20	-1.16	15.2	3.30	25.7	0.4
37BB	24	-0.97	17.9	3.04	24.7	0.0
37BB	28	-1.02	21.4	3.04	24.7	0.0
37BB	32	-1.03	24.9	3.02	24.7	0.8
37BB	36	-1.19	28.4	2.99	24.6	0.1
37BB	40	-1.21	31.1	2.87	24.0	0.0
37BB	44	-1.27	33.8	2.86	24.2	0.0
37BB	48	-1.26	36.4	3.01	24.6	0.0
37BB	52	-1.41	39.1	2.81	24.0	0.0
37BB	56	-1.39	42.0	2.96	24.4	0.4
37BB	60	-1.42	48.4	2.98	24.5	0.2
37BB	64	-1.38	52.6	3.07	24.6	0.7
37BB	68	-1.41	55.7	2.99	24.5	0.0
37BB	72	-1.36	58.0	3.14	25.1	0.0
37BB	76	-1.30	61.5	2.92	24.2	0.3
37BB	80	-1.39	64.4	2.88	24.4	0.0
37BB	84	-1.21	67.7	2.83	24.2	0.0
37BB	88	-1.37	71.2	2.99	24.7	0.3
37BB	92	-1.32	74.1	2.93	24.2	0.5
37BB	100	-1.65	80.5	3.32	25.9	0.0
37BB	104	-1.64	83.0	3.27	25.8	0.1
37BB	112	-1.50	89.0	3.10	25.2	0.0
37BB	116	-1.59	92.1	3.17	25.4	0.0
37BB	120	-1.74	95.2	3.30	25.8	0.2
37BB	124	-1.86	99.1	3.27	25.7	0.2
37BB	128	-1.64	104.0	3.31	26.1	0.6
37BB	132	-1.66	108.7	3.39	26.5	0.0
37BB	136	-1.76	113.5	3.36	26.3	0.0
37BB	140	-1.97	117.5	3.88	27.9	0.0
37BB	144	-1.95	123.7	3.92	27.7	0.2
37BB	148	-1.90	127.5	3.94	27.7	0.4
37BB	152	-1.58	131.0	3.98	27.8	0.1
37BB	156	-1.14	134.1	3.80	27.2	0.0
37BB	160	-0.99	137.5	3.39	25.7	0.4
37BB	164	-0.88	141.0	3.20	25.3	0.4
37BB	168	-0.94	144.1	3.05	24.8	0.4
37BB	172	-0.97	148.5	3.16	25.1	0.8

37BB	176	-0.95	153.0	3.24	25.4	0.6
37BB	180	-0.81	156.1	3.24	25.4	0.2
37BB	184	-0.98	159.9	3.14	25.1	0.5
37BB	188	-0.86	163.6	3.14	25.1	0.3
37BB	192	-1.06	168.2	3.22	25.3	0.1
37BB	196	-1.14	174.0	3.01	24.6	0.2
37BB	200	-1.22	180.0	2.97	24.4	0.0

REFERENCES

Adkins, J. F., & Schrag, D. P. (2001). Pore fluid constraints on deep ocean temperature and salinity during the last glacial maximum. *Geophysical Research Letters*, *28*(5), 771–774.

Amante, C., & Eakins, B. W. (2009). ETOPO1 1 arc-minute global relief model: Procedures, data sources and analysis. *NOAA Tech. Mem. NESDIS*. https://doi.org/10.1594/PANGAEA.769615

An, S. Il, & Choi, J. (2014). Mid-Holocene tropical Pacific climate state, annual cycle, and ENSO in PMIP2 and PMIP3. *Climate Dynamics*, *43*(3–4), 957–970. https://doi.org/10.1007/s00382-013-1880-z

Anand, P., Elderfield, H., & Conte, M. H. (2003). Calibration of Mg/Ca thermometry in planktonic foraminifera from a sediment trap time series. *Paleoceanography*, *18*(2). https://doi.org/10.1029/2002PA000846

Anderson, D. M., & Archer, D. (2002). Glacial-interglacial stability of ocean pH inferred from foraminifer dissolution rates. *Nature*, *416*(6876), 70–73. https://doi.org/10.1038/416070a

Annan, J. D., & Hargreaves, J. C. (2013). A new global reconstruction of temperature changes at the Last Glacial Maximum. *Climate of the Past*, *9*(1), 367–376. https://doi.org/10.5194/cp-9-367-2013

Arbuszewski, J., deMenocal, P., Kaplan, A., & Farmer, E. C. (2010). On the fidelity of shell-derived δ18Oseawater estimates. *Earth and Planetary Science Letters*, *300*(3–4), 185–196. https://doi.org/10.1016/j.epsl.2010.10.035

Arrhenius, G. (1952). Sediment cores from the east Pacific. *Reports of the Swedish Deep-Sea Expedition, 1947-1948*, *5*, 201p

Ballantyne, A. P., Lavine, M., Crowley, T. J., Liu, J., & Baker, P. B. (2005). Meta-analysis of tropical surface temperatures during the Last Glacial Maximum. *Geophysical Research Letters*, *32*(5), 1–4. https://doi.org/10.1029/2004GL021217

Barker, S., Greaves, M., & Elderfield, H. (2003). A study of cleaning procedures used for foraminiferal Mg/Ca paleothermometry. *Geochemistry, Geophysics, Geosystems*, *4*(9), 1–20. https://doi.org/10.1029/2003GC000559

Bemis, B. E., Spero, H. J., & Lea, D. W. (1998). Reevaluation of the oxygen isotopic composition of planktonic foraminifera : Experimental results and revised paleotemperature equations. *Paleoceanography*, *13*(2), 150–160.

Benway, H. M., Mix, A. C., Haley, B. A., & Klinkhammer, G. P. (2006). Eastern Pacific Warm Pool paleosalinity and climate variability: 0-30 kyr. *Paleoceanography*. https://doi.org/10.1029/2005PA001208

Bolliet, T., Holbourn, A., Kuhnt, W., Laj, C., Kissel, C., Beaufort, L., … Garbe-Schöberg, D. (2011). Mindanao Dome variability over the last 160 kyr: Episodic

glacial cooling of the West Pacific Warm Pool. *Paleoceanography*, *26*(1). https://doi.org/10.1029/2010PA001966

Bova, S., Rosenthal, Y., Liu, Z., Godad, S. P., & Yan, M. (2021). Seasonal origin of the thermal maxima at the Holocene and the last interglacial. *Nature*, *589*(July 2020). https://doi.org/10.1038/s41586-020-03155-x

Boyer, T. P., Antonov, J. I., Baranova, O. K., Coleman, C., Garcia, H. E., Grodsky, A., … Sullivan, K. D. (2013). World Ocean Database 2013, NOAA Atlas NESDIS 72. *Sydney Levitus, Ed.; Alexey Mishonoc, Technical Ed., NOAA Atlas*, 209 pp. https://doi.org/10.7289/V5NZ85MT

Boyle, E. A. (1983). Manganese carbonate overgrowths on foraminifera tests. *Geochimica et Cosmochimica Acta*, *47*(10), 1815–1819. https://doi.org/10.1016/0016-7037(83)90029-7

Boyle, E., & Rosenthal, Y. (1996). Chemical Hydrography of the South Atlantic During the Last Glacial Maximum: Cd vs. δ13C. In *The South Atlantic* (pp. 423–443). Berlin, Heidelberg: Springer Berlin Heidelberg. https://doi.org/10.1007/978-3-642-80353-6_23

Braconnot, P., Otto-Bliesner, B., Harrison, S., Joussaume, S., Peterchmitt, J. Y., Abe-Ouchi, A., … Zhao, Y. (2007). Results of PMIP2 coupled simulations of the Mid-Holocene and last glacial maximum - Part 1: Experiments and large-scale features. *Climate of the Past*, *3*(2), 261–277. https://doi.org/10.5194/cp-3-261-2007

Brady, E. C., Otto-Bliesner, B. L., Kay, J. E., & Rosenbloom, N. (2013). Sensitivity to glacial forcing in the CCSM4. *Journal of Climate*, *26*(6), 1901–1925. https://doi.org/10.1175/JCLI-D-11-00416.1

Chalk, T. B., Foster, G. L., & Wilson, P. A. (2019). Dynamic storage of glacial CO 2 in the Atlantic Ocean revealed by boron 3] and pH records. *Earth and Planetary Science Letters*, *510*, 1–11. https://doi.org/10.1016/j.epsl.2018.12.022

CLIMAP Project Members. (1976). Modeling the ice-age climate. *Science (New York, N.Y.)*, *191*(4232), 1138–1144. https://doi.org/10.1126/science.191.4232.1138

Colleoni, F., Wekerle, C., Näslund, J.-O., Brandefelt, J., & Masina, S. (2016). Constraint on the penultimate glacial maximum Northern Hemisphere ice topography (~140 kyrs BP), *137*. https://doi.org/10.1016/j.quascirev.2016.01.024

Crowley, T. J. (2000). CLIMAP SSTs re-revisited. *Climate Dynamics*, *16*, 241–255.

Dai, Y., Yu, J., deMenocal, P., & Hyams-Kaphzan, O. (2019). Influences of Temperature and Secondary Environmental Parameters on Planktonic Foraminiferal Mg/Ca: A New Core-Top Calibration. *Geochemistry, Geophysics, Geosystems*, 1–12. https://doi.org/10.1029/2019gc008526

Dang, H., Jian, Z., Wang, Y., Mohtadi, M., Rosenthal, Y., Ye, L., … Kuhnt, W. (2020). Pacific warm pool subsurface heat sequestration modulated Walker circulation and ENSO activity during the Holocene, 1–9.

de Garidel-Thoron, T., Rosenthal, Y., Bassinot, F., & Beaufort, L. (2005). Stable sea surface temperatures in the western Pacific warm pool over the past 1.75 million years. *Nature*. https://doi.org/10.1038/nature03189

de Garidel-Thoron, T., Rosenthal, Y., Beaufort, L., Bard, E., Sonzogni, C., & Mix, A. C. (2007). A multiproxy assessment of the western equatorial Pacific hydrography during the last 30 kyr. *Paleoceanography*, *22*(3), 1–18. https://doi.org/10.1029/2006PA001269

Dekens, P. S., Lea, D. W., Pak, D. K., & Spero, H. J. (2002). Core top calibration of Mg/Ca in tropical foraminifera: Refining paleotemperature estimation. *Geochemistry, Geophysics, Geosystems*, *3*(4), 1–29. https://doi.org/10.1029/2001gc000200

Dickson, A. G., & Millero, F. J. (1987). A comparison of the equilibrium constants for the dissociation of carbonic acid in seawater media. *Deep Sea Research Part A, Oceanographic Research Papers*. https://doi.org/10.1016/0198-0149(87)90021-5

Dickson, Andrew G. (1990). Standard potential of the reaction: AgCl(s) + 1 2H2(g) = Ag(s) + HCl(aq), and and the standard acidity constant of the ion HSO4- in synthetic sea water from 273.15 to 318.15 K. *The Journal of Chemical Thermodynamics*. https://doi.org/10.1016/0021-9614(90)90074-Z

DiNezio, P., Clement, A., Vecchi, G. A., Soden, B., Broccoli, A. J., Otto-Bliesner, B. L., & Braconnot, P. (2011). The response of the Walker circulation to Last Glacial Maximum forcing: Implications for detection in proxies. *Paleoceanography*, *26*(3), 1–21. https://doi.org/10.1029/2010PA002083

Dyez, K. A., & Ravelo, A. C. (2013). Late Pleistocene tropical Pacific temperature sensitivity to radiative greenhouse gas forcing. *Geology*, *41*(1), 23–26. https://doi.org/10.1130/G33425.1

Dyez, K. A., & Ravelo, A. C. (2014). Dynamical changes in the tropical Pacific warm pool and zonal SST gradient during the Pleistocene. *Geophysical Research Letters*, *41*(21), 7626–7633. https://doi.org/10.1002/2014GL061639

Dyke, A. S., Andrews, J. T., Clark, P. U., England, J. H., Miller, G. H., Shaw, J., & Veillette, J. J. (2002). The Laurentide and Innuitian ice sheets during the Last Glacial Maximum, *21*, 9–31.

Evans, D., Wade, B. S., Henehan, M., Erez, J., & Müller, W. (2016). Revisiting carbonate chemistry controls on planktic foraminifera Mg / Ca: implications for sea surface temperature and hydrology shifts over the Paleocene–Eocene Thermal Maximum and Eocene–Oligocene transition. *Climate of the Past*, *12*(4), 819–835. https://doi.org/10.5194/cp-12-819-2016

Farrell, J. W., & Prell, W. L. (1989). Climatic change and CaCO3 preservation: An 800,000 year bathymetric Reconstruction from the central equatorial Pacific Ocean. *Paleoceanography*, *4*(4), 447–466. https://doi.org/10.1029/PA004i004p00447

Fehrenbacher, J., & Martin, P. (2011). Western equatorial Pacific deep water carbonate chemistry during the Last Glacial Maximum and deglaciation: Using planktic foraminiferal Mg/Ca to reconstruct sea surface temperature and seafloor dissolution. *Paleoceanography*, *26*(2), https://doi.org/10.1029/2010PA002035

Ferguson, J. E., Henderson, G. M., Kucera, M., & Rickaby, R. E. M. (2008). Systematic change of foraminiferal Mg/Ca ratios across a strong salinity gradient. *Earth and Planetary Science Letters*, *265*(1–2), 153–166. https://doi.org/10.1016/j.epsl.2007.10.011

Gray, W. R., & Evans, D. (2019). Nonthermal Influences on Mg/Ca in Planktonic Foraminifera: A Review of Culture Studies and Application to the Last Glacial Maximum. *Paleoceanography and Paleoclimatology*, *34*(3), 306–315. https://doi.org/10.1029/2018PA003517

Gray, W. R., Weldeab, S., Lea, D. W., Rosenthal, Y., Gruber, N., Donner, B., & Fischer, G. (2018). The effects of temperature, salinity, and the carbonate system on Mg/Ca in Globigerinoides ruber (white): A global sediment trap calibration. *Earth and Planetary Science Letters*, *482*, 607–620. https://doi.org/10.1016/j.epsl.2017.11.026

Greene, C. A., Thirumalai, K., Kearney, K. A., Delgado, J. M., Schwanghart, W., Wolfenbarger, N. S., et al. (2019). The climate data toolbox for MATLAB. *Geochemistry, Geophysics, Geosystems*, 20, 3774– 3781. https://doi.org/10.1029/2019GC008392

Greaves, M., Caillon, N., Rebaubier, H., Bartoli, G., Bohaty, S., Cacho, I., … Eggins, S. (2008). Interlaboratory comparison study of calibration standards for foraminiferal Mg/Ca thermometry. *Geochemistry Geophysics Geosystems*, *9*(8). https://doi.org/10.1029/2008GC001974

Gwizd, S. J., & Lea, D. W. (2020). Marine Micropaleontology A new Upper and Middle Pleistocene stratigraphic and dissolution record from the Carnegie Platform , Eastern Equatorial Paci fi c. *Marine Micropaleontology*, *157*, 101857. https://doi.org/10.1016/j.marmicro.2020.101857

Hargreaves, J. C., Annan, J. D., Yoshimori, M., & Abe-Ouchi, A. (2012). Can the Last Glacial Maximum constrain climate sensitivity? *Geophysical Research Letters*, *39*(24), 2014. https://doi.org/10.1029/2012GL053872

Hertzberg, J. E., & Schmidt, M. W. (2013). Refining Globigerinoides ruber Mg/Ca paleothermometry in the Atlantic Ocean. *Earth and Planetary Science Letters*, *383*, 123–133. https://doi.org/10.1016/j.epsl.2013.09.044

Hertzberg, J. E., Schmidt, M. W., Bianchi, T. S., Smith, R. K., Shields, M. R., & Marcantonio, F. (2016). Comparison of eastern tropical Pacific TEX86 and Globigerinoides ruber Mg/Ca derived sea surface temperatures: Insights from the Holocene and Last Glacial Maximum. *Earth and Planetary Science Letters*, *434*, 320–332. https://doi.org/10.1016/j.epsl.2015.11.050

Hoffman, J. S., Parnell, A. C., & He, F. (2017). Regional and global sea-surface

temperatures during the last interglaciation, *Science, 279*, 276–279.

Hollstein, M., Mohtadi, M., Rosenthal, Y., Moffa Sanchez, P., Oppo, D., Martínez Méndez, G., … Hebbeln, D. (2017). Stable Oxygen Isotopes and Mg/Ca in Planktic Foraminifera From Modern Surface Sediments of the Western Pacific Warm Pool: Implications for Thermocline Reconstructions. *Paleoceanography*, *32*(11), 1174–1194. https://doi.org/10.1002/2017PA003122

Hopcroft, P. O., & Valdes, P. J. (2015). Last glacial maximum constraints on the Earth System model HadGEM2-ES. *Climate Dynamics*, *45*(5–6), 1657–1672. https://doi.org/10.1007/s00382-014-2421-0

IPCC (2021). *Climate Change 2021. The Physical Science Basis. Contribution of Working Group 1 to Sixth Assessment Report of the Intergovernmental Panel on Climate Change*.

Jacobel, A. W., McManus, J. F., Anderson, R. F., & Winckler, G. (2017). Climate-related response of dust flux to the central equatorial Pacific over the past 150 kyr. *Earth and Planetary Science Letters*, *457*, 160–172. https://doi.org/10.1016/j.epsl.2016.09.042

Khider, D., Huerta, G., Jackson, C., Stott, L. D., & Emile-Geay, J. (2015). A Bayesian, multivariate calibration for Globigerinoides ruber Mg/Ca. *Geochemistry, Geophysics, Geosystems*. https://doi.org/10.1002/2015GC005844

Kienast, M., Steinke, S., Stattegger, K., & Calvert, S. E. (2001). Synchronous Tropical South China Sea SST Change and Greenland Warming During Deglaciation. *Science*, *291*(5511), 2132–2134. https://doi.org/10.1126/SCIENCE.1057131

Kim, S. T., & O'Neil, J. R. (1997). Equilibrium and nonequilibrium oxygen isotope effects in synthetic carbonates. *Geochimica et Cosmochimica Acta*, *61*(16), 3461–3475. https://doi.org/10.1016/S0016-7037(97)00169-5

Kisakürek, B., Eisenhauer, A., Böhm, F., Garbe-Schönberg, D., & Erez, J. (2008). Controls on shell Mg/Ca and Sr/Ca in cultured planktonic foraminiferan, Globigerinoides ruber (white). *Earth and Planetary Science Letters*, *273*(3–4), 260–269. https://doi.org/10.1016/j.epsl.2008.06.026

Knutti, R.., Rugenstein, M.A.A., & Hegerl, G.C. (2017) Beyond equilibrium climate sensitivity. *Nature Geoscience*, 10, 727-736.

Koutavas, A, Lynch-Stieglitz, J., Marchitto, T. M., & Sachs, J. P. (2002). El Niño-like pattern in ice age tropical Pacific sea surface temperature. *Science, 297*, 226–230. Retrieved from http://dx.doi.org/10.1126/science.1072376

Koutavas, A, & Sachs, J. P. (2008). Northern timing of deglaciation in the eastern equatorial Pacific from alkenone paleothermometry. *Paleoceanography*, 4205. https://doi.org/10.1029/2008PA001593

Koutavas, Athanasios, & Joanides, S. (2012). El Niño-Southern Oscillation extrema in the Holocene and Last Glacial Maximum. *Paleoceanography, 27*(4), 1–15. https://doi.org/10.1029/2012PA002378

Lalicata, J. J., & Lea, D. W. (2011). Pleistocene carbonate dissolution fluctuations in the eastern equatorial Pacific on glacial timescales: Evidence from ODP Hole 1241. *Marine Micropaleontology*, *79*(1–2), 41–51. https://doi.org/10.1016/J.MARMICRO.2011.01.002

Lambeck, K., & Chappell, J. (2001). Sea Level Change Through the Last Glacial Cycle, *292*(April), 679–687.

Lea, D. W., Mashiotta, T. A., & Spero, H. J. (1999). Controls on magnesium and strontium uptake in planktonic foraminifera determined by live culturing. *Geochimica et Cosmochimica Acta*, *63*(16), 2369–2379. https://doi.org/10.1016/S0016-7037(99)00197-0

Lea, D. W., Pak, D. K., & Spero, H. J. (2000). Climate impact of late quaternary equatorial Pacific sea surface temperature variations. *Science*, *289*(5485), 1719–1724. https://doi.org/10.1126/science.289.5485.1719

Lea, David W. (2004). The 100 000-yr cycle in tropical SST, greenhouse forcing, and climate sensitivity. *Journal of Climate*, *17*(11), 2170–2179. https://doi.org/10.1175/1520-0442(2004)017<2170:TYCITS>2.0.CO;2

Lea, D. W., Pak, D. K., & Paradis, G. L. (2005). Influence of volcanic shards on foraminiferal Mg/Ca in a core from.the Galápagos region. *Geochemistry, Geophysics, Geosystems*, *6*(11).

Lea, David W., Pak, D. K., Belanger, C. L., Spero, H. J., Hall, M. A., & Shackleton, N. J. (2006). Paleoclimate history of Galápagos surface waters over the last 135,000 yr. *Quaternary Science Reviews*, *25*(11–12), 1152–1167. https://doi.org/10.1016/J.QUASCIREV.2005.11.010

Lea, David W, Pak, D. K., Peterson, L. C., & Hughen, K. A. (2003). Synchroneity of Tropical and High-Latitude Atlantic Temperatures over the Last Glacial Termination. *Science*, *301*, 1361–1365.

Leduc, G., Vidal, L., Tachikawa, K., Rostek, F., Sonzogni, C., Beaufort, L., & Bard, E. (2007). Moisture transport across Central America as a positive feedback on abrupt climatic changes. *Nature*, *445*(7130), 908–911. https://doi.org/10.1038/nature05578

LeGrande, A. N., & Schmidt, G. A. (2006). Global gridded data set of the oxygen isotopic composition in seawater. *Geophysical Research Letters*, *33*(12), 1–5. https://doi.org/10.1029/2006GL026011

Levitus, S., & Boyer, T. P. (1994). *World Ocean Atlas 1994*. *Temperature, NOAA Atlas NESDIS 4*.

Lewis, E., & Wallace, D. W. R. (1998). CO2SYS - Program developed for the CO2 system calculations. *ORNL/CDIAC-105 (Ed Center CDIA)*. https://doi.org/4735

Lin, L., Khider, D., Lisiecki, L. E., & Lawrence, C. E. (2014). Probabilistic sequence alignment of stratigraphic records. *Paleoceanography*, *29*, 976–989.

Liu, Z., Herbert, T. (2004) High-latitude influence on the eastern equatorial Pacific climate in the early Pleistocene epoch. *Nature* **427,** 720–723. https://doi.org/10.1038/nature02338

Lynch-Stieglitz, J., Polissar, P. J., Jacobel, A. W., Hovan, S. A., Pockalny, R. A., Lyle, M., … Xie, R. C. (2015). Glacial-interglacial changes in central tropical Pacific surface seawater property gradients. *Paleoceanography*, *30*(5), 423–438. https://doi.org/10.1002/2014PA002746

Marchitto, T. M., Lynch-Stieglitz, J., & Hemming, S. R. (2005). Deep Pacific CaCO3 compensation and glacial-interglacial atmospheric CO2. *Earth and Planetary Science Letters*. https://doi.org/10.1016/j.epsl.2004.12.024

Mathien-Blard, E., & Bassinot, F. (2009). Salinity bias on the foraminifera Mg/Ca thermometry: Correction procedure and implications for past ocean hydrographic reconstructions. *Geochemistry, Geophysics, Geosystems*, *10*(12). https://doi.org/10.1029/2008GC002353

McKay, N. P., Overpeck, J. T., & Otto-Bliesner, B. L. (2011). The role of ocean thermal expansion in Last Interglacial sea level rise. *Geophysical Research Letters*, *38*(14), 4–9. https://doi.org/10.1029/2011GL048280

Mehrbach, C., Culberson, C. H., Hawley, J. E., & Pytkowicx, R. M. (1973). MEASUREMENT OF THE APPARENT DISSOCIATION CONSTANTS OF CARBONIC ACID IN SEAWATER AT ATMOSPHERIC PRESSURE. *Limnology and Oceanography*. https://doi.org/10.4319/lo.1973.18.6.0897

Mix, A. C., Morey, A. E., Pisias, N. G., & Hostetler, S. W. (1999). Foraminiferal faunal estimates of paleotemperature: Circumventing the no-analog problem yields cool ice age tropics. *Paleoceanography*, *14*(3), 350–359.

Monteagudo, M., Lynch-Stieglitz, J., Marchitto, T. M., & Schmidt, M. W. (2021). Central Equatorial Pacific Cooling During the Last Glacial Maximum. *Geophysical Research Letters*, *48*. https://doi.org/10.1029/2020GL088592

Nürnberg, D., Bijma, J., & Hemleben, C. (1996). Assessing the reliability of magnesium in foraminiferal calcite as a proxy for water mass temperatures. *Geochimica et Cosmochimica Acta*, *60*(5), 803–814. https://doi.org/10.1016/0016-7037(95)00446-7

Otto-Bliesner, B. L., Schneider, R., Brady, E. C., Kucera, M., Abe-Ouchi, A., Bard, E., … Yu, Y. (2009). A comparison of PMIP2 model simulations and the MARGO proxy reconstruction for tropical sea surface temperatures at last glacial maximum. *Climate Dynamics*, *32*(6), 799–815. https://doi.org/10.1007/s00382-008-0509-0

Otto-Bliesner, B. L., Brady, E. C., Zhao, A., Brierley, C. M., Axford, Y., Capron, E., … Tzedakis, P. C. (2021). Large-scale features of Last Interglacial climate : results from evaluating the lig127k simulations for the Coupled Model Intercomparison Project (CMIP6)– Paleoclimate Modeling Intercomparison Project (PMIP4), 63–94.

Otto-Bliesner, B. L., Rosenbloom, N., Stone, E. J., Mckay, N. P., Lunt, D. J., Brady, E. C., & Overpeck, J. T. (2013). How warm was the last interglacial? new model-data comparisons. *Philosophical Transactions of the Royal Society A: Mathematical, Physical and Engineering Sciences*, *371*(2001). https://doi.org/10.1098/rsta.2013.0097

Pelejero, C., Grimalt, J., Heilig, S; Kienast, M., Wang, L. (1999) High-resolution UK37 temperature reconstructions in the South China Sea over the past 220 kyr. Paleoceanography, 14(2), 224-231, https://doi.org/10.1029/1998PA900015

Prahl, F. G., Muehlhausen, L. A., & Zahnle, D. L. (1988). Further evaluation of long-chain alkenones as indicators of paleoceanographic conditions. *Geochimica et Cosmochimica Acta*. https://doi.org/10.1016/0016-7037(88)90132-9

Qin, B., Li, T., Xiong, Z., Algeo, T. J., & Chang, F. (2017). Deepwater carbonate ion concentrations in the western tropical Pacific since 250 ka: Evidence for oceanic carbon storage and global climate influence. *Paleoceanography*, *32*(4), 351–370. https://doi.org/10.1002/2016PA003039

Rabineau, M., Berné, S., Olivet, J., Aslanian, D., Guillocheau, F., & Joseph, P. (2006). Paleo sea levels reconsidered from direct observation of paleoshoreline position during Glacial Maxima (for the last 500,000 yr), *252*, 119–137. https://doi.org/10.1016/j.epsl.2006.09.033

Regenberg, M., Regenberg, A., Garbe-Schönberg, D., & Lea, D. W. (2014). Global dissolution effects on planktonic foraminiferal Mg/Ca ratios controlled by the calcite-saturation state of bottom waters. *Paleoceanography*, *29*, 127–142. https://doi.org/10.1002/2013PA002492.

Reimer, P. J., Bard, E., Beck, A., Blackwell, J. W., Ramsey, B., & Van Der Plicht, C. (2013). IntCal13 and Marine13 Radiocarbon Age Calibration Curves 0-50,000 Years Cal BP. *Radiocarbon*, *55*(4), 1869–1887. https://doi.org/10.2458/azu_js_rc.55.16947

Rincón-Martínez, D., Lamy, F., Contreras, S., Leduc, G., Bard, E., Saukel, C., Blanz, T., Mackensen, A., and Tiedemann, R. (2010), More humid interglacials in Ecuador during the past 500 kyr linked to latitudinal shifts of the equatorial front and the Intertropical Convergence Zone in the eastern tropical Pacific, *Paleoceanography*, 25, PA2210, doi:10.1029/2009PA001868.

Rind, D., & Peteet, D. (1985). Terrestrial conditions at the Last Glacial Maximum and CLIMAP sea-surface temperature estimates: Are they consistent? *Quaternary Research*, *24*(1), 1–22. https://doi.org/10.1016/0033-5894(85)90080-8

Rippert, N., Nürnberg, D., Raddatz, J., Maier, E., Hathorne, E., Bijma, J., & Tiedemann, R. (2016). Constraining foraminiferal calcification depths in the western Pacific warm pool. *Marine Micropaleontology*, *128*, 14–27. https://doi.org/10.1016/j.marmicro.2016.08.004

Rongstad, B. L., Marchitto, T. M., & Herguera, J. C. (2017). Understanding the Effects of

Dissolution on the Mg/Ca Paleothermometer in Planktic Foraminifera: Evidence From a Novel Individual Foraminifera Method. *Paleoceanography*, *32*(12), 1386–1402. https://doi.org/10.1002/2017PA003179

Rongstad, B. L., Marchitto, T. M., Marks, G. S., Koutavas, A., Mekik, F., & Ravelo, A. C. (2019). *Investigating ENSO-related temperature variability in equatorial Pacific core-tops using Mg/Ca in individual planktic foraminifera*. *Paleoceanography and Paleoclimatology*. https://doi.org/10.1029/2019PA003774

Rosell-Melé, A., Bard, E., Emeis, K. C., Grieger, B., Hewitt, C., Müller, P. J., & Schneider, R. R. (2004). Sea surface temperature anomalies in the oceans at the LGM estimated from the alkenone-U37K′ index: Comparison with GCMs. *Geophysical Research Letters*, *31*(3), 1–4. https://doi.org/10.1029/2003GL018151

Rosenthal, Y., Oppo, D. W., & Linsley, B. K. (2003). The amplitude and phasing of climate change during the last deglaciation in the Sulu Sea, western equatorial Pacific. *Geophysical Research Letters*, *30*(8). https://doi.org/10.1029/2002GL016612

Russell, A. D., Hönisch, B., Spero, H. J., & Lea, D. W. (2004). Effects of seawater carbonate ion concentration and temperature on shell U, Mg, and Sr in cultured planktonic foraminifera. *Geochimica et Cosmochimica Acta*, *68*(21), 4347–4361. https://doi.org/10.1016/j.gca.2004.03.013

Rustic, G. T., Ravelo, A. C., & White, S. M. (2020). Modulation of late Pleistocene ENSO strength by the tropical Pacific thermocline. *Nature Communications*, https://doi.org/10.1038/s41467-020-19161-6

Seager, R., Cane, M. A., & Clement, A. C. (1999). Orbital controls on the El Nino/Southern Oscillation and the tropical climate. *Paleoceanography*, *14*(4), 441–456.

Saenger, C. P., & Evans, M. N. (2019). Calibration and Validation of Environmental Controls on Planktic Foraminifera Mg/Ca Using Global Core-Top Data. *Paleoceanography and Paleoclimatology*, *34*(8), 1249–1270. https://doi.org/10.1029/2018pa003507

Sagawa, T., Yokoyama, Y., Ikehara, M., & Kuwae, M. (2012). Shoaling of the western equatorial Pacific thermocline during the last glacial maximum inferred from multispecies temperature reconstruction of planktonic foraminifera. *Palaeogeography, Palaeoclimatology, Palaeoecology*, *346–347*, 120–129. https://doi.org/10.1016/j.palaeo.2012.06.002

Schiebel, R., & Hemleben, C. (2005). Modern planktic foraminifera. *Paläontologische Zeitschrift*, *79*(1), 135–148. https://doi.org/10.1007/bf03021758

Schmidt, G. A., Annan, J. D., Bartlein, P. J., Cook, B. I., Guilyardi, E., Hargreaves, J. C., … Yiou, P. (2014). Using palaeo-climate comparisons to constrain future projections in CMIP5. *Climate of the Past*, *10*(1), 221–250. https://doi.org/10.5194/cp-10-221-2014

Schmidtko, S., Johnson, G. C., & Lyman, J. M. (2013). MIMOC: A global monthly isopycnal upper-ocean climatology with mixed layers. *Journal of Geophysical*

Research: Oceans, *118*(4), 1658–1672. https://doi.org/10.1002/jgrc.20122

Sexton, P. F., Wilson, P. A., & Pearson, P. N. (2006). Microstructural and geochemical perspectives on planktic foraminiferal preservation: "Glassy" versus "Frosty." *Geochemistry, Geophysics, Geosystems*, *7*(12).

Spero, H. J., & Lea, D. W. (1993). Intraspecific stable isotope variability in the planktic foraminifera Globigerinoides sacculifer: Results from laboratory experiments. *Marine Micropaleontology*, *22*(3), 221–234. https://doi.org/10.1016/0377-8398(93)90045-Y

Steinke, S., Chiu, H. Y., Yu, P. Sen, Shen, C. C., Erlenkeuser, H., Löwemark, L., & Chen, M. Te. (2006). On the influence of sea level and monsoon climate on the southern South China Sea freshwater budget over the last 22,000 years. *Quaternary Science Reviews*, *25*(13–14), 1475–1488. https://doi.org/10.1016/j.quascirev.2005.12.008

Stott, L., Poulsen, C., Lund, S., & Thunell, R. (2002). Super ENSO and Global Climate Time Oscillations at Millennial Scales. *Science*, *297*(5579), 222–226. https://doi.org/10.1126/science.1071627

Stott, L., Timmermann, A., & Thunell, R. (2007). Southern Hemisphere and deep-sea warming led deglacial atmospheric CO2 rise and tropical warming. *Science (New York, N.Y.)*, *318*(5849), 435–438. https://doi.org/10.1126/science.1143791

Svendsen, J.I., Alexanderson, H., Astakhov, V., Demidov, I., Dowdeswell, J.A., Funder, S., Gataullin, V., Henriksen, M., Hjort, C., Houmark-Nielsen, M., Hubberten, H., Ingólfsson, Ó.A., Jakobsson, M., Kjær, K.H., Larsen, E., Lokrantz, H., Lunkka, J.P., Lysså, A., Mangerud, J., Matiouchkov, A., Murray, A.S., Möller, P., Niessen, F., Nikolskaya, O.K., Polyak, L., Saarnisto, M., Siegert, C., Siegert, M.J., Spielhagen, R.F., & Stein, R. (2004). Late quaternary ice sheet history of northern Eurasia. *Quaternary Science Reviews,* 23, 1229-1271.

Thirumalai, K., DiNezio, P. N., Tierney, J. E., Puy, M., & Mohtadi, M. (2019). An El Niño Mode in the Glacial Indian Ocean? *Paleoceanography and Paleoclimatology*, *34*(8), 1316–1327. https://doi.org/10.1029/2019PA003669

Tierney, J. E., Malevich, S. B., Gray, W., Vetter, L., & Thirumalai, K. (2019). Bayesian Calibration of the Mg/Ca Paleothermometer in Planktic Foraminifera. *Paleoceanography and Paleoclimatology*, *34*(12), 2005–2030. https://doi.org/10.1029/2019PA003744

Tierney, J. E., & Tingley, M. P. (2017). BAYSPLINE : A New Calibration for the Alkenone Paleothermometer. *Paleoceanography and Paleoclimatology*, *33*, 281–301. https://doi.org/10.1002/2017PA003201

Tierney, J. E., Zhu, J., King, J., Malevich, S. B., Hakim, G. J., & Poulsen, C. J. (2020). Glacial cooling and climate sensitivity revisited. *Nature*, *584*(December 2019). https://doi.org/10.1038/s41586-020-2617-x

Timmermann, A., Sachs, J., & Timm, O. E. (2014). Assessing divergent SST behavior during the last 21 ka derived from alkenones and G. ruber-Mg/Ca in the equatorial Pacific. *Paleoceanography*, *29*(6), 680–696. https://doi.org/10.1002/2013PA002598

Tripati, A. K., Sahany, S., Pittman, D., Eagle, R. A., Neelin, J. D., Mitchell, J. L., & Beaufort, L. (2014). Modern and glacial tropical snowlines controlled by sea surface temperature and atmospheric mixing. *Nature Geoscience*, *7*(3), 205–209. https://doi.org/10.1038/ngeo2082

Waelbroeck, C., Paul, A., Kucera, M., Rosell-Melé, A., Weinelt, M., Schneider, R., … Turon, J. L. (2009). Constraints on the magnitude and patterns of ocean cooling at the Last Glacial Maximum. *Nature Geoscience*, *2*(2), 127–132. https://doi.org/10.1038/ngeo411

Webster, P. J., & Streten, N. A. (1978). Late Quaternary ice age climates of tropical Australasia: Interpretations and reconstructions. *Quaternary Research*, *10*(3), 279–309. https://doi.org/10.1016/0033-5894(78)90024-8

Wekerle, C., Colleoni, F., Näslund, J., Brandefelt, J., & Masina, S. (2016). Numerical reconstructions of the penultimate glacial maximum Northern Hemisphere ice sheets : sensitivity to climate forcing and model parameters, *62*, 607–622. https://doi.org/10.1017/jog.2016.45

White, S. M., Ravelo, A. C., & Polissar, P. J. (2018). Dampened El Niño in the Early and Mid-Holocene Due To Insolation-Forced Warming/Deepening of the Thermocline. *Geophysical Research Letters*, *45*(1), 316–326. https://doi.org/10.1002/2017GL075433

Wycech, J. B., Kelly, D. C., Kitajima, K., Kozdon, R., Orland, I. J., & Valley, J. W. (2018). Combined Effects of Gametogenic Calcification and Dissolution on δ18O Measurements of the Planktic Foraminifer Trilobatus sacculifer. *Geochemistry, Geophysics, Geosystems*, *19*(11), 4487–4501. https://doi.org/10.1029/2018GC007908

Xu, J., Kuhnt, W., Holbourn, A., Regenberg, M., & Andersen, N. (2010). Indo-pacific warm pool variability during the holocene and last glacial maximum. *Paleoceanography*, *25*(4). https://doi.org/10.1029/2010PA001934

Yu, J., Broecker, W. S. W. S., Elderfield, H. H., Zhangdong, J., McManus, J. F., Zhang, F., … Zhang, F. (2010). Loss of carbon from the deep sea since the last glacial maximum. *Science*, *330*(6007), 1084–1087. https://doi.org/10.1126/science.1193221

Yu, J., Anderson, R. F., Jin, Z., Rae, J. W. B., Opdyke, B. N., & Eggins, S. M. (2013). Responses of the deep ocean carbonate system to carbon reorganization during the Last Glacial e interglacial cycle. *Quaternary Science Reviews*, *76*, 39–52. https://doi.org/10.1016/j.quascirev.2013.06.020

Yuan, V. (2018). *Late Pleistocene Cenral Equatorial Pacific Temperature Drivers*. UC

Santa Cruz. Retrieved from https://escholarship.org/uc/item/3d41w5qn

Zelinka, M. D., Myers, T. A., McCoy, D. T., Po-Chedley, S., Caldwell, P. M., Ceppi, P., … Taylor, K. E. (2020). Causes of Higher Climate Sensitivity in CMIP6 Models. *Geophysical Research Letters*, *47*(1), 1–12. https://doi.org/10.1029/2019GL085782

Zhu, J., Otto-bliesner, B. L., Brady, E. C., & Poulsen, C. J. (2021). Assessment of Equilibrium Climate Sensitivity of the Community Earth System Model Version 2 Through Simulation of the Last Glacial Maximum Geophysical Research Letters, *2*. https://doi.org/10.1029/2020GL091220